uOttawa

L'Université canadienne
Canada's university

FACULTÉ DES ÉTUDES SUPÉRIEURES ET POSTOCTORALES

uOttawa

L'Université canadienne
Canada's university

FACULTY OF GRADUATE AND POSDOCTORAL STUDIES

Walid Abediseid

AUTEUR DE LA THÈSE / AUTHOR OF THESIS

M.A.Sc. (Electrical Engineering)

GRADE / DEGREE

School of Information Technology and Engineering

FACULTÉ, ÉCOLE, DÉPARTEMENT / FACULTY, SCHOOL, DEPARTMENT

A Linearizing Approach to Coding for Generalized MSK

TITRE DE LA THÈSE / TITLE OF THESIS

Dr. Galko

DIRECTEUR (DIRECTRICE) DE LA THÈSE / THESIS SUPERVISOR

CO-DIRECTEUR (CO-DIRECTRICE) DE LA THÈSE / THESIS CO-SUPERVISOR

EXAMINATEURS (EXAMINATRICES) DE LA THÈSE / THESIS EXAMINERS

Dr. D'Amours

Dr. El-Tanany

Gary W. Slater

Le Doyen de la Faculté des études supérieures et postdoctorales / Dean of the Faculty of Graduate and Postdoctoral Studies

A Linearizing Approach to Coding for Generalized MSK

by

Walid AbedIseid

A thesis submitted in conformity with the requirements
for the degree of Master of Applied Science
Ottawa-Carleton Institute for Electrical and Computer Engineering
University of Ottawa

Your file Votre référence
ISBN: 978-0-494-32429-5
Our file Notre référence
ISBN: 978-0-494-32429-5

Abstract

Minimum shift keying as an instance of continuous-phase frequency shift keying is a nonlinear modulation which makes designing error correcting codes for it difficult as Euclidean distances between signals and the Hamming distances between symbol sequences do not linearly correspond. We show that the nonlinearity disappears if we employ a sequence mapping we term precoding arising from the equivalence of this modulation to a form of offset quadrature phase shift keying. When we consider the modified forms of this modulation (generalized MSK) to achieve improved spectral efficiency, the nonlinearity and memory make the coding design problem more difficult, and precoding does not resolve the issue. We show that the nonlinearity can be removed in the cases involving pulse shapes of two and three symbol period duration using two stages of coding, the last being a double or quadruple repetition code.

Using the Laurent representation of continuous-phase modulation as amplitude modulated pulses, a simple inphase-quadrature modulator can be implemented to generate such coded generalized MSK signals. The inphase and quadrature pulses are shown to be linear combinations of the Laurent pulses. It is shown that the coded signals can be demodulated using a simple inphase-quadrature receiver without sacrificing the performance. It is shown that no intersymbol interference is introduced at the sampled output of the matched filter and in additive white Gaussian noise environment, the noise samples are independent. Therefore, the detection problem for the recovery of the symbols sequence from the decision variable sequence is one corresponding to memoryless linear modulation, avoiding the use of the maximum likelihood sequence detection which would otherwise be needed for optimal performance. Furthermore, it is shown that by applying repetition code to these modulation schemes, the Euclidean distance between different signals is directly related to the Hamming distance between corresponding coded sequences. This may simplify the task of search for good codes applied to the considered case of generalized MSK signals.

Dedication

This thesis is dedicated to my wonderful parents, Mohammed and Hana, who have raised me to be the person I am today. You have been with me every step of the way, through good times and bad. Thank you for all the unconditional love, guidance, and support that you have always given me, helping me to succeed and instilling in me the confidence that I am capable of doing anything I put my mind to. Thank you for everything.

I love you!

♡

Acknowledgment

First and foremost, I would like to take this opportunity to thank my Thesis advisor Dr. Peter Galko for the endless support and guidance over the past several years. He is an excellent teacher whose enthusiasm in teaching infects me with the determination to perform at my best. I am extremely proud to have been his student and honored to have been able to work with him. His keen eye for details have saved me from many a pitfall.

I owe an eternal debt to Sh. Mahmoud Mehrez and his great family. I am indebted to him for inspiring and encouraging me to pursue and continuing my graduate studies. Nothing could have been achieved without his support, thank you is not enough.

There are a number of people who should be recognized as well. The first person to be acknowledged is my best friend Hamza Al Shawaf for his unceasing support, encouragement and the many pep talks he has given me whenever I was frustrated. To my friends that I have met in Ottawa, Safwat, Hassan, Thaer, Ebrahim, Yaman, Sharief, Talal and Ahmad Mehrez, thanks for the fun times and for the shoulders that only friends can give.

I would like to express my sincere thanks to my uncle Omar and his great wife Sawsan for always keeping in touch with me, and providing me with advice when I needed them. Not to forget my wonderful cousins Osama, Mohammed and Dania, for considering me their favourite cousin. I would like also to thanks Mohammed Al Ramahi for his advice and being there to help whenever I needed him.

I would also like to place on record my gratitude towards my wonderful bother Wajdi, and my lovely sisters Lubna, Deema, Ayat and Amani, who have always supported me

in my academic pursuits and encouraged me to do my best, I love you all. I would like also to thanks Dr. Mohammed Al Qaffaf for his ecouragement and support during my studies. Again I would like to thank my parents for their love and encouragement that carried me through all the difficulties.

I would like to thank my wife, my father-in-law, Abu Mustapha, his wife, and their sons Mustapha and Tariq, for the trust and support during my studies.

During my tenure at the University of Ottawa, I courted the woman of my dreams. I was and will always be most honored that she became my wife this past year. Fatima, I love you with all my heart. I look forward to being with you for the rest of my life, to our children that are yet a twinkle in your eye, to being your lifelong friend, and to growing old with you. Fatima, my all forever belongs to you.

Finally, the financial support provided by the government of Ontario (OGS) is gratefully acknowledged. I thank also the University of Ottawa for providing me with financial assistance throughout this work.

Contents

List of Tables

List of Figures

List of Acronyms

AMF	Average Matched Filter
AOF	Asymptotic Optimal Filter
AWGN	Additive White Gaussian Noise Channel
BPSK	Binary Phase-Shift Keying
CG	Coding Gain
CPFSK	Continuous Phase Frequency Shift Keying
CPM	Continuous Phase Modulation
DMSK	Duobinary Minimum Shift Keying
GMSK	Gaussian Minimum Shift Keying
I-Q	Inphase and Quadrature
ISI	Intersymbol Interference
MLSD	Maximum Likelihood Sequence Detection
MLSE	Maximum Likelihood Sequence Estimator
MSK	Minimum Shift Keying
NSED	Normalized Squared Euclidean Distance
NSFED	Normalized Squared Free Euclidean Distance
PAM	Pulse Amplitude Modulation
OQPSK	Offset Quadrature Phase Shift Keying
QAM	Quadrature Amplitude Modulation
SNR	Signal to Noise Ratio
TFM	Tamed Frequency Modulation
VA	Viterbi Algorithm

List of Symbols

a_n	Source symbol
b_n	Input symbol to CPFSK-MSK modulator
c_n	Output symbol of the cascaded channel encoder $\mathbf{W}$
$\mathbf{c}^i$	Output coded sequence of encoder $\mathbf{W}$
$\mathbf{c}'^i$	Output coded sequence of outer encoder $\mathbf{W}^o$
C_W	Cascaded convolutional code
C_{W^o}	Outer convolutional code
$C_k(t)$	The k^{th} Laurent pulse
$\|C_k(t)\|^2$	Energy of the Laurent pulse $C_k(t)$
$\langle C_m(t), C_n(t)\rangle$	Inner product between the Laurent pulses $C_m(t)$ and $C_n(t)$
D	Symbol delay element
E	Average energy transmitted per symbol
E_b	Average energy transmitted per bit
f_c	Carrier frequency
$\mathbf{G}$	Channel encoder for CPFSK-MSK system
$h(t)$	Premodulation pulse shape
$H_W(\mathbf{c}^i, \mathbf{c}^j)$	Hamming distance between two coded sequences $\mathbf{c}^i$ and $\mathbf{c}^j$
H_{min}^W	Minimum Hamming distance of encoder $\mathbf{W}$
$H_{\text{min}}^{W^o}$	Minimum Hamming distance of encoder $\mathbf{W^o}$
$\Im\{\}$	Imaginary part of a complex number
$I(t)$	Inphase channel signal
k_i	Coding polynomial coefficients
L	Modulation memory
$n(t)$	White Gaussian noise process
$n_I(t)$	Inphase component of $n(t)$

$n_Q(t)$	Quadrature component of $n(t)$
n_m	Noise samples of the output of matched filter at time mT
$\bar{n}_m$	Averaged noise samples of the output of matched filter at time mT
$\mathcal{N}_o$	Noise level
$p(t)$	Inphase channel pulse
$\tilde{p}(t)$	Quadrature channel pulse
$\mathcal{P}_b$	Bit error probability
$\mathcal{P}_{b,\text{asymp}}$	Asymptotic bit error probability
$Q(x)$	The Q-function
$\mathbf{Q}$	Precoder
$Q(t)$	Quadrature channel signal
$\Re\{\}$	Real part of a complex number
R_c	Rate of cascaded encoder $\mathbf{W}$
R_o	Rate of outer encoder $\mathbf{W}^o$
$r(t)$	Receiver signal
$s(t)$	Transmitted generalized MSK signal
$s_l(t)$	Lowpass equivalent generalized MSK signal
T	Symbol period
v_n	Real and Imaginary part of $\beta_{1,n}$
$\mathbf{W}$	The generator matrix of cascaded channel encoder
$\mathbf{W}^o$	The generator matrix of outer channel encoder
$\mathbf{W}^i$	The generator matrix of inner channel encoder
$\mathbf{W}(D)$	$\mathcal{D}$-transform representation of the generator matrix of cascaded channel encoder
$\mathbf{W}^o(D)$	$\mathcal{D}$-transform representation of the generator matrix of outer channel encoder
$\mathbf{W}^i(D)$	$\mathcal{D}$-transform representation of the generator matrix of inner channel encoder
$\mathbf{W}^i_l(D)$	Enlarged inner encoder's generator matrix by l
$w^o_{i,j}(D)$	Entries of the outer encoder's generator matrix
x_n	Real and Imaginary part of $\beta_{2,n}$
y_n	Real part of $\beta_{3,n}$
z_n	Sampled output of matched filter at time nT
$\bar{z}_n$	Averaged sampled output of matched filter at time nT
$\phi(t)$	Excess phase
ϕ_0	Arbitrary initial phase

$\beta_{k,n}$ Laurent coefficient

ν Constraint length of cascaded convolutional encoder $\mathbf{W}$

ν^o Constraint length of outer convolutional encoder $\mathbf{W}^o$

Chapter 1

Introduction

1.1 Preface

Digital modulation can be divided into two classes: linear and nonlinear modulation. Modulation techniques such as M-ary pulse amplitude modulation (PAM) and M-ary quadrature amplitude modulation (QAM) are considered linear in the sense that the signal can be expressed as a linear function of the transmitted data. Typically, these modulation schemes produce a signal with non-constant envelopes which make the schemes unsuitable for use in power limited situations such as wireless communications. In these cases, the amplifiers that generate the RF signals need to be operated in saturation to achieve the most efficient use of battery power. In saturation, these amplifiers display significant non-linear characteristics described by a non-linear input-amplitude to output-amplitude (AM/AM) characteristic and a non-constant input-power to output-power (AM/PM) characteristic [1], [2]. The effect of these characteristics on a signal with non-constant envelope is to distort that signal by causing a growth of spectral sidelobes of the transmitted signal (i.e., broadening the bandwidth of the signal) and producing undesirable inter-symbol interference (ISI) which invariably significantly decreases the detection performance of the system. Attempts have been made by researchers to com-

pensate for the nonlinearities introduced by the power amplifier to reduce the amount of distortion in the transmitted signal. Predistortion is one technique that is most widely used for such purposes. However, it suffers from many drawbacks such as high complexity, bandwidth limitations and sensitivity to component drift (see [2] for example, for more details about this subject).

Constant envelope modulation schemes such as *continuous-phase modulation* (CPM) avoid these difficulties. CPM is a non-linear modulation that is widely used in wireless and mobile communication systems, due to its power and bandwidth-efficiency [3]. In CPM, the phase is continuous and as a result, the signal on a symbol interval depends on many symbols and so this modulation is said to have memory. To best recover the symbols requires this memory to be taken into account which requires we use a maximum-likelihood sequence estimator (MLSE) receiver (e.g. a Viterbi receiver) [4],[5]. Receivers based on maximum likelihood sequence estimation are generally complex to implement in comparison to symbol-by-symbol detectors.

Among the CPM schemes there is one case of special note to which some of the above remarks do not apply. This is the case of minimum-shift keying (MSK) which is an instant of binary continuous-phase frequency-shift keying (CPFSK) in which the transmitted signal always has one of two instantaneous frequencies that are separated by half the symbol rate. MSK is particularly important amongst constant envelope modulation schemes as it produces signals with a relatively small bandwidth and can be also expressed in the form of two binary antipodal pulse amplitude modulated (PAM) signals with non-overlapping pulses (a form of offset quadrature phase shift keying [OQPSK] to be precise). Thus, MSK has the performance of binary antipodal signalling in noise, and can be optimally demodulated using a simple inphase-quadrature receiver performing *symbol-by-symbol* detection.

To further improve upon the spectral efficiency of MSK, it can be modified with smoother pulse shapes extending beyond a symbol interval. However, for more signifi-

cant changes, the ability to express the resulting scheme as binary pulse amplitude in quadrature is lost, requiring again we resort to complex MLSE receivers for optimal detection. If we restrict the modifications in some small way to a class of schemes termed *generalized* MSK, it has been shown [6] that it remains possible to use simple receivers to successfully detect the modulated signals, with possibly only small losses in performance compared to a MLSE receiver. Such generalized MSK schemes are used in practice, most notably perhaps being the instance of generalized MSK using a pulse with a Gaussian shape; resulting in Gaussian MSK (used in wireless mobile applications such as GSM systems) [23].

Unfortunately, the improvements of spectral properties that generalized MSK can provide come at the expense of some loss in performance in noise even if a MLSE receiver is used. To improve this performance, a natural thought would be to employ error control coding. Designing such codes for generalized MSK represents a challenge arising from the non-linear relationship between channel symbols and the generated signals, and the memory in the modulation. This is the task we would like to address in this thesis—how to design an error correcting code for generalized MSK signals, keeping in mind the complexity of the detection system.

Using a decomposition of CPM signals as a sum of pulse amplitude modulated signals developed by Laurent [7], we shall show that combining *double* and *quadruple* repetition codes to "precoded" generalized MSK signals with pulse durations $2T$ and $3T$ respectively, the information symbols sequence can be *optimally* detected using a simple I-Q receiver employing symbol-by-symbol detection. These simple codes can achieve relatively small coding gains compared to the uncoded case. For further improvement in the power-efficiency, an outer (convolutional) encoder is combined with the repetition code generating a *cascaded* channel encoder [34, p.466].

It will be shown that using the repetition codes mentioned above, an exact inphase and quadrature (I-Q) representation of such a coded signal may be given which allows

us to generate the coded signal using a simple I-Q modulator. Another significant result of applying such coding schemes is that no inter-symbol interference (ISI) is introduced at the output of the matched filters in the I-Q receiver. Therefore, the use of post equalization is avoided which provides a reduction in the complexity of the optimum receiver. Another important result that would have the advantage of simplifying the search for the good (convolutional) codes applied to generalized MSK, is the proportionality of the Euclidean distance between generated signals to the corresponding Hamming distance between sequences generated by channel encoder. The cost of applying such coding schemes to increase the performance of the optimum receiver is an expansion in the bandwidth of the transmitted signal and an increase in decoder complexity.

1.2 Previous Work

Extensive work and research has been performed previously in the design of optimum and sub-optimum receivers for generalized MSK signals. In 1982, P. Galko [8] showed that generalized MSK can be demodulated sub-optimally using an I-Q receiver where the impulse response of the predetection filter is shown to be a linear combination of all possible signals at the input of the filter. The optimum (minimum probability of error) predetection filter is determined numerically and depends on the value of the signal-to-noise ratio (SNR). The problem of designing the optimum filter can be simplified in the two asymptotic cases of a very low and a very high SNR leading to the solution of the "Average Matched Filter" (AMF) and the "Asymptotically Optimal Filter" (AOF). Filter design based on a zero ISI constraint for PAM-based approximations of the signals was also considered.

In [9], El-Tanany and Mahmoud discuss the design of predetection filters that minimize the mean square ISI when the filter noise bandwidth is held constant. M. Luise and U. Mengali [10] have developed a method of approximating a generalized MSK as an

OQPSK signal using a minimum mean-square error criterion, where it has been shown that the filter matched to the pulse of the best approximating OQPSK signal is just the AMF.

Other work that has been published in literature [11]-[15] for designing optimum receiver for generalized MSK was based on Viterbi detection which is considered complex. The reduction in complexity for such receiver was based on reducing the number of trellis states in the Viterbi detector. A. Svensson, C. Sundberg and T. Aulin [11], proposed a reduced complexity Viterbi detector, where the main idea was to use a shorter length frequency pulse for the Viterbi receiver.

The complexity of the optimum (Viterbi) receiver can be significantly reduced by the use of PAM representation of CPM signals developed by Laurent [7]. Kaleh [16] exploited Laurent's representation of CPM to allow for simple implementation of coherent receivers for such modulation, in particular, for the case of Gaussian MSK. Two forms of such receivers were considered, namely, a simplification of the Viterbi receiver and a linear MSK-*type* receiver, both for which yielded small degradation relative to the true optimum receiver. The idea is to approximate the CPM signal (with memory $L \geq 3$) by the first and/or second Laurent pulse(s), since they contain most of the energy of the CPM signal. This leads to a reduced-complexity Viterbi receiver which can achieve near-optimal performance.

With regards to the problem of code design, some research has been performed previously in the search for good codes combined with generalized MSK such as *duobinary* MSK (DMSK), *tamed-frequency* modulation (TFM) and Gaussian MSK. J. Fonseka [31] has considered the study of block coding combined with various forms of CPM modulation to increase the performance of the overall CPM system. The code design was based on preventing merging states with small Euclidean distance from occurring. It was shown that some block codes have performance equivalent to the one achieved using convolutional codes.

S. Pizzi and S. Wilson [33] have considered the combination of some convolutional error-correcting codes with CPM signals to maximize the minimum Euclidean distance between signal paths. The design of the convolutional code depends on the mapping rule to reduce the search. G. Benelli and R. Fantacci [32] have analyzed the combination of some Hamming codes and binary CPFSK modulation, where it was shown that the error performance depends on the configuration of the parity-check matrix of the block encoder. The search for good block codes was considered difficult in the sense that no analytical method has been found to determine the best code configuration. Therefore, all previous work has been done using computer searches.

The idea of using "coding" to reduce the complexity of the optimum receiver for CPM signals while achieving good coding gains was first introduced by Moreno [15]. In his PhD thesis, special convolutional codes, called matched codes, are applied to the CPM systems such that the number of states in the (soft-decision) Viterbi receiver is minimized. This receiver still exhibits a significantly high level of complexity when it is compared to the (optimum) I-Q receiver that is used to demodulate MSK signal (or suboptimal in the case of generalized MSK).

1.3 Thesis structure

Chapter 2 provides some background information on generalized MSK and their optimum and sub-optimum receiver structure. Using the OQPSK description of MSK a special precoder is designed which is then used with other generalized MSK systems. In Chapter 3, the use of Laurent representation of generalized MSK as a PAM signal is discussed in detail. An analytical expression of the Euclidean distance, for generalized MSK with memory $L = 2$ and $L = 3$, is derived.

In Chapter 4, we introduce most of the new concepts and results of this thesis, where the role of repetition codes in improving the performance of the overall system while

reducing the complexity of optimum receiver is investigated. Using repetition codes an exact I-Q representation of generalized MSK with memory $L = 2$ and $L = 3$ is derived analytically. A simple I-Q modulator for generating coded generalized MSK signals is proposed. Moreover, a linear (matched) receiver is designed for optimum detection of such coded signals where symbol-by-symbol detection may be applied for recovering the coded sequence. The results of a complete search for the optimal convolutional codes (for some code rates and constraint length) applied to such systems are reported.

Finally, conclusions are given in Chapter 5. The proof of some results in this thesis is given in the appendices.

Chapter 2

Generalized MSK

2.1 Minimum-Shift Keying

Minimum-shift keying (MSK) may be described as an instance of binary continuous-phase frequency-shift keying (CPFSK) with frequencies separated by half the symbol rate. As such, it represents a non-linear modulation scheme that generates constant-envelope signals with an attractive spectral and power efficiency [17]. The signal produced in MSK may also be described as a form of *offset* quadrature phase-shift keying (OQPSK) with a half-cycle sinusoidal pulse shape [18], which is a linear modulation. The power efficiency of MSK can be further improved using error control coding, but the task of designing codes for MSK signals using its CPFSK description (CPFSK-MSK) is difficult due to the nonlinearity and memory of the modulation. Previous work in this area [15], [19] has optimized the code design with certain constraints using a numerical search. Fortunately, the coding design problem can be simplified by the use of the OQPSK description of MSK (OQPSK-MSK).

2.1.1 CPFSK-OQPSK MSK

The CPFSK description of the MSK signal can be mathematically expressed as

$$s(t) = \sqrt{\frac{2E}{T}}\cos(2\pi f_c t + \phi(t) + \theta_0), \qquad nT \le t < (n+1)T, \tag{2.1}$$

where E is the average energy transmitted per symbol, T is the symbol period, f_c is the carrier frequency, θ_0 is an initial phase, and $\phi(t)$ is the excess-phase given by

$$\phi(t) = \frac{\pi}{2T}\int_0^t \sum_m b_m h(\tau - mT)d\tau, \tag{2.2}$$

where $\{..., b_{-2}, b_{-1}, b_0, b_1, b_2, ...\}$ is a binary symbol stream (using an alphabet $\{-1, 1\}$) input to the CPFSK-MSK modulator, and $h(t)$ is given by

$$h(t) = \begin{cases} 1, & 0 \le t \le T; \\ 0, & \text{otherwise.} \end{cases} \tag{2.3}$$

The excess-phase $\phi(t)$ for $t \in [nT, (n+1)T)$ can be written as,

$$\phi(t) = \frac{\pi(t - nT)}{2T} b_n + \phi_n,$$

where

$$\phi_n = \phi(nT) = \begin{cases} \frac{\pi}{2}\sum_{m=0}^{n-1} b_m, & \text{if } n \ge 1; \\ 0, & \text{if } n = 0; \\ -\frac{\pi}{2}\sum_{m=n}^{-1} b_m, & \text{if } n \le -1; \end{cases}$$

which can only be one of exactly four values (modulo 2π): $-\pi/2, 0, \pi/2$ or π. The sequence of values ϕ_n can be described by a finite state machine with state transition diagram shown in Fig. 2.1. The excess-phase can also be described by the trellis diagram shown in Fig. 2.2, which is a plot of the possible trajectories of $\phi(t)$, modulo 2π.

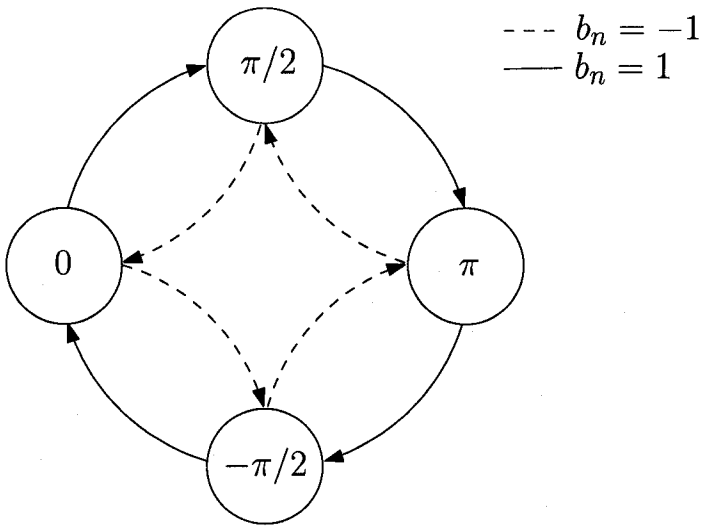

Fig. 2.1: The state transition diagram of a finite state machine describing the relation between the sequence of excess-phase values ϕ_n and the symbols $\{b_n\}$ for CPFSK-MSK. Transitions between states are governed by the value of the symbol b_n.

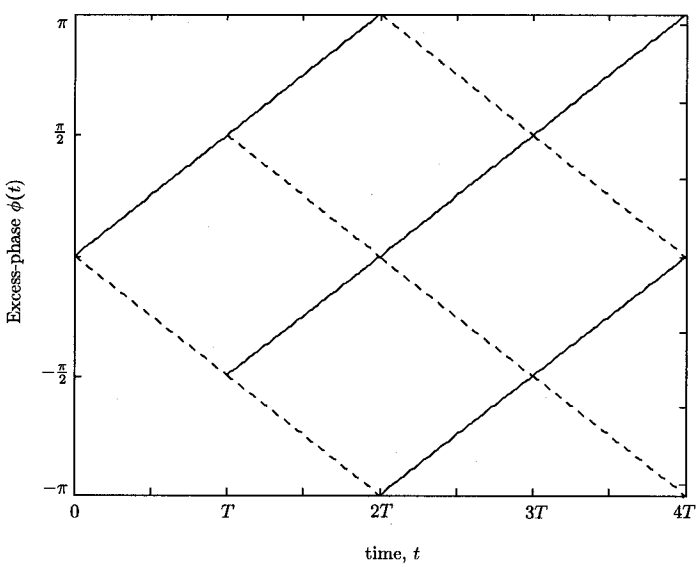

Fig. 2.2: The excess-phase trellis of MSK for $t \geq 0$. Solid lines are for a symbol value $b_n = 1$, dashed lines correspond to $b_n = -1$.

It is well-known [18], that MSK can be viewed as a special case of offset quadrature phase-shift keying (OQPSK) with half-period sinusoidal pulses, i.e., the signal in (2.1)–(2.3) can also be expressed as

$$\begin{aligned} s(t) &= A\left[\sum_{n \text{ odd}} c_n p(t-nT)\right]\cos(2\pi f_c t + \phi_0) \\ &\quad + A\left[\sum_{n \text{ even}} c_n p(t-nT)\right]\sin(2\pi f_c t + \phi_0), \end{aligned} \tag{2.4}$$

where $\{..., c_{-2}, c_{-1}, c_0, c_1, c_2...\}$ is a binary symbol stream with an alphabet $\{-1, 1\}$ and

$$p(t) = \begin{cases} \sin(\frac{\pi t}{2T}), & t \in [0, 2T]; \\ 0, & \text{otherwise.} \end{cases} \tag{2.5}$$

Note that the $\{b_n\}$ and $\{c_n\}$ symbol streams share the same alphabet but are not the same. It can be shown [8] that for the formulation of the MSK signal in (2.1)–(2.3) and (2.4),(2.5) to be equal, the binary symbol streams $\{b_n\}$ and $\{c_n\}$ must be related by a non-linear relation

$$b_n = (-1)^{n+1} c_n c_{n-1}, \tag{2.6}$$

with $c_{-1} = 1$ (since $\phi(t)$ at $t = 0$ is 0).

If we were to use coding on each of these forms for expressing MSK, we produce the systems depicted in Fig. 2.3. At time t a binary k-tuple $(a_t^{(1)}, a_t^{(2)}, ..., a_t^{(k)})$ produces at the output of encoders $\mathbf{G}$ and $\mathbf{W}$ a binary l-tuple $(b_t^{(1)}, b_t^{(2)}, ..., b_t^{(l)})$ and $(c_t^{(1)}, c_t^{(2)}, ..., c_t^{(l)})$ which is transmitted serially to the CPFSK-MSK and OQPSK-MSK modulators, respectively. Therefore, both encoders $\mathbf{G}$ and $\mathbf{W}$ have a code rate of k/l.

2.1.2 Precoded CPFSK-MSK system

The nonlinear relationship between the input symbol stream (the $\{b_n\}$ sequence) and the transmitted signal $s(t)$ in CPFSK-MSK is quite inconvenient for code design as Hamming distances between sequences do not directly relate to Euclidean distances between corresponding transmitted signals. Thus the performance of the coded CPFSK-MSK cannot

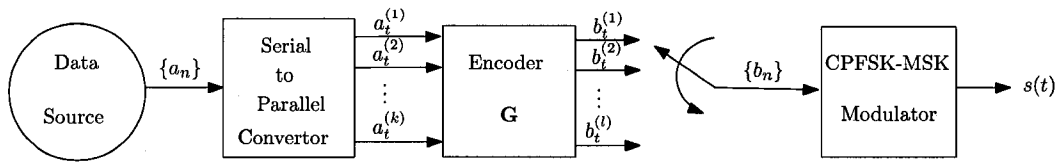

a. Coded CPFSK-MSK system.

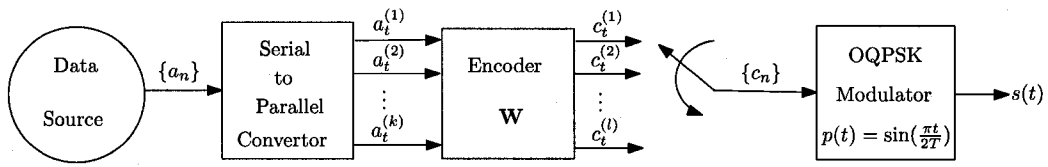

b. Coded OQPSK-MSK system.

Fig. 2.3: Two equivalent coded MSK systems.

be related to the Hamming distance properties of the code (on which much of the code design is based). Since the OQPSK-MSK does not have this difficulty (see Appendix A), it suggests a strategy to eliminate the problem by beginning with the OQPSK-MSK input symbols and converting this sequence to the $\{b_n\}$ sequence with a mapping we term "precoding" followed by a CPFSK-MSK modulator as depicted in Fig. 2.4. The precoder can be viewed as linearizing CPFSK-MSK.

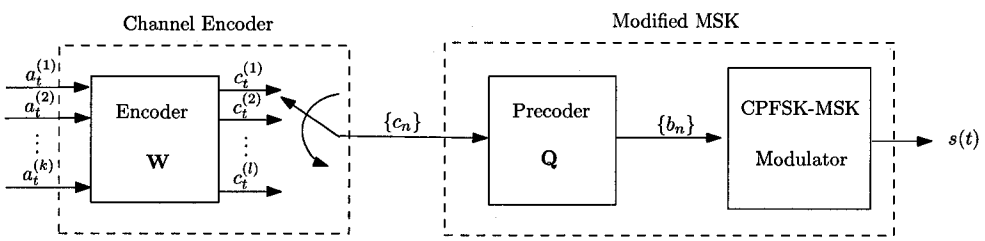

Fig. 2.4: Modified coded CPFSK-MSK system.

The precoder **Q** can be described by the block diagram shown in Fig. 2.5. This precoder consists of two parts: a feed-forward differential-type encoder followed by an alternating (periodic) sequence $\{-1, 1, -1, ...\}$.

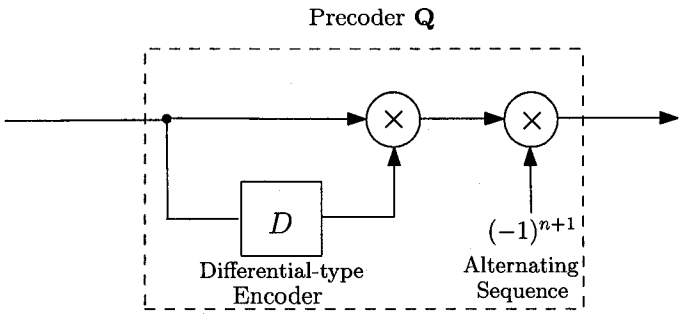

Fig. 2.5: Structure of Precoder **Q**. The D block represents a one symbol delay.

2.2 Generalized MSK

In MSK, while the excess-phase $\phi(t)$ is continuous and limited to changing $\pi/2$ or $-\pi/2$, the instantaneous frequency can change abruptly so that the second derivative of $s(t)$ is discontinuous, limiting the decay rate of the mean power spectral density function. If we replace the pulse shape $h(t)$ by a smoother pulse than the NRZ pulse of (2.3), yet with the same area T, this situation could be improved. Such considerations lead us to consider the modulation schemes that produce a transmitted signal as given by (2.1) with excess phase given by (2.2), but with $h(t)$ some other pulse of area T and duration possibly greater than T. Such modulation schemes are instances of what is referred as continuous phase modulation (CPM) for the specific choice of a modulation index of 0.5 ("$h = 1/2$") [3].

For our discussion here we consider a causal pulse shape with duration not more than LT, so we are considering a pulse that satisfies the property

$$\int_0^t h(\tau)\, d\tau = \begin{cases} 0, & t \leq 0; \\ T, & t \geq LT. \end{cases} \tag{2.7}$$

The parameter L in the above expression is the number of symbol intervals over which the pulse shape is spread. The greatest spectral efficiencies achieved by using other pulse shapes $h(t)$ occur when $L > 1$. One means of achieving the effect of a pulse shape spread over more than one interval is through the use of correlative coding (also termed

partial response signalling). Correlative coding can be viewed as a means to introduce a controlled amount of intersymbol interference into a PAM signal and has many possible implementations. Fig. 2.6 represents one means to do so. The pulse shape $g(t)$ in this

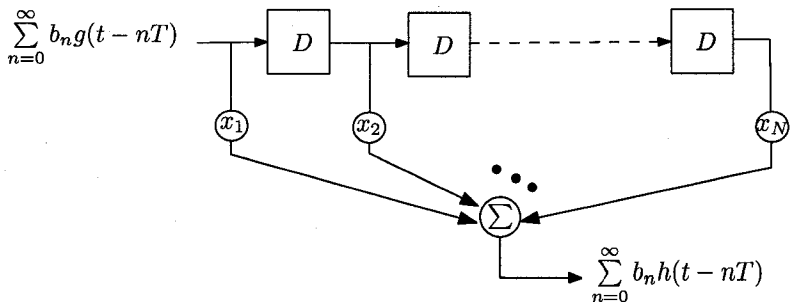

Fig. 2.6: One scheme to implement correlative coding. Each box represents a one symbol period delay.

scheme would be required to satisfy

$$\int_0^t g(\tau)\, d\tau = \begin{cases} 0, & t < 0; \\ T, & t \geq T. \end{cases}$$

Correlative coding schemes are usually identified by their "coding polynomial" $x(D) = \sum_{i=0}^{N} x_i D^i$, where D representing an operator corresponding to a symbol period delay. The degree of the polynomial is $N = L - 1$, and so that (2.7) holds, $\sum_{i=0}^{L-1} x_i = 1$. Duobinary MSK (DMSK) and tamed frequency modulation (TFM) [22] are two well-known instances of such modified MSK that may be described as employing correlative coding using coding polynomials $(1+D)/2$ and $(1+2D+D^2)/4 = (1+D)^2/4$ respectively.

Now any signal in this family (i.e., one defined by (2.1), (2.2) and (2.7)) can be expressed as

$$s(t) = \sqrt{\frac{2E}{T}}\Big\{\cos\phi(t)\cos(2\pi f_c t + \theta_0) - \sin\phi(t)\sin(2\pi f_c t + \theta_0)\Big\},$$

and we know that in the instance of MSK (i.e., $h(t)$ given by (2.3)), $\cos\phi(t)$ and $\sin\phi(t)$ can be expressed as

$$\cos\phi(t) = \sum_{n \text{ odd}} c_n p(t-nT), \quad \text{and} \quad \sin\phi(t) = \sum_{n \text{ even}} c_n p(t-nT), \tag{2.8}$$

where $p(t)$ is given by (2.5). This is the basis of the OQPSK description of MSK. With modified pulse shapes for $h(t)$, it has been shown in [8] that the equivalence of the resulting modified MSK scheme to a form of OQPSK is affected. It was shown that if $h(t)$ satisfies (2.7) for $L = 1$, then $\cos\phi(t)$ and $\sin\phi(t)$ can be expressed as in (2.8), but $p(t)$ is some other pulse other than given by (2.5), though its duration is limited $[-T, T]$ and has the value 1 at $t = 0$. In other words, in this case the modified scheme still can be expressed by (2.4) but with the pulse shape has been altered. The modified MSK scheme in this case is termed an MSK-*like* scheme.

In the case of MSK or MSK-*like* schemes, the samples of $\cos\phi(t)$ and $\sin\phi(t)$ at even and odd multiples of T respectively are just the values of the symbol stream $\{c_n\}$:

$$\cos[\phi(2nT)] = c_{2n-1}, \quad \text{and} \quad \sin[\phi([2n+1]T)] = c_{2n}. \tag{2.9}$$

This can be described as there being no intersymbol interference in the $\cos\phi(t)$ and $\sin\phi(t)$ components at the sampling instants. This feature can be preserved in more general circumstances if the pulse shape $h(t)$ satisfies the condition

$$\int_{mT}^{(m+1)T} h(t)\, dt = \begin{cases} T, & m = 0; \\ 0, & m \neq 0. \end{cases} \tag{2.10}$$

Schemes where (2.10) holds are termed MSK-*type*; unless it is also an MSK-*like* scheme, it has been shown that $\cos\phi(t)$ and $\sin\phi(t)$ cannot be expressed as PAM, but (2.9) holds, so an I-Q receiver still could recover the $\{c_n\}$ symbol sequence.

The condition (2.10) can be interpreted as a "no intersymbol interference" or "fully open eye" condition for the I-Q representation and the recovery of the symbol stream $\{c_n\}$ using a simple I-Q receiver. If we consider further generalizations of the pulse shape, it has been shown in [8] if the pulse shape meets certain mild conditions, the symbol stream $\{c_n\}$ can be recovered using a simple I-Q receiver, though the carriers employed would be possibly phase offset, and the sampling instants in the inphase and quadrature arms of the receiver may be delayed by some amount τ_0. The sufficient condition given in [8] for

this (which merely guarantees an open eye for the inphase and quadrature components at the sampling instants) is that

$$\sum_{l=1}^{\infty}\left\{\left|\sum_{j=l}^{\infty} k_j\right| + \left|\sum_{j=l}^{\infty} k_{-j}\right|\right\} < T, \tag{2.11}$$

where

$$k_j \triangleq \int_{jT}^{(j+1)T} h(t+\tau_0)\, dt.$$

(For pulse shapes $h(t)$ restricted to $[0, LT]$, we would usually expect some near symmetry on that interval and thus usually want the time offset to be $\tau_0 = (L-1)T/2$). Schemes that meet this condition—the modified forms of MSK that would still allow a simple I-Q receiver to recover the symbol stream $\{c_n\}$ directly—are referred to as *generalized* MSK. The schemes DMSK and TFM mentioned before are examples of generalized MSK modulation that are not MSK-*like* or MSK-*type* schemes. Another significant instance of this is Gaussian MSK [23],[24], one of the most important schemes used in some widely used wireless communication systems. Gaussian MSK is generalized MSK with a pulse shape given by

$$h(t) = \begin{cases} Q\left(\frac{2\pi BT}{\sqrt{\ln 2}}\frac{t-(L+1)\frac{T}{2}}{T}\right) - Q\left(\frac{2\pi BT}{\sqrt{\ln 2}}\frac{t-(L-1)\frac{T}{2}}{T}\right), & 0 < t < LT; \\ 0, & \text{otherwise}, \end{cases} \tag{2.12}$$

where $Q(x)$ is the familiar "Q-function" given by

$$Q(x) = \int_{x}^{\infty} \frac{1}{\sqrt{2\pi}} e^{-t^2/2}\, dx.$$

and $L \geq \lfloor 1/BT \rfloor$. The parameter BT is termed the bandwidth-time product of the Gaussian MSK scheme[2].

[2]GMSK with $BT = 0.3$ and 0.5 is being employed in Global System for Mobile (GSM) and cellular digital packet data (CDPD), respectively. Lower values of BT which has the effect of increasing the bandwidth-efficiency of GMSK signals can be found in many important applications such as commercial and military narrowband systems [25],[26].

2.3 Optimum and Sub-Optimum Receivers for Generalized MSK in AWGN Channel

Consider first the detection of MSK signals with no channel coding (i.e., where $\mathbf{W}$ is the identity mapping $a_n = c_n$). Since the transmitted signal $s(t)$ can be expressed in OQPSK form, it follows that provided $f_c T \gg 1$, an MSK signal (or more generally MSK-*like* signals) in additive white Gaussian noise (AWGN) can be optimally demodulated with respect to errors in $\{c_n\}$ (or $\{a_n\}$) by an I-Q receiver depicted in Fig. 2.7.*a*. The output of the matched filter on each channel z_{2m+1} and z_{2m} are *sufficient statistics* for making a decision on the sequence $\{c_n\}$ (or $\{a_n\}$) [34]. The performance of this receiver (i.e., the bit error probability $\mathcal{P}_b$) is well-known to be [17]

$$\mathcal{P}_b = Q\left(\sqrt{\frac{2E_b}{\mathcal{N}_o}}\right). \tag{2.13}$$

If we employ error control coding as depicted in Fig. 2.4, the performance of the over all coded MSK system with respect to the source symbols $\{a_n\}$ will depend on the type of decoding (*hard-decision* or *soft-decision* decoding) used at the decoder for the code $\mathbf{W}$. If hard-decision decoding is employed at the receiver (see Fig. 2.7.*b*) then the sampled output of the matched filter is first detected using a slicer and then passed to the decoder for the code $\mathbf{W}$. If convolutional code is applied at the channel encoder, then the bit error probability $\mathcal{P}_b$ can be upper bounded by [34, p. 490]

$$\mathcal{P}_b < \frac{1}{k} \sum_{d=H_{\text{free}}^W}^{\infty} \beta_d \left[4\mathcal{P}_e(1-\mathcal{P}_e)\right]^{d/2}, \tag{2.14}$$

where H_{free}^W is the free (minimum) Hamming distance of the convolutional code $\mathbf{W}$, β_d is a constant that depends on the properties of the code $\mathbf{W}$, and $\mathcal{P}_e = Q(\sqrt{2R_c E_b/\mathcal{N}_o})$. Although hard-decision decoding is simple to implement compared to soft-decision, it is not optimum in the sense of minimizing the bit error probability $\mathcal{P}_b$.

If we consider the optimum decoding for coded MSK signals (see Fig. 2.7.*c*), then the

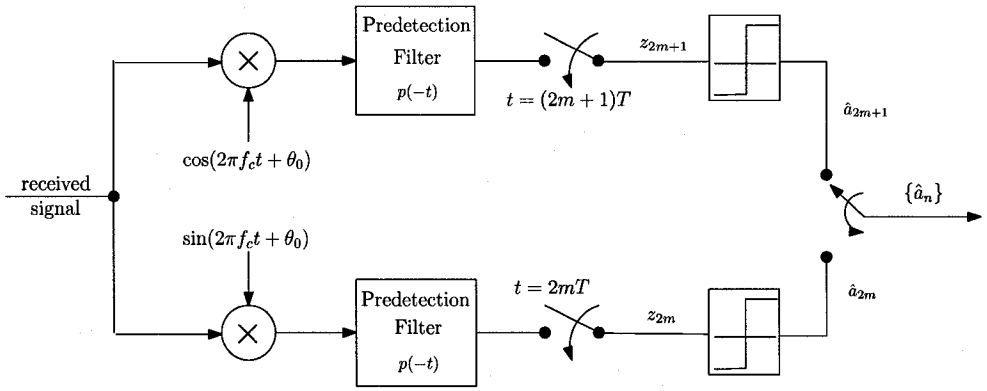

a. Optimum *I-Q* receiver for uncoded MSK.

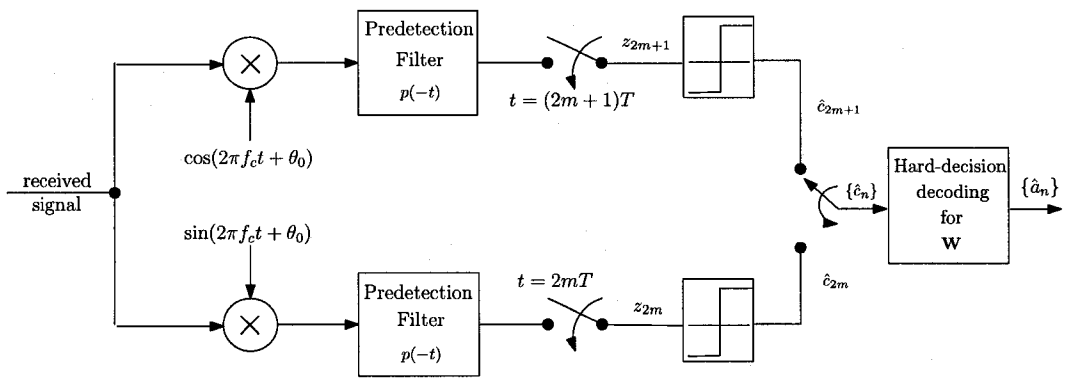

b. Sub-optimum receiver for coded MSK employing hard-decision decoding.

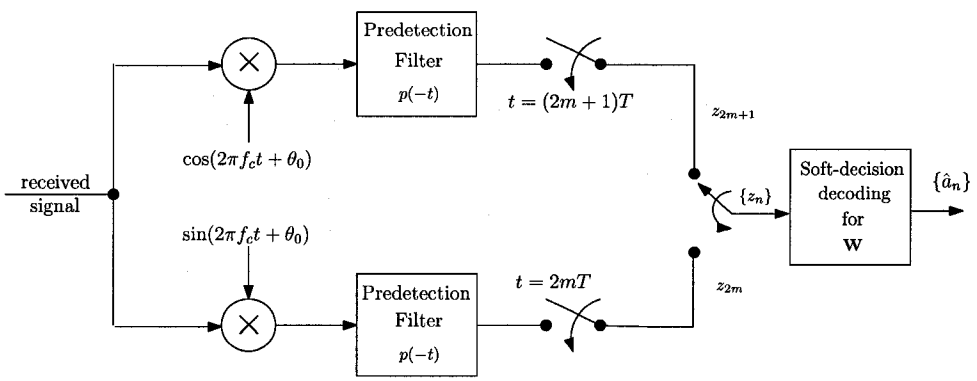

c. Optimum receiver for coded MSK employing soft-decision decoding.

Fig. 2.7: *I-Q* receivers for uncoded and coded MSK signals

output of the I-Q demodulator (i.e., $\{z_n\}$) is passed directly to the soft-decision decoder. If the channel encoder is a convolutional encoder, then the performance of the decoder (employing Viterbi algorithm), i.e., the bit error probability $\mathcal{P}_b$ is upper bounded by [34, p. 488]

$$\mathcal{P}_b < \frac{1}{k} \sum_{d=H_{\text{free}}^W}^{\infty} \beta_d \, Q\left(\sqrt{2R_c d \frac{E_b}{\mathcal{N}_o}}\right). \tag{2.15}$$

The symbol-by-symbol detection described above for the case of MSK (see Fig. 2.7.a) is not the optimum detection scheme for other generalized MSK signals due to the memory inherent in the received signal. This requires the use of MLSE receiver for optimum detection usually implemented using the Viterbi Algorithm (VA) [27]. This optimum receiver is quite complex in the sense that the number of filters and number of states in VA can be quite large and the computational efforts required per symbol is equally large. However, generalized MSK signals can still be demodulated, suboptimally, using the I-Q receiver similar to that depicted in Fig. 2.7.a (the predetection filter may change). It was shown [8] that the impulse response of the optimum filter is matched to a linear combination of all possible signals at its input and depends on the noise level (SNR) at the input of the filter. The filter design problem can be simplified by considering the two asymptotic situations, the extremely low and extremely high SNR leading to the solutions of the "Averaged Matched Filter" (AMF) and "Asymptotically Optimal Filter" (AOF).

The problem of demodulating generalized MSK signals using such near-optimal filter, is the difficulty in the evaluation of the performance of the I-Q receiver. This is because, these filters are constructed based on numerical approach and no exact representation is given for such filters. Another important issue is that these filters have an impulse duration greater than $2T$ which causes intersymbol interference (ISI) in the sampled output of the matched filter. Moreover, in AWGN channel, the noise samples are correlated and thus post equalization is required. As such, the upper bounds of the bit error probability derived for coded MSK (for hard and soft decision decoding) given in (2.14) and (2.15)

are not valid anymore for other coded generalized MSK signals detected using the I-Q receiver.

Using the analysis developed by Laurent [7] (discussed in Chapter 3) to express any CPM signal as superposition of PAM signals, an optimum Viterbi receiver in AWGN channel can be implemented as shown in Fig. 2.8. The performance of such optimum receiver (i.e., the bit error probability) can be upper bounded by [43]

$$\mathcal{P}_b \leq \sum_{d=d_{\min}}^{\infty} C_d \, Q\left(\sqrt{d^2 \frac{E_b}{N_o}}\right),$$

where C_d is a constant that depends on the combined coded-modulation trellis structure. Again, the difficulty that arises here is that no analytical expression is found for the Euclidean distance and computer search and evaluation is required.

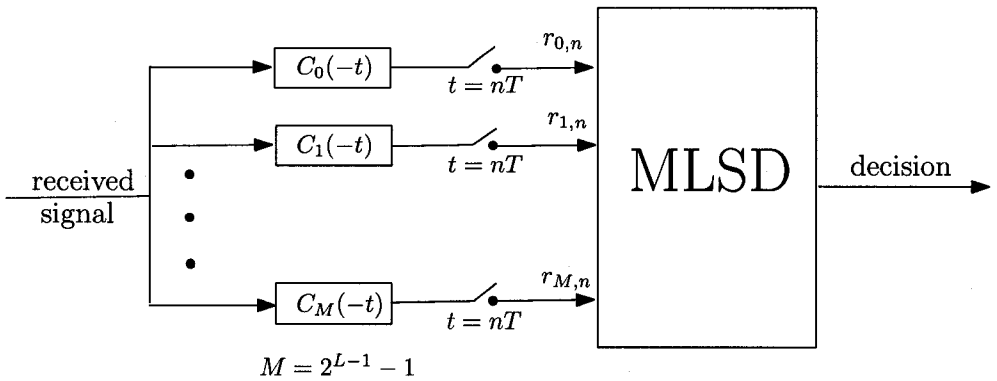

Fig. 2.8: Optimum CPM receiver based on Laurent representation in AWGN channel

Different approaches have been followed after the work proposed by Laurent, in order to reduce the complexity of the optimum receiver. The reduction in complexity was based on reducing the number of matched filters and/or reducing the number of trellis states in the Viterbi algorithm [28]–[30]. These different techniques lead to reduced complexity detectors with near optimum performance. The reduction in the optimum receiver complexity is achieved by truncating the main PAM components of the CPM signal, which contains most of the signal energy. However, the output of the matched

filters contains ISI and the noise samples are correlated. This causes a degradation in performance and post equalization such as decision-feedback equalization is required to reduce the effect of the ISI. This post processing requires additional computational load and makes the receiver structure more complex.

In this thesis we will show (Chapter 4) that by applying repetition coding prior to modulation, a simple I-Q receiver, depicted in Fig. 2.9, can be constructed to optimally demodulate generalized MSK signals. A significant result is that (as shown in Fig. 2.9) no post equalization is required at the receiver, since the matched filter applied to the received signal is shown to produce zero-ISI at the output and the noise samples, in AWGN channel, are independent. Therefore, *symbol-by-symbol* detection can be applied to optimally detect the coded symbols (output of demodulator). A result, the detection problem is simplified, just as in the linear memoryless modulation case (e.g., binary phase-shift keying (BPSK) and QPSK).

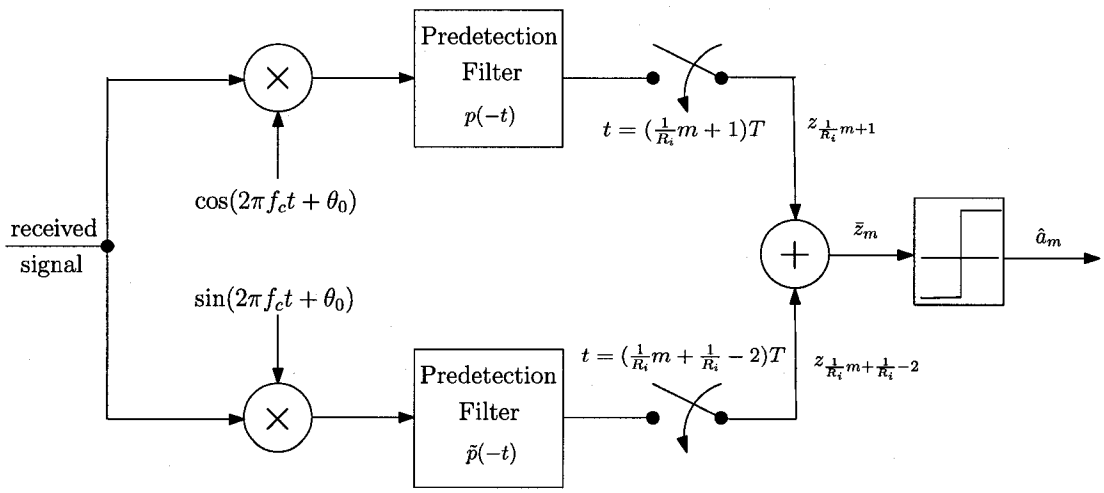

Fig. 2.9: Structure of proposed optimum matched filter receiver used for demodulating coded generalized MSK with pulse shape duration $2T$ and $3T$ employing double and quadruple repetition code respectively, in AWGN channel. R_i is the rate of the repetition code.

Chapter 3

Laurent Decomposition of Generalized MSK

3.1 Introduction

Fig. 3.1 shows a block diagram for a coded generalized MSK system employing precoding.

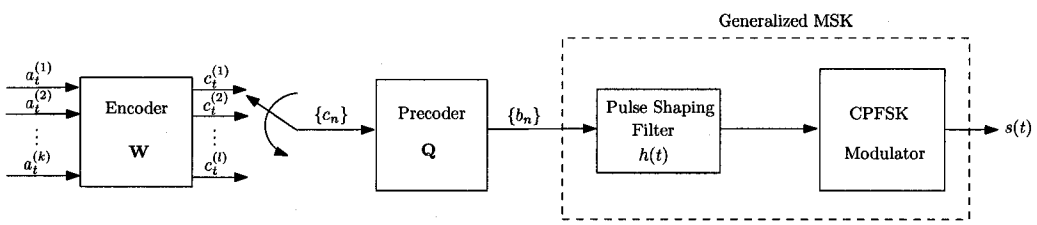

Fig. 3.1: Coded Generalized MSK system using premodulation pulse shaping filter $h(t)$.

Following the development given by Laurent [7], binary CPM signals may be represented by a linear superposition of a finite number of amplitude-modulated pulse trains (PAM). We will only consider such decomposition for generalized MSK signals with modulation memory $L = 2$ and $L = 3$ (i.e., with $h(t)$ of length $2T$ and $3T$). It will be shown (Chapter 4) that such decomposition helps to simplify the optimum receiver design problem. It will be demonstrated that for any generalized MSK, using the precoder $\mathbf{Q}$ (see

Fig. 3.1) discussed in Chapter 2, the transmitted signal $s(t)$ will be proportional to the coded symbols $\{c_n\}$ carried by the first Laurent pulse train which may simplify the code design problem.

The lowpass equivalent of generalized MSK signal with respect to the carrier frequency f_c is (assuming $f_cT \gg 1$)

$$s_l(t) = \sqrt{\frac{2E}{T}} e^{j\phi(t)}, \tag{3.1}$$

where the excess-phase $\phi(t)$ is still given by (2.2), $b_m \in \{-1, 1\}$, and the pulse $h(t)$ is zero outside the interval $t \in [0, LT]$ with

$$\int_0^{LT} h(t)\, dt = T. \tag{3.2}$$

The PAM representation of $s_l(t)$ from [7] is

$$s_l(t) = \sqrt{\frac{2E}{T}} \sum_{k=0}^{2^{L-1}-1} \sum_{n=-\infty}^{\infty} \beta_{k,n} C_k(t - nT), \tag{3.3}$$

where $\beta_{k,n}$ is given by

$$\beta_{k,n} = e^{j\frac{\pi}{2}A_{k,n}}, \tag{3.4}$$

in which

$$A_{k,n} = \sum_{i=0}^{n} b_i - \sum_{m=1}^{L-1} b_{n-m}\alpha_{k,m}, \tag{3.5}$$

and b_n satisfies (2.6); $C_k(t)$ is the Laurent pulse given by

$$C_k(t) = \begin{cases} S(t) \prod_{m=1}^{L-1} S[t + (m + L\alpha_{k,m})T], & 0 \le t \le T \cdot \min_{m=1}^{L-1}\{L(2 - \alpha_{k,m}) - m\}; \\ 0, & \text{otherwise}, \end{cases} \tag{3.6}$$

where the $\alpha_{k,n} \in \{0, 1\}$ are obtained from $L-1$ bit binary representation of the index k, i.e.,

$$k = \sum_{m=1}^{L-1} 2^{m-1}\alpha_{k,m} \qquad 0 \le k \le 2^{L-1} - 1, \quad \alpha_{k,n} \in \{0, 1\}, \tag{3.7}$$

and $S(t)$ has the following form

$$S(t) = \begin{cases} \sin\left(\frac{\pi}{2T}\int_0^t h(\tau)d\tau\right), & t \in [0, LT]; \\ \cos\left(\frac{\pi}{2T}\int_0^{t-LT} h(\tau)d\tau\right), & t \in [LT, 2LT]; \\ 0, & \text{otherwise}. \end{cases} \tag{3.8}$$

Let us consider the simple example of representing precoded CPFSK-MSK signal, generated by the system shown in Fig. 2.4, as a PAM signal using the analysis given in the previous section. MSK signal is considered binary full response CPM (i.e., $L = 1$) where $h(t)$ is a rectangular pulse with duration T. The pulse $S(t)$ can be expressed as

$$S(t) = \begin{cases} \sin(\frac{\pi t}{2T}), & t \in [0, 2T]; \\ 0, & \text{otherwise.} \end{cases} \tag{3.9}$$

The index k is equal to $\alpha_{0,0}$, therefore $k = 0$. Hence, there is only one Laurent pulse, $C_0(t) = S(t)$, that entirely represents MSK as a PAM signal. The baseband signal $s_l(t)$ can then be expressed as

$$s_l(t) = \sum_{n=-\infty}^{\infty} \beta_{0,n} C_0(t - nT). \tag{3.10}$$

From (3.4), $\beta_{k,n}$ is generally a non-linear function of the coded sequence $\{c_n\}$. However, for $k = 0$

$$\beta_{0,n} = e^{j\left(\frac{\pi}{2}\phi_n + \frac{\pi}{2}b_n\right)}, \tag{3.11}$$

where $\phi_n = \sum_{i=0}^{n-1} b_i$. By taking the real and imaginary parts of $\beta_{0,n}$, both parts happen to be a linear function of the odd and even symbols of $\{c_n\}$ respectively as shown below:

$$\begin{aligned} \Re\{\beta_{0,n}\} &= \cos(\phi_n) \underbrace{\cos(\frac{\pi}{2}b_n)}_{=0} - \sin(\phi_n) \underbrace{\sin(\frac{\pi}{2}b_n)}_{=b_n} \\ &= \begin{cases} -b_n \sin(\phi_n) = c_n, & \text{for } n \text{ odd } (\phi_n = \pm\frac{\pi}{2}); \\ 0, & \text{for } n \text{ even } (\phi_n = 0, \pi), \end{cases} \end{aligned} \tag{3.12}$$

and

$$\begin{aligned} \Im\{\beta_{0,n}\} &= \cos(\phi_n) \underbrace{\sin(\frac{\pi}{2}b_n)}_{=b_n} + \sin(\phi_n) \underbrace{\cos(\frac{\pi}{2}b_n)}_{=0} \\ &= \begin{cases} b_n \cos(\phi_n) = -c_n, & \text{for } n \text{ even;} \\ 0, & \text{for } n \text{ odd.} \end{cases} \end{aligned} \tag{3.13}$$

A detailed proof of this result is given in [8, Appendix A].

The actual transmitted precoded MSK signal can then be expressed as

$$s(t) = \Re\{s_l(t) e^{j(2\pi f_c t + \theta_0)}\}$$

$$= \sqrt{\frac{2E}{T}}\left[\sum_{n\ \text{odd}} c_n C_0(t-nT)\right]\cos(2\pi f_c t+\theta_0)$$
$$+\sqrt{\frac{2E}{T}}\left[\sum_{n\ \text{even}} c_n C_0(t-nT)\right]\sin(2\pi f_c t+\theta_0). \tag{3.14}$$

where $\{..., c_{-1}, c_0, c_1, ...\}$ ($c_n \in \{-1, 1\}$) is equivalent to the output binary stream generated by encoder **W** shown in Fig. 2.4. It can be easily verified that (3.14) is equivalent to the equation given in (2.4) where $C_0(t) = p(t)$.

3.2 PAM representation of Generalized MSK with Pulse Shape of Length $2T$

We would like to consider in this section the PAM representation of a subclass of generalized MSK signals with pulse shape $h(t)$ of duration $2T$ (i.e., $L = 2$). In this case, the baseband signal $s_l(t)$ can be expressed as the sum of two simple PAM signals given by

$$s_l(t) = \sqrt{\frac{2E}{T}}\left[\sum_{n=-\infty}^{\infty}\beta_{0,n}C_0(t-nT) + \sum_{n=-\infty}^{\infty}\beta_{1,n}C_1(t-nT)\right], \tag{3.15}$$

where the Laurent pulses, $C_0(t)$ and $C_1(t)$, are given respectively by

$$C_0(t) = \begin{cases} S(t)S(t+T), & 0 \le t \le 3T; \\ 0, & \text{otherwise.} \end{cases} \tag{3.16}$$

$$C_1(t) = \begin{cases} S(t)S(t+3T), & 0 \le t \le T; \\ 0, & \text{otherwise.} \end{cases} \tag{3.17}$$

The Laurent coefficient $\beta_{0,n}$ has been already derived in the previous section. Noting that $\alpha_{1,1} = 1$ and $A_{1,n} = A_{0,n} - b_{n-1}$, the other coefficient $\beta_{1,n}$ can be expressed as

$$\beta_{1,n} = e^{j\frac{\pi}{2}A_{1,n}} = \underbrace{e^{j\frac{\pi}{2}A_{0,n}}}_{\beta_{0,n}} e^{-j\frac{\pi}{2}b_{n-1}} = \beta_{0,n}e^{-j\frac{\pi}{2}b_{n-1}}. \tag{3.18}$$

The inphase and quadrature channel signals, $I(t)$ and $Q(t)$, for any generalized MSK with modulation memory $L = 2$ can be expressed as

$$I(t) = \sqrt{\frac{2E}{T}}\cos\phi(t)$$

$$= \sqrt{\frac{2E}{T}}\left[\sum_{n=-\infty}^{\infty}\Re\{\beta_{0,n}\}C_0(t-nT)+\sum_{n=-\infty}^{\infty}\Re\{\beta_{1,n}\}C_1(t-nT)\right], \quad (3.19)$$

and

$$\begin{aligned} Q(t) &= \sqrt{\frac{2E}{T}}\sin\phi(t) \\ &= \sqrt{\frac{2E}{T}}\left[\sum_{n=-\infty}^{\infty}\Im\{\beta_{0,n}\}C_0(t-nT)+\sum_{n=-\infty}^{\infty}\Im\{\beta_{1,n}\}C_1(t-nT)\right]. \end{aligned} \quad (3.20)$$

The real and imaginary parts of $\beta_{1,n}$ can be derived in a similar manner as for $\beta_{0,n}$. The real part of $\beta_{1,n}$ can be expressed as

$$\begin{aligned} \Re\{\beta_{1,n}\} &= \Re\{\beta_{0,n}e^{-j\frac{\pi}{2}b_{n-1}}\} \\ &= \Re\{\beta_{0,n}\}\underbrace{\cos(-\frac{\pi}{2}b_{n-1})}_{=0} - \Im\{\beta_{0,n}\}\underbrace{\sin(-\frac{\pi}{2}b_{n-1})}_{=-b_{n-1}} \\ &= \begin{cases} -b_{n-1}c_n, & n \text{ even;} \\ 0, & \text{otherwise,} \end{cases} \end{aligned} \quad (3.21)$$

while the imaginary part of $\beta_{1,n}$ can be expressed as

$$\begin{aligned} \Im\{\beta_{1,n}\} &= \Im\{\beta_{0,n}e^{-j\frac{\pi}{2}b_{n-1}}\} \\ &= \Re\{\beta_{0,n}\}\underbrace{\sin(-\frac{\pi}{2}b_{n-1})}_{=-b_{n-1}} + \Im\{\beta_{0,n}\}\underbrace{\cos(-\frac{\pi}{2}b_{n-1})}_{=0} \\ &= \begin{cases} -b_{n-1}c_n, & n \text{ odd;} \\ 0, & \text{otherwise.} \end{cases} \end{aligned} \quad (3.22)$$

Therefore, the expressions given in (3.19) and (3.20) can be rewritten as

$$I(t) = \sqrt{\frac{2E}{T}}\left[\sum_{n \text{ odd}} c_nC_0(t-nT)+\sum_{n \text{ even}} v_nC_1(t-nT)\right], \quad (3.23)$$

$$Q(t) = \sqrt{\frac{2E}{T}}\left[-\sum_{n \text{ even}} c_nC_0(t-nT)+\sum_{n \text{ odd}} v_nC_1(t-nT)\right], \quad (3.24)$$

where $\{v_n\}$ is a binary symbol stream ($v_n \in \{-1,1\}$) that satisfies the following equation

$$v_n = -b_{n-1}c_n = (-1)^{n+1}c_nc_{n-1}c_{n-2}. \quad (3.25)$$

We can see that the non-linearity inherent in this type of signals is embodied in the symbol sequence $\{v_n\}$. It will be shown later in this thesis that by appropriately encoding the information symbols this non-linearity may be removed.

3.2.1 PAM representation of Generalized MSK with first degree correlative coding

Consider now the more specific case of generalized MSK using correlative coding with first degree coding polynomial given by $(k_0 + k_1 D)$, where k_0 and k_1 are real numbers, and a rectangular pulse shape $g(t)$ of duration T (Fig. 2.6). For such signals, the pulse shaping filter $h(t)$ has the following expression

$$h(t) = \begin{cases} k_0, & 0 \leq t < T; \\ k_1, & T \leq t < 2T; \\ 0, & \text{otherwise}, \end{cases} \tag{3.26}$$

where $k_0 + k_1 = 1$. Fig. 3.2 shows a plot for the pulse shape $h(t)$ given in (3.26).

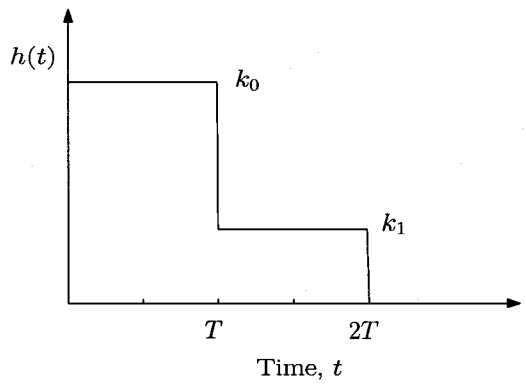

Fig. 3.2: A pulse $h(t)$ given in (3.26) used to preshape the input symbols prior modulation for $L = 2$ generalized MSK signals.

Evaluating (3.8) for this case, we find $S(t)$ can be expressed as

$$S(t) = \begin{cases} \sin(\frac{k_0 \pi t}{2T}), & 0 \leq t < T; \\ \sin(\frac{k_1 \pi t}{2T} + [k_0 - k_1]\frac{\pi}{2}), & T \leq t < 2T; \\ \cos(\frac{k_0 \pi t}{2T} - k_0 \pi), & 2T \leq t < 3T; \\ \cos(\frac{k_1 \pi t}{2T} + [k_0 - 3k_1]\frac{\pi}{2}), & 3T \leq t < 4T; \\ 0, & \text{otherwise}. \end{cases} \tag{3.27}$$

The Laurent pulses $C_0(t)$ and $C_1(t)$ can then be found using (3.16) and (3.17) respectively. A plot of these two pulses are shown in Fig. 3.3 for $k_0 = 1/2$ (the case for Duobinary

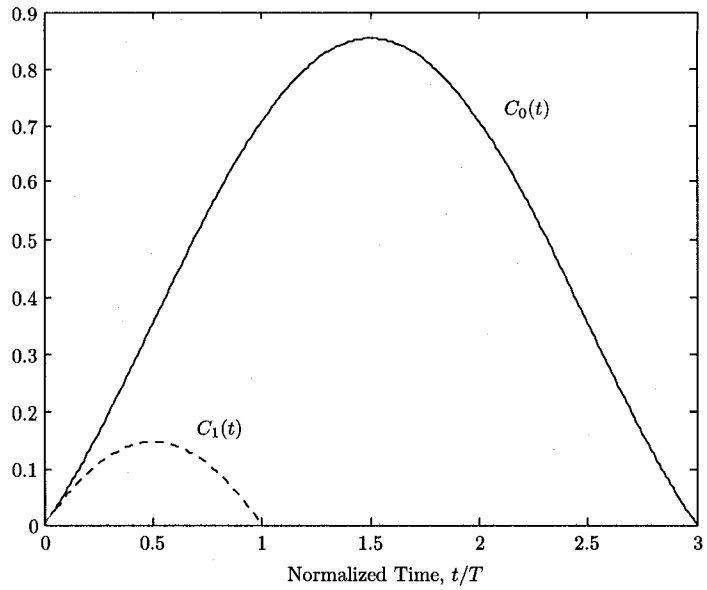

(a)

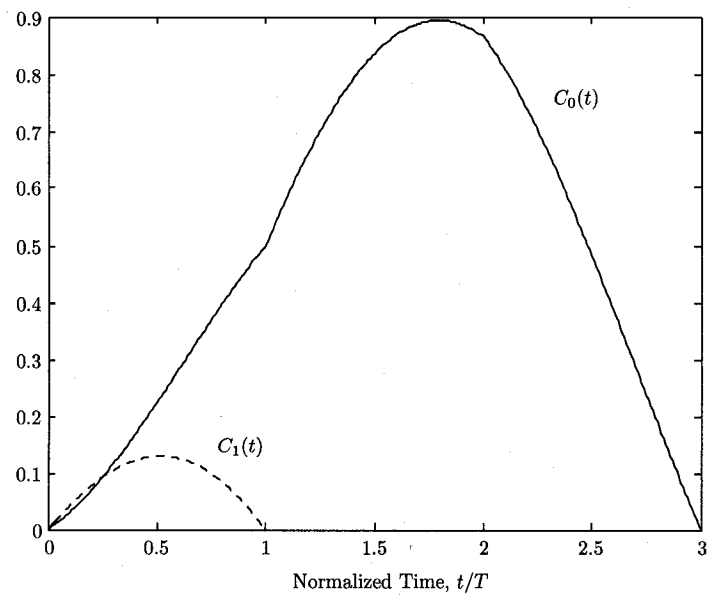

(b)

Fig. 3.3: Laurent pulses $C_k(t)$ for generalized MSK with $h(t)$ given in (3.26). (*a*) $k_0 = 1/2$ (Duobinary MSK), (*b*) $k_0 = 1/3$.

MSK) and $k_0 = 1/3$. As in these examples, the Laurent pulse $C_0(t)$ usually contains most of the energy in the transmitted signal $s(t)$. Therefore, generalized MSK signals with modulation memory $L = 2$ usually can be well-approximated by the Laurent pulse train with the pulse shape $C_0(t)$.

3.3 PAM representation of Generalized MSK with Pulse Shape of Length $3T$

Consider now expressing precoded generalized MSK signals that are generated using a pulse shape $h(t)$ of duration $3T$. The baseband signal for such generalized MSK signal is represented by the sum of four PAM signals given by

$$s_l(t) = \sqrt{\frac{2E}{T}} \sum_{k=0}^{3} \sum_{n=-\infty}^{\infty} \beta_{k,n} C_k(t - nT). \tag{3.28}$$

The four Laurent pulses are given by

$$C_0(t) = \begin{cases} S(t)S(t+T)S(t+2T), & 0 \le t \le 4T; \\ 0, & \text{otherwise;} \end{cases} \tag{3.29}$$

$$C_1(t) = \begin{cases} S(t)S(t+2T)S(t+4T), & 0 \le t \le 2T; \\ 0, & \text{otherwise;} \end{cases} \tag{3.30}$$

$$C_2(t) = \begin{cases} S(t)S(t+T)S(t+5T), & 0 \le t \le T; \\ 0, & \text{otherwise;} \end{cases} \tag{3.31}$$

$$C_3(t) = \begin{cases} S(t)S(t+4T)S(t+5T), & 0 \le t \le T; \\ 0, & \text{otherwise;} \end{cases} \tag{3.32}$$

where the pulse $S(t)$ is given by

$$S(t) = \begin{cases} \sin\left(\frac{\pi}{2T} \int_0^t h(\tau)d\tau\right), & t \in [0, 3T]; \\ \cos\left(\frac{\pi}{2T} \int_0^{t-3T} h(\tau)d\tau\right), & t \in [3T, 6T]; \\ 0, & \text{otherwise.} \end{cases} \tag{3.33}$$

The Laurent coefficients $\beta_{k,n}$ are given by

$$\begin{aligned}\beta_{k,n} = e^{j\frac{\pi}{2}A_{k,n}} &= e^{j\frac{\pi}{2}\left[\sum_{i=0}^{n} b_i - \left(b_{n-1}\alpha_{k,1}+b_{n-2}\alpha_{k,2}\right)\right]}, \\ &= e^{j\frac{\pi}{2}\left[A_{0,n}-\left(b_{n-1}\alpha_{k,1}+b_{n-2}\alpha_{k,2}\right)\right]}, \\ &= \beta_{0,n}e^{-j\frac{\pi}{2}\left(b_{n-1}\alpha_{k,1}+b_{n-2}\alpha_{k,2}\right)}, \end{aligned} \tag{3.34}$$

where Table 3.1 gives the relationship between the index k and the values of $\alpha_{k,1}$ and $\alpha_{k,2}$.

Table 3.1: Index $k = \alpha_{k,1} + 2\alpha_{k,2}$.

k	$\alpha_{k,1}$	$\alpha_{k,2}$
0	0	0
1	1	0
2	0	1
3	1	1

We would like now to find the real and imaginary parts for each Laurent coefficient. The real and imaginary parts of $\beta_{0,n}$ and $\beta_{1,n}$ have been derived previously in (3.12), (3.13), (3.21) and (3.22), leaving only the $\beta_{2,n}$ and $\beta_{3,n}$ terms. The real part of $\beta_{2,n}$ is given by

$$\begin{aligned}\Re\{\beta_{2,n}\} &= \Re\{\beta_{0,n}e^{-j\frac{\pi}{2}b_{n-2}}\} \\ &= \Re\{\beta_{0,n}\}\underbrace{\cos(-\frac{\pi}{2}b_{n-2})}_{=0} - \Im\{\beta_{0,n}\}\underbrace{\sin(-\frac{\pi}{2}b_{n-2})}_{=-b_{n-2}} \\ &= \begin{cases} -b_{n-2}c_n, & n \text{ even}; \\ 0, & \text{otherwise}, \end{cases} \end{aligned} \tag{3.35}$$

while the imaginary part of $\beta_{2,n}$ can be expressed as

$$\begin{aligned}\Im\{\beta_{2,n}\} &= \Im\{\beta_{0,n}e^{-j\frac{\pi}{2}b_{n-2}}\} \\ &= \Re\{\beta_{0,n}\}\underbrace{\sin(-\frac{\pi}{2}b_{n-2})}_{=-b_{n-2}} + \Im\{\beta_{0,n}\}\underbrace{\cos(-\frac{\pi}{2}b_{n-2})}_{=0}\end{aligned}$$

$$= \begin{cases} -b_{n-2}c_n, & n \text{ odd}; \\ 0, & \text{otherwise}. \end{cases} \tag{3.36}$$

The real part of $\beta_{3,n}$ is given by

$$\begin{aligned} \Re\{\beta_{3,n}\} &= \Re\{\beta_{0,n}e^{-j\frac{\pi}{2}(b_{n-1}+b_{n-2})}\} \\ &= \Re\{\beta_{0,n}\}\underbrace{\cos(-\frac{\pi}{2}[b_{n-1}+b_{n-2}])}_{=-b_{n-1}b_{n-2}} - \Im\{\beta_{0,n}\}\underbrace{\sin(-\frac{\pi}{2}[b_{n-1}+b_{n-2}])}_{=0} \\ &= \begin{cases} -b_{n-1}b_{n-2}c_n, & n \text{ odd}; \\ 0, & \text{otherwise}, \end{cases} \end{aligned} \tag{3.37}$$

while the imaginary part of $\beta_{3,n}$ can be expressed as

$$\begin{aligned} \Im\{\beta_{3,n}\} &= \Im\{\beta_{0,n}e^{-j\frac{\pi}{2}(b_{n-1}+b_{n-2})}\} \\ &= \Re\{\beta_{0,n}\}\underbrace{\sin(-\frac{\pi}{2}[b_{n-1}+b_{n-2}])}_{=0} + \Im\{\beta_{0,n}\}\underbrace{\cos(-\frac{\pi}{2}[b_{n-1}+b_{n-2}])}_{=-b_{n-1}b_{n-2}} \\ &= \begin{cases} b_{n-1}b_{n-2}c_n, & n \text{ even}; \\ 0, & \text{otherwise}. \end{cases} \end{aligned} \tag{3.38}$$

Therefore, the inphase and quadrature channel signals can be expressed as

$$\begin{aligned} I(t) = \sqrt{\frac{2E}{T}}\Big\{ &\sum_{n \text{ odd}} c_n C_0(t-nT) + \sum_{n \text{ even}} v_n C_1(t-nT) \\ &+ \sum_{n \text{ even}} x_n C_2(t-nT) + \sum_{n \text{ odd}} y_n C_3(t-nT)\Big\}, \end{aligned} \tag{3.39}$$

$$\begin{aligned} Q(t) = \sqrt{\frac{2E}{T}}\Big\{ &-\sum_{n \text{ even}} c_n C_0(t-nT) + \sum_{n \text{ odd}} v_n C_1(t-nT) \\ &+ \sum_{n \text{ odd}} x_n C_2(t-nT) - \sum_{n \text{ even}} y_n C_3(t-nT)\Big\}, \end{aligned} \tag{3.40}$$

where v_n is given by (3.25), $\{x_n\}$ and $\{y_n\}$ are binary symbol streams ($x_n, y_n \in \{-1, 1\}$) that satisfy the following equations

$$x_n = -b_{n-2}c_n = (-1)^n c_n c_{n-2} c_{n-3}, \tag{3.41}$$

$$y_n = -b_{n-1}b_{n-2}c_n = c_n c_{n-1} c_{n-3}. \tag{3.42}$$

3.3.1 PAM representation of Generalized MSK with second degree Correlative Coding

We will consider now the exact analysis of decomposing correlatively coded generalized MSK generated by a coding polynomial given by $(k_0 + k_1 D + k_2 D^2)$, where k_0, k_1 and k_2 are real numbers, with a rectangular pulse shape $g(t)$ of duration T. For such signals, the pulse shape $h(t)$ has the following expression

$$h(t) = \begin{cases} k_0, & 0 \leq t < T; \\ k_1, & T \leq t < 2T; \\ k_2, & 2T \leq t < 3T; \\ 0, & \text{otherwise}, \end{cases} \tag{3.43}$$

where $k_0 + k_1 + k_2 = 1$. Fig. 3.4 shows a plot for the pulse $h(t)$.

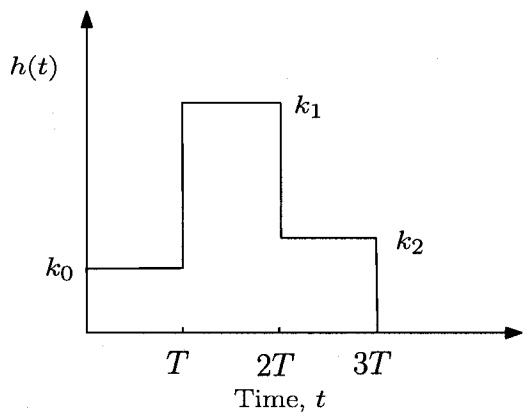

Fig. 3.4: A pulse $h(t)$ given in (3.43) used to preshape the input symbols prior modulation for $L = 3$ generalized MSK signals.

By evaluating the integrals that are given in (3.8), for each sub-interval of length T, for generalized MSK signals with pulse shape $h(t)$ given in (3.43), $S(t)$ can be expressed

as

$$S(t) = \begin{cases} \sin(\frac{k_0\pi t}{2T}), & 0 \le t < T; \\ \sin(\frac{k_1\pi t}{2T} + [k_0 - k_1]\frac{\pi}{2}), & T \le t < 2T; \\ \sin(\frac{k_2\pi t}{2T} + [k_0 + k_1 - 2k_2]), & 2T \le t < 3T; \\ \cos(\frac{k_0\pi t}{2T} - \frac{3\pi}{2}k_0), & 3T \le t < 4T; \\ \cos(\frac{k_1\pi t}{2T} + [k_0 - 4k_1]\frac{\pi}{2}), & 4T \le t < 5T; \\ \cos(\frac{k_2\pi t}{2T} + [k_0 + k_1 - 5k_2]\frac{\pi}{2}), & 5T \le t < 6T; \\ 0, & \text{otherwise.} \end{cases} \tag{3.44}$$

The Laurent pulses $C_0(t)$, $C_1(t)$, $C_2(t)$ and $C_3(t)$ can be found using (3.29), (3.30), (3.31) and (3.32) respectively. A plot of these pulses is shown in Fig. 3.5 for $k_1 = 1/2$ and $k_0 = k_2 = 1/4$ (the case for TFM), and $k_0 = k_1 = k_2 = 1/3$. As in these cases, usually the energy of $C_0(t)$ is significantly more than the energy of $C_1(t)$, which is significantly more than the energy of $C_2(t)$ and that of $C_3(t)$. Thus such generalized MSK signals can usually be well-approximated by the superposition of the pulse trains for $C_0(t)$ and $C_1(t)$—or indeed by the single PAM signal involving $C_0(t)$.

3.4 The Squared Euclidean Distance

In this section we will consider the derivation of the exact expression for squared Euclidean distance between different generalized MSK signals with modulation memory of $L = 2$ and $L = 3$. It is to be expected that the Euclidean distance depends on the shape of the $h(t)$ [22].

The normalized squared Euclidean distance (**NSED**) between any two (coded) generalized MSK signals, say $s_i(t)$ and $s_j(t)$, for $t \ge 0$ is defined by

$$\mathbf{NSED}(i,j) \triangleq \frac{1}{2E_b}\|s_i(t) - s_j(t)\|^2 = \frac{1}{2E_b}\int_0^\infty |s_i(t) - s_j(t)|^2\, dt. \tag{3.45}$$

It can be shown that, assuming $f_cT \gg 1$, the expression given in (3.45) can be

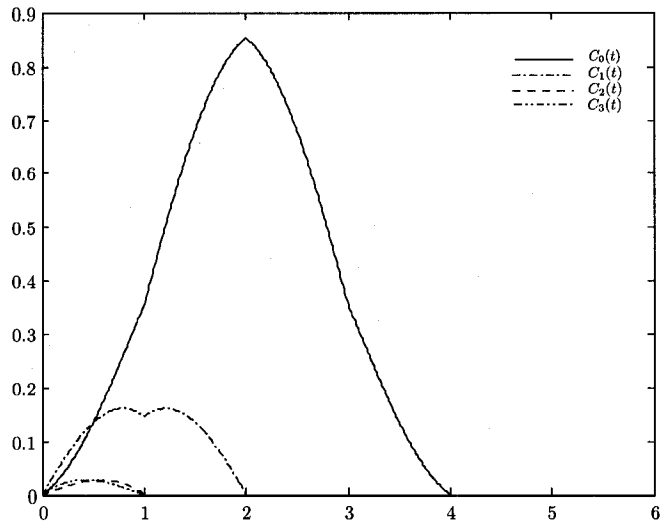

(a)

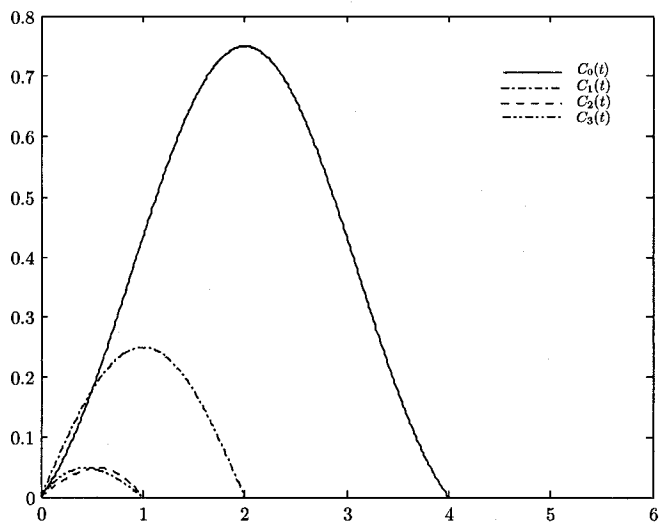

(b)

Fig. 3.5: Laurent pulses $C_k(t)$ for generalized MSK with $h(t)$ given in (3.43). (a) $k_0 = k_2 = 1/4$, $k_1 = 1/2$ (TFM). (b) $k_0 = k_1 = k_2 = 1/3$.

expressed as

$$\mathbf{NSED}(i,j) = \frac{R_c}{2}\left\{\frac{1}{T}\int_0^{\infty}\left[\cos\phi_i(t)-\cos\phi_j(t)\right]^2 dt + \frac{1}{T}\int_0^{\infty}\left[\sin\phi_i(t)-\sin\phi_j(t)\right]^2 dt\right\}, \tag{3.46}$$

where R_c is the rate of channel encoder $\mathbf{W}$

Let $I_{i,j}$ and $Q_{i,j}$ be equal to the following

$$I_{i,j} = \frac{1}{T}\int_0^{\infty}\left[\cos\phi_i(t)-\cos\phi_j(t)\right]^2\ dt, \tag{3.47}$$

$$Q_{i,j} = \frac{1}{T}\int_0^{\infty}\left[\sin\phi_i(t)-\sin\phi_j(t)\right]^2\ dt. \tag{3.48}$$

Using (3.23) and (3.24) we find that for generalized MSK with modulation memory $L=2$, (3.47) and (3.48) can be expressed as

$$\begin{aligned} I_{i,j} &= \sum_{n\text{ odd}}\sum_{m\text{ odd}}\left[c_n^i-c_n^j\right]\left[c_m^i-c_m^j\right]\frac{1}{T}\int_0^{\infty}C_0(t-nT)C_0(t-mT)\,dt \\ &+\sum_{n\text{ even}}\sum_{m\text{ even}}\left[v_n^i-v_n^j\right]\left[v_m^i-v_m^j\right]\frac{1}{T}\int_0^{\infty}C_1(t-nT)C_1(t-mT)\,dt \\ &+2\sum_{n\text{ odd}}\sum_{m\text{ even}}\left[c_n^i-c_n^j\right]\left[v_m^i-v_m^j\right]\frac{1}{T}\int_0^{\infty}C_0(t-nT)C_1(t-mT)\,dt, \end{aligned} \tag{3.49}$$

and

$$\begin{aligned} Q_{i,j} &= \sum_{n\text{ even}}\sum_{m\text{ even}}\left[c_n^i-c_n^j\right]\left[c_m^i-c_m^j\right]\frac{1}{T}\int_0^{\infty}C_0(t-nT)C_0(t-mT)\,dt \\ &+\sum_{n\text{ odd}}\sum_{m\text{ odd}}\left[v_n^i-v_n^j\right]\left[v_m^i-v_m^j\right]\frac{1}{T}\int_0^{\infty}C_1(t-nT)C_1(t-mT)\,dt \\ &-2\sum_{n\text{ even}}\sum_{m\text{ odd}}\left[c_n^i-c_n^j\right]\left[v_m^i-v_m^j\right]\frac{1}{T}\int_0^{\infty}C_0(t-nT)C_1(t-mT)\,dt, \end{aligned} \tag{3.50}$$

where we have that,

$$\int_0^{\infty}C_0(t-nT)C_0(t-mT)\,dt = \begin{cases} \|C_0(t)\|^2, & n=m; \\ \langle C_0(t), C_0(t+2T)\rangle, & |n-m|=2; \\ 0, & \text{otherwise}; \end{cases} \tag{3.51}$$

$$\int_0^\infty C_1(t-nT)C_1(t-mT)\,dt = \begin{cases} \|C_1(t)\|^2, & n=m; \\ 0, & \text{otherwise;} \end{cases} \tag{3.52}$$

$$\int_0^\infty C_0(t-nT)C_1(t-mT)\,dt = \begin{cases} \langle C_0(t), C_1(t-T)\rangle = \langle C_0(t+T), C_1(t)\rangle\,, & m-n=1; \\ 0, & \text{otherwise.} \end{cases} \tag{3.53}$$

where $\langle C_i(t), C_j(t)\rangle$ refers to the usual inner product between the two pulses $C_i(t)$ and $C_j(t)$.

For the case of generalized MSK with correlative coding with $(k_0 + k_1 D)$ as its coding polynomial and a rectangular pulse $g(t)$, we can evaluate these expressions more explicitly in terms of k_0 and k_1. In this case $h(t)$ is given by (3.26) and we find

$$\int_0^\infty C_0(t-nT)C_0(t-mT)\,dt = \begin{cases} \frac{T}{4}\left[3 + \left(\frac{1}{k_0k_1} - 1\right)\frac{\sin(k_0\pi)}{\pi}\right], & n=m; \\ \frac{T}{4\pi}\sin(k_0\pi), & |n-m|=2; \\ 0, & \text{otherwise.} \end{cases}$$

$$\int_0^\infty C_1(t-nT)C_1(t-mT)\,dt = \begin{cases} \frac{T}{4}\left[1 - \left(\frac{1}{k_0k_1} - 1\right)\frac{\sin(k_0\pi)}{\pi}\right], & n=m; \\ 0, & \text{otherwise;} \end{cases}$$

$$\int_0^\infty C_0(t-nT)C_1(t-mT)\,dt = \begin{cases} \frac{T}{4\pi}\sin(k_0\pi), & m-n=1; \\ 0, & \text{otherwise.} \end{cases}$$

Since $k_1 = 1 - k_0$, we find we can express $I_{i,j}$ and $Q_{i,j}$ as

$$\begin{aligned} I_{i,j} \;=\; & \left\{\frac{1}{4}\left[3 + \left(\frac{1}{k_0(1-k_0)} - 1\right)\frac{1}{\pi}\sin(k_0\pi)\right]\sum_{n\text{ odd}}\left[c_n^i - c_n^j\right]^2\right. \\ & + \frac{1}{4}\left[1 - \left(\frac{1}{k_0(1-k_0)} - 1\right)\frac{1}{\pi}\sin(k_0\pi)\right]\sum_{n\text{ even}}\left[v_n^i - v_n^j\right]^2 \\ & + \frac{1}{2\pi}\sin(k_0\pi)\sum_{n\text{ odd}}\left[c_n^i - c_n^j\right]\left[c_{n-2}^i - c_{n-2}^j\right] \\ & \left. + \frac{1}{2\pi}\sin(k_0\pi)\sum_{n\text{ even}}\left[v_n^i - v_n^j\right]\left[c_{n-1}^i - c_{n-1}^j\right]\right\}, \end{aligned} \tag{3.54}$$

and

$$\begin{aligned} Q_{i,j} &= \left\{\frac{1}{4}\left[3+\left(\frac{1}{k_0(1-k_0)}-1\right)\frac{1}{\pi}\sin(k_0\pi)\right]\sum_{n\text{ even}}\left[c_n^i-c_n^j\right]^2\right. \\ &\quad +\frac{1}{4}\left[1-\left(\frac{1}{k_0(1-k_0)}-1\right)\frac{1}{\pi}\sin(k_0\pi)\right]\sum_{n\text{ odd}}\left[v_n^i-v_n^j\right]^2 \\ &\quad +\frac{1}{2\pi}\sin(k_0\pi)\sum_{n\text{ even}}\left[c_n^i-c_n^j\right]\left[c_{n-2}^i-c_{n-2}^j\right] \\ &\quad \left.-\frac{1}{2\pi}\sin(k_0\pi)\sum_{n\text{ odd}}\left[v_n^i-v_n^j\right]\left[c_{n-1}^i-c_{n-1}^j\right]\right\}. \end{aligned} \tag{3.55}$$

Noticing that $\sum_n [c_n^i - c_n^j]^2 = 4H(\mathbf{c}^i, \mathbf{c}^j)$ and $\sum_n [v_n^i - v_n^j]^2 = 4H(\mathbf{v}^i, \mathbf{v}^j)$, where $H(\mathbf{a}\ , \mathbf{b})$ is defined to be the Hamming distance between two symbol sequences denoted by $\mathbf{a}$ and $\mathbf{b}$, $\mathbf{NSED}(i,j)$ can then be expressed as

$$\begin{aligned} \mathbf{NSED}(i,j) &= \frac{R_c}{2}\left\{\left[3+\left(\frac{1}{k_0(1-k_0)}-1\right)\frac{1}{\pi}\sin(k_0\pi)\right]H(\mathbf{c}^i,\mathbf{c}^j)\right. \\ &\quad \left.+\left[1-\left(\frac{1}{k_0(1-k_0)}-1\right)\frac{1}{\pi}\sin(k_0\pi)\right]H(\mathbf{v}^i,\mathbf{v}^j)+\frac{2}{\pi}\sin(k_0\pi)\chi(i,j)\right\} \\ &= \frac{R_c}{2}\left\{\left(4-\left[1-\left(\frac{1}{k_0(1-k_0)}-1\right)\frac{1}{\pi}\sin(k_0\pi)\right]\right)H(\mathbf{c}^i,\mathbf{c}^j)\right. \\ &\quad +\left[1-\left(\frac{1}{k_0(1-k_0)}-1\right)\frac{1}{\pi}\sin(k_0\pi)\right]H(\mathbf{v}^i,\mathbf{v}^j) \\ &\quad \left.+\frac{2}{\pi}\sin(k_0\pi)\chi(i,j)\right\}, \end{aligned} \tag{3.56}$$

where the function $\chi(i,j)$ is given by

$$\begin{aligned} \chi(i,j) &= \sum_n\left[c_n^i-c_n^j\right]\left[c_{n-2}^i-c_{n-2}^j\right] \\ &\quad +\sum_{n\text{ even}}\left[v_n^i-v_n^j\right]\left[c_{n-1}^i-c_{n-1}^j\right] \\ &\quad -\sum_{n\text{ odd}}\left[v_n^i-v_n^j\right]\left[c_{n-1}^i-c_{n-1}^j\right]. \end{aligned} \tag{3.57}$$

As expected, the (normalized) squared Euclidean distance, $\mathbf{NSED}(i,j)$, is affected by the shape of the pulse $h(t)$ (i.e., it depends on the value of k_0) which can be clearly seen from the expression given in (3.56). Moreover, the computations of both functions $H(\mathbf{v}^i, \mathbf{v}^j)$ and $\chi(i,j)$ are somehow complex for all $i \neq j$ (i.e., for all different sequences generated by encoder $\mathbf{W}$). This is why the calculation of **NSED** for generalized MSK analytically is considered difficult and a computer evaluation is required.

The above results can be generalized by letting the pulse shape $h(t)$ be an arbitrary pulse of duration $2T$, providing

$$\int_0^{2T} h(t)\, dt = T. \tag{3.58}$$

Substituting (3.51)–(3.53) into (3.49) and (3.50), the normalized square Euclidean distance in that case can be expressed as

$$\begin{aligned}\mathbf{NSED}(i,j) \;=\; & \frac{R_c}{2}\cdot\frac{1}{T}\Big\{4\|C_0(t)\|^2 H(\mathbf{c}^i,\mathbf{c}^j) + 4\|C_1(t)\|^2 H(\mathbf{v}^i,\mathbf{v}^j) \\ & +2\left\langle C_0(t), C_0(t+2T)\right\rangle \sum_{n} \left[c_n^i - c_n^j\right]\left[c_{n-2}^i - c_{n-2}^j\right] \\ & +2\left\langle C_0(t+T), C_1(t)\right\rangle \sum_{n \text{ even}} \left[v_n^i - v_n^j\right]\left[c_{n-1}^i - c_{n-1}^j\right] \\ & -2\left\langle C_0(t), C_1(t-T)\right\rangle \sum_{n \text{ odd}} \left[v_n^i - v_n^j\right]\left[c_{n-1}^i - c_{n-1}^j\right]\Big\},\end{aligned} \tag{3.59}$$

We can show that for any $h(t)$ of duration $2T$,

$$\|C_0(t)\|^2 + \|C_1(t)\|^2 = T, \tag{3.60}$$

and

$$\left\langle C_0(t), C_0(t+2T)\right\rangle = \left\langle C_0(t+T), C_1(t)\right\rangle = \left\langle C_0(t), C_1(t-T)\right\rangle. \tag{3.61}$$

To demonstrate this, we begin by letting

$$f(t) = \frac{\pi}{2T}\int_0^t h(\tau)\, d\tau.$$

Then

$$\begin{aligned}\|C_0(t)\|^2 \;+\; \|C_1(t)\|^2 &= \int_0^{3T} S^2(t)S^2(t+T)\, dt + \int_0^{T} S^2(t)S^2(t+3T)\, dt \\ &= \int_0^{T} \sin^2\left[f(t)\right]\sin^2\left[f(t+T)\right]\, dt + \int_T^{2T} \sin^2\left[f(t)\right]\cos^2\left[f(t-T)\right]\, dt \\ &\quad + \int_{2T}^{3T} \cos^2\left[f(t-2T)\right]\cos^2\left[f(t-T)\right]\, dt + \int_0^{T} \sin^2\left[f(t)\right]\cos^2\left[f(t+T)\right]\, dt.\end{aligned}$$

By a change of variable ($t' = t - T$) in the third integral we get

$$\begin{aligned}\|C_0(t)\|^2 + \|C_1(t)\|^2 &= \int_0^T \sin^2[f(t)] \underbrace{\left(\sin^2[f(t+T)] + \cos^2[f(t+T)]\right)}_{=1} dt \\ &\quad + \int_T^{2T} \cos^2[f(t-T)] \underbrace{\left(\sin^2[f(t)] + \cos^2[f(t)]\right)}_{=1} dt.\end{aligned}$$

By the same change of variable in the second integral we get

$$\begin{aligned}\|C_0(t)\|^2 + \|C_1(t)\|^2 &= \int_0^T \underbrace{\left(\sin^2[f(t)] + \cos^2[f(t)]\right)}_{=1} dt \\ &= T.\end{aligned}$$

Equation (3.61) can be established as follows:

$$\begin{aligned}\langle C_0(t), C_0(t+2T)\rangle &= \int_0^T S(t)S(t+T)S(t+2T)S(t+3T)\, dt, \\ \langle C_0(t+T), C_1(t)\rangle &= \int_0^T S(t+T)S(t+2T)S(t)S(t+3T)\, dt \\ &= \int_0^T S(t)S(t+T)S(t+2T)S(t+3T)\, dt, \\ \langle C_0(t), C_1(t-T)\rangle &= \int_T^{2T} S(t)S(t+T)S(t-T)S(t+2T)\, dt \\ &= \int_0^T S(t)S(t+T)S(t+2T)S(t+3T)\, dt.\end{aligned}$$

Using (3.60) and (3.61), (3.59) can be rewritten as

$$\mathbf{NSED}(i,j) = \frac{R_c}{2}\left\{4\left(1 - \frac{\|C_1(t)\|^2}{T}\right)H(\mathbf{c}^i, \mathbf{c}^j) + 4\frac{\|C_1(t)\|^2}{T}H(\mathbf{v}^i, \mathbf{v}^j) + 2a\chi(i,j)\right\}, \quad (3.62)$$

where $a = \langle C_0(t), C_0(t+2T)\rangle / T = \langle C_0(t+T), C_1(t)\rangle / T = \langle C_0(t), C_1(t-T)\rangle / T$.

It is well-known that the minimum value of $\mathbf{NSED}(i,j)$ between all transmitted possible signals is the most important parameter in determining the asymptotic (high

SNR) performance of the over all coded modulation system. This parameter is usually referred to as the squared *free* Euclidean distance (**NSFED**)

$$\mathbf{NSFED} = \min_{i,j} \mathbf{NSED}(i,j). \tag{3.63}$$

For generalized MSK with modulation memory $L = 2$, using (3.62), the **NSFED** can be expressed as

$$\mathbf{NSFED} = \frac{R_c}{2}\left\{4\left(1 - \frac{\|C_1(t)\|^2}{T}\right)H^W_{\min} + 4\frac{\|C_1(t)\|^2}{T}H^V_{\min} + 2a\chi_{\min}\right\}, \tag{3.64}$$

where $H^W_{\min}$ is the minimum Hamming distance between all possible sequences generated by encoder $\mathbf{W}$, $H^V_{\min}$ is the Hamming distance between the sequences $\mathbf{v}^i$ and $\mathbf{v}^j$ that are related to the sequences $\mathbf{c}^i$ and $\mathbf{c}^j$ by (3.25) such that $H(\mathbf{c}^i, \mathbf{c}^j) = H^W_{\min}$. The expression given by (3.57) for $\chi_{\min}$, is calculated using the sequences $\mathbf{c}^i$ and $\mathbf{c}^j$ that corresponds to $H^W_{\min}$ and the sequences $\mathbf{v}^i$ and $\mathbf{v}^j$ which corresponds to $H^V_{\min}$.

The evaluation of the **NSFED** for any coded generalized MSK generated by encoder $\mathbf{W}$ is generally a difficult task. This is because $H^V_{\min}$ and $\chi_{\min}$ are still nonlinear functions in terms of the coded sequence $\{c_n\}$ and they are hard to evaluate analytically for all channel codes C_W. As such, the calculation is usually performed using computer evaluation. However, it is possible to find a closed expression of **NSFED** for the *uncoded* case of generalized MSK with pulse shape of duration $2T$.

Let us consider finding the exact expression of **NSFED** for the uncoded case of generalized MSK with modulation memory $L = 2$, where $R_c = 1$. Encoder $\mathbf{W}$ is just the identity mapping (i.e., $c_n = a_n$). Therefore $H^W_{\min} = 1$ and the values of $H^V_{\min}$ and $\chi_{\min}$ can be found as follows:

NSFED for the uncoded case corresponds to the sequences $\mathbf{a}^i$ and $\mathbf{a}^j$ where $a^i_0 \neq a^j_0$ and $a^i_n = a^j_n$ for $n > 0$. Let

$$\begin{aligned} \mathbf{a}^i &= \mathbf{c}^i = \{-1, -1, -1, ...\}, \\ \mathbf{a}^j &= \mathbf{c}^j = \{1, -1, -1, ...\}. \end{aligned}$$

Clearly, $H^W_{\min} = H(\mathbf{a}^i, \mathbf{a}^j) = 1$, and applying (3.25) to each sequence of $\mathbf{a}^i$ and $\mathbf{a}^j$ we get

$$\begin{aligned} \mathbf{v}^i &= \{1, -1, 1, -1, 1, -1, ...\}, \\ \mathbf{v}^j &= \{-1, 1, -1, -1, 1, -1, ...\}. \end{aligned}$$

Therefore, $H^V_{\min} = H(\mathbf{v}^i, \mathbf{v}^j) = 3$, and finally evaluating (3.57) for the same two sequences $\mathbf{a}^i$ and $\mathbf{a}^j$ we get

$$\chi_{\min} = \chi(i, j) = 0 + 0 - (-2)(-2) = -4.$$

Substituting $H^W_{\min}$, $H^V_{\min}$ and $\chi_{\min}$ in (3.62), we get

$$\mathbf{NSFED} = 2 + 4\frac{\|C_1(t)\|^2}{T} - 4a. \tag{3.65}$$

An interesting result of using (3.65) is that, one does not have to look through the excess-phase trellis to calculate the minimum Euclidean distance between generated generalized MSK signals with pulse shape $h(t)$ of length $2T$, as mentioned in [3]. Instead, we only need to calculate the quantities $\|C_1(t)\|^2/T$ and a to find the exact value of **NSFED** for such signals. Table 3.2 below shows the calculation of **NSFED** for some generalized MSK signals with modulation memory $L = 2$. The special case of MSK is shown in the table for the sake of comparison.

Example 1. Let us determine the exact expression of **NSFED** for generalized MSK with pulse shape $h(t)$ given in (3.26). The values of $\|C_1(t)\|^2$ and a are given by (3.52) and (3.53) respectively. Thus,

$$\begin{aligned} \mathbf{NSFED} &= 2 + 4\frac{\frac{T}{4}\left[1 - \left(\frac{1}{k_0(1-k_0)} - 1\right)\right]\frac{\sin(k_0\pi)}{\pi}}{T} - 4\frac{\frac{T}{4\pi}\sin(k_0\pi)}{T} \\ &= 3 - \frac{\sin(\pi k_0)}{\pi k_0(1-k_0)}. \end{aligned} \tag{3.66}$$

Fig. 3.6 shows a plot of **NSFED** as a function of the correlative polynomial coefficient k_0. It is shown that for $k_0 = 1$, **NSFED** is equal to 2 which corresponds to the special case where the modulation is MSK. It is interesting to note that the minimum **NSFED** occurs when $k_0 = 0.5$ (duobinary MSK) where the minimum value of **NSFED** is 1.727.

Generalized MSK Scheme	Pulse Shape	$\|C_1(t)\|^2/T$	a	**NSFED**
DMSK	$h(t) = \begin{cases} \frac{1}{2}, & 0 \le t \le 2T; \\ 0, & \text{otherwise.} \end{cases}$	0.0113	0.0796	1.727
2-Raised Cosine	$h(t) = \begin{cases} \frac{1}{2}\left(1 - \cos(\frac{\pi t}{T})\right), & 0 \le t \le 2T; \\ 0, & \text{otherwise.} \end{cases}$	1.3370×10^{-4}	0.0085	1.967
Gaussian MSK ($BT = 0.5$)	$h(t) = \begin{cases} Q\left(\frac{2\pi BT}{\sqrt{\ln 2}} \frac{t-\frac{3T}{2}}{T}\right) - Q\left(\frac{2\pi BT}{\sqrt{\ln 2}} \frac{t-\frac{T}{2}}{T}\right), & 0 < t < 2T; \\ 0, & \text{otherwise.} \end{cases}$	3.2526×10^{-4}	0.0149	1.942
MSK	$h(t) = \begin{cases} 1, & 0 \le t \le T; \\ 0, & \text{otherwise.} \end{cases}$	0	0	2.0

Table 3.2: NSFED for some commonly used generalized MSK signals with pulse shapes $h(t)$ of length $2T$.

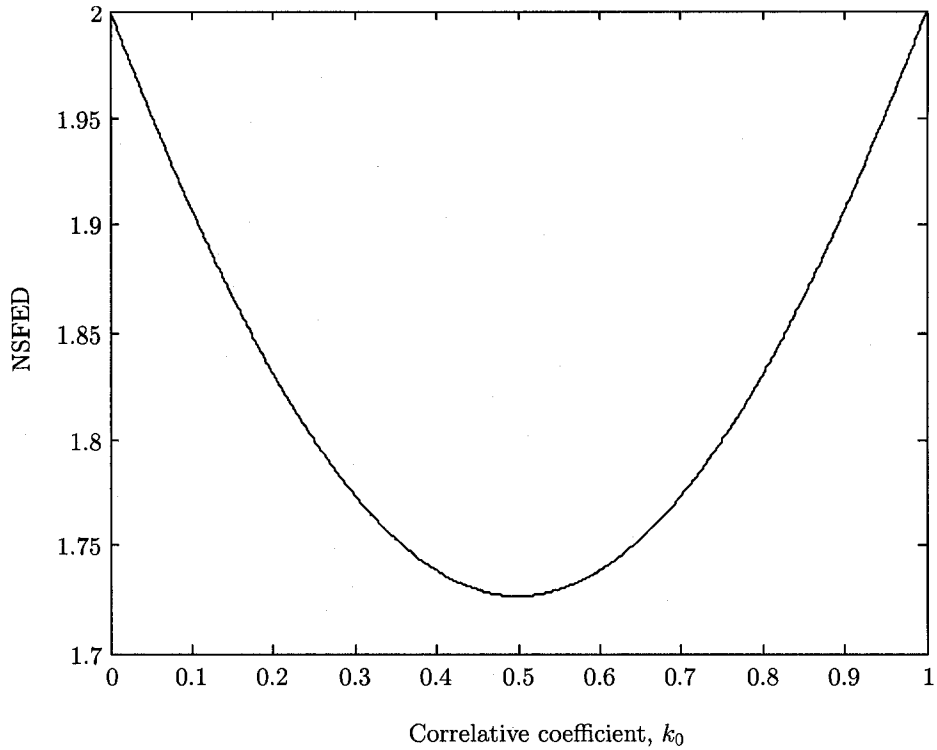

Fig. 3.6: NSFED as a function of k_0 for correlatively coded generalized MSK with rectangular pulse shape and coding polynomial $(k_0 + k_1 D)$ where $k_1 = 1 - k_0$.

Consider now the computation of the squared Euclidean distance for generalized MSK signals with premodulation pulse shape $h(t)$ given in (3.43). In general, the **NSED** for coded generalized MSK with modulation memory $L = 3$ can be expressed exactly as (see Appendix B)

$$\begin{aligned}\mathbf{NSED}(i,j) \;=\; & \frac{R_c}{2T}\Big\{4\|C_0(t)\|^2 H(\mathbf{c}^i,\mathbf{c}^j) + 4\|C_1(t)\|^2 H(\mathbf{v}^i,\mathbf{v}^j) \\ & +4\|C_2(t)\|^2 H(\mathbf{x}^i,\mathbf{x}^j) + 4\|C_3(t)\|^2 H(\mathbf{y}^i,\mathbf{y}^j) \\ & +2\left\langle C_0(t), C_0(t-2T)\right\rangle \chi(i,j) + 2\left\langle C_0(t-T), C_1(t)\right\rangle \eta(i,j) + \\ & 2\left\langle C_0(t-T), C_1(t-4T)\right\rangle \lambda(i,j) + 2\left\langle C_0(t-T), C_2(t-4T)\right\rangle \zeta(i,j) \\ & +2\left\langle C_0(t-T), C_3(t-T)\right\rangle \delta(i,j)\Big\}, \end{aligned} \tag{3.67}$$

where the functions $\chi(i,j)$, $\eta(i,j)$, $\lambda(i,j)$, $\zeta(i,j)$, and $\delta(i,j)$ are all as defined in Appendix B.

When the memory of the modulation increases (i.e., for large values of L) the exact computations of **NSED** gets more complex and time consuming especially for the coded case. Therefore, let us consider only finding the exact expression of the *free* (normalized) squared Euclidean distance (the most important parameter in determining the performance of the overall modulation system) for the uncoded case ($R_c = 1$) . In that situation, **NSFED** can be written as

$$\begin{aligned}\textbf{NSFED} \;=\; \frac{1}{2T}\Big\{ & 4\|C_0(t)\|^2 H^W_{\min} + 4\|C_1(t)\|^2 H^V_{\min} + 4\|C_2(t)\|^2 H^X_{\min} + 4\|C_3(t)\|^2 H^Y_{\min} \\ & +2\left\langle C_0(t), C_0(t-2T)\right\rangle \chi_{\min} + 2\left\langle C_0(t-T), C_1(t)\right\rangle \eta_{\min} \\ & +2\left\langle C_0(t-T), C_1(t-4T)\right\rangle \lambda_{\min} + 2\left\langle C_0(t-T), C_2(t-4T)\right\rangle \zeta_{\min} \\ & +2\left\langle C_0(t-T), C_3(t-T)\right\rangle \delta_{\min}\Big\}. \end{aligned} \tag{3.68}$$

Again, **NSFED** for the uncoded case corresponds to the sequences $\mathbf{a}^i$ and $\mathbf{a}^j$ where $a^i_0 \neq a^j_0$ and $a^i_n = a^j_n$ for $n > 0$. Let

$$\begin{aligned}\mathbf{a}^i &= \mathbf{c}^i = \{-1,-1,-1,...\}, \\ \mathbf{a}^j &= \mathbf{c}^j = \{1,-1,-1,...\}.\end{aligned}$$

Clearly, $H^W_{\min} = H(\mathbf{a}^i, \mathbf{a}^j) = 1$, and applying (3.25), (3.41) and (3.42) to each sequence of $\mathbf{a}^i$ and $\mathbf{a}^j$ we get

$$\begin{aligned}\mathbf{v}^i &= \{1,-1,1,-1,1,-1,1...\}, \\ \mathbf{v}^j &= \{-1,1,-1,-1,1,-1,1...\}, \\ \mathbf{x}^i &= \{-1,1,-1,1,-1,1,-1...\}, \\ \mathbf{x}^j &= \{1,-1,1,1,-1,1,-1...\}, \\ \mathbf{y}^i &= \{-1,-1,-1,-1,-1,-1,...\}, \\ \mathbf{y}^j &= \{1,1,-1,1,1,-1,1,...\}.\end{aligned}$$

Therefore, $H^V_{\min} = H(\mathbf{v}^i, \mathbf{v}^j) = 3$, $H^X_{\min} = H(\mathbf{x}^i, \mathbf{x}^j) = 3$, $H^Y_{\min} = H(\mathbf{y}^i, \mathbf{y}^j) = 3$, and finally evaluating (3.57) and (B.18)-(B.21) for the same two sequences $\mathbf{a}^i$ and $\mathbf{a}^j$ we get

$$\chi_{\min} = -4, \quad \eta_{\min} = 0, \quad \lambda_{\min} = 0, \quad \zeta_{\min} = -4, \text{ and } \quad \delta_{\min} = -4.$$

It can be shown (see Appendix C, C.13) that

$$\sum_{k=0}^{3} \|C_k(t)\|^2 = T.$$

In that case, **NSFED** becomes

$$\textbf{NSFED} = 6 - 4\frac{\|C_0(t)\|^2}{T} - 4b, \tag{3.69}$$

where $b = \Big(\langle C_0(t), C_0(t-2T)\rangle + \langle C_0(t-T), C_2(t-4T)\rangle + \langle C_0(t-T), C_3(t-T)\rangle\Big)/T$.

Again, one does not have to go through the excess-phase trellis for such generalized MSK signals to calculate the minimum Euclidean distance. Instead, one has to find the values of $\|C_0(t)\|^2/T$ and b to calculate **NSFED**. Table 3.3 below shows the calculation of **NSFED** for some generalized MSK signals with modulation memory $L = 3$. The special case of MSK is shown in table for the sake of comparison.

Example 2. Let us determine the exact expression of **NSFED** for generalized MSK with pulse shape $h(t)$ shown in Fig. 3.4. The values of $\|C_0(t)\|^2$ and b can be found using simple integration, and can be shown to be equal to:

$$\begin{aligned}
\|C_0(t)\|^2 &= \frac{T}{4}\Big\{2 + \frac{1}{\pi(1-k_0-k_1)}\sin(\pi\,[k_0+k_1]) + \frac{1}{\pi k_0}\sin(\pi k_0) \\
&+ \frac{1}{2\pi(1-k_0)}\left[\sin(\pi\,[1+k_0+k_1]) - \sin(\pi\,[2k_0+k_1])\right] \\
&+ \frac{1}{2\pi(1-k_0-2k_1)}\left[\sin(\pi\,[1-k_0-k_1]) + \sin(\pi k_1)\right] \\
&+ \frac{1}{2\pi(k_0+k_1)}\left[\sin(\pi\,[2k_0+k_1]) + \sin(\pi k_0)\right] \\
&+ \frac{1}{2\pi(k_1-k_0)}\left[\sin(\pi k_1) + \sin(\pi k_0)\right]\Big\},
\end{aligned}$$

$$\begin{aligned}
b &= \frac{T}{8}\Big\{\frac{1}{\pi(1-k_0-2k_1)}\left[\sin(\pi\,[1-k_0-k_1]) + \sin(\pi k_1)\right] \\
&- \frac{1}{2\pi(1-k_0)}\left[\sin(\pi\,[1+k_0+k_1]) + \sin(\pi\,[2k_0+k_1])\right] +
\end{aligned}$$

Generalized MSK Scheme	Pulse Shape	$\|C_0(t)\|^2/T$	b	**NSFED**
3-REC	$h(t) = \begin{cases} \frac{1}{3}, & 0 \le t \le 3T; \\ 0, & \text{otherwise.} \end{cases}$	0.9351	0.2284	1.346
TFM	$h(t) = \begin{cases} \frac{1}{4}, & 0 \le t \le T; \\ \frac{1}{2}, & 0 \le t \le 2T; \\ \frac{1}{4}, & 0 \le t \le 3T; \\ 0, & \text{otherwise.} \end{cases}$	0.9684	0.1683	1.454
3-Raised Cosine	$h(t) = \begin{cases} \frac{1}{3}\left(1 - \cos(\frac{2\pi t}{3T})\right), & 0 \le t \le 3T; \\ 0, & \text{otherwise.} \end{cases}$	0.9948	0.0640	1.765
Gaussian MSK ($BT = 0.3$)	$h(t) = \begin{cases} Q\left(\frac{2\pi BT}{\sqrt{\ln 2}} \frac{t-2T}{T}\right) - Q\left(\frac{2\pi BT}{\sqrt{\ln 2}} \frac{t-T}{T}\right), & 0 < t < 3T; \\ 0, & \text{otherwise.} \end{cases}$	0.9963	0.0568	1.787
MSK	$h(t) = \begin{cases} 1, & 0 \le t \le T; \\ 0, & \text{otherwise.} \end{cases}$	1.0	0	2.0

Table 3.3: NSFED for some commonly used generalized MSK signals with pulse shapes $h(t)$ of length $3T$.

$$\frac{1}{2\pi(k_1 - k_0)}\left[\sin(\pi k_1) + \sin(\pi k_0)\right]$$
$$-\frac{1}{2\pi(k_0 + k_1)}\left[\sin(\pi\left[2k_0 + k_1\right]) + \sin(\pi k_0)\right]\Big\}.$$

Therefore, **NSFED** reduces to,

$$\begin{aligned}\textbf{NSFED} \;=\; 4 - \Big\{ & \frac{1}{\pi k_0}\sin(\pi k_0) + \frac{1}{\pi(1 - k_0 - k_1)}\sin(\pi\left[k_0 + k_1\right]) \\ & + \frac{1}{\pi(1 - k_0 - 2k_1)}\left[\sin(\pi\left[1 - k_0 - k_1\right]) - \sin(\pi k_1)\right] \\ & + \frac{1}{\pi(k_1 - k_0)}\left[\sin(\pi k_1) - \sin(\pi k_0)\right]\Big\}. \end{aligned} \tag{3.70}$$

Fig. 3.7 shows a contour plot of **NSFED** as a function of the correlative polynomial coefficients k_0 and k_1. Let us consider plotting **NSEFD** with respect to k_0 by fixing the value of the coefficient k_1 at $1/4$ and $1/2$. It is shown (Fig. 3.8.*a*) that for $k_1 = 1/4$, the minimum value of **NSFED** is equal to 1.326 which corresponds to $k_0 = k_2 = 3/8$. It is interesting to note that, for $k_1 = 1/2$, the minimum **NSFED** occurs when $k_0 = 1/4$ (tamed-frequency modulation, TFM) where the minimum value of **NSFED** is 1.453 (see Fig. 3.8.*b*).

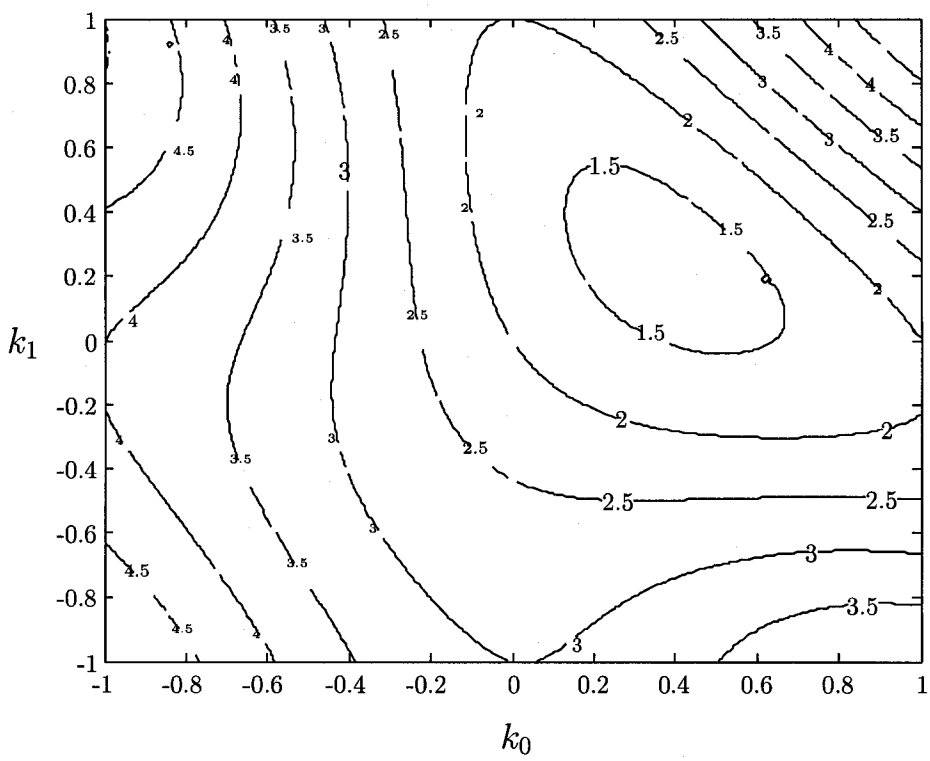

Fig. 3.7: A contour plot of **NSFED** as a function of k_0 and k_1 for correlatively coded generalized MSK with rectangular pulse shape and coding polynomial $(k_0 + k_1 D + k_2 D^2)$ where $k_2 = 1 - k_0 - k_1$.

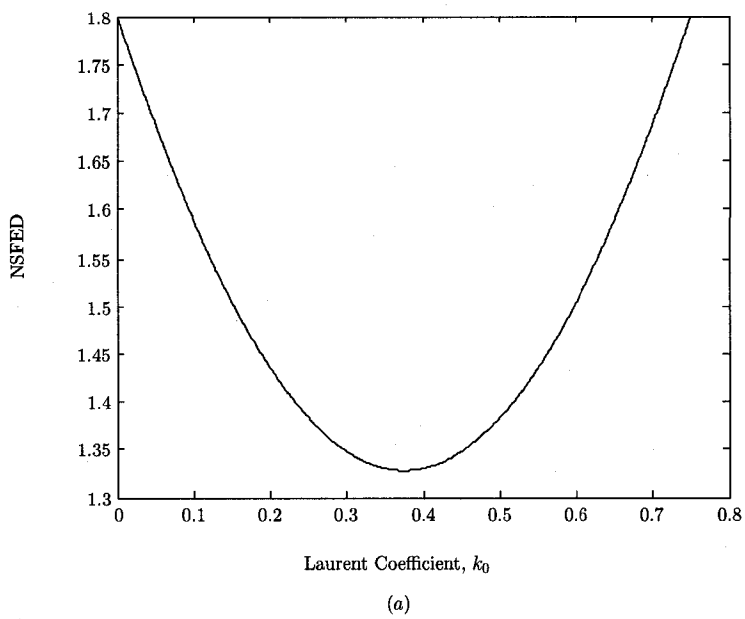

(a)

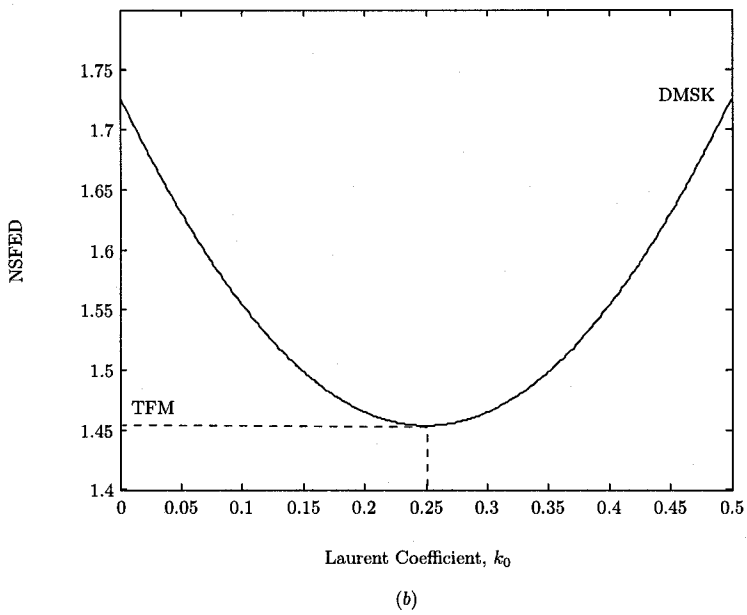

(b)

Fig. 3.8: NSFED as a function of k_0 for correlatively coded generalized MSK with rectangular pulse and coding polynomial $(k_0 + k_1 D + k_2 D^2)$ where (a) corresponds to $k_1 = 1/4$ and (b) corresponds to $k_1 = 1/2$.

Chapter 4

Special Coding Design for Generalized MSK

4.1 Introduction

It is to be expected that the error performance of generalized MSK modulation systems can be improved by the use of channel coding. The redundancy introduced by error control coding increases the power efficiency of the coded modulation system, an effect that is termed *coding gain*. For a fixed information rate, employing error control coding increases the required transmission bandwidth. In order to compensate for the increase in bandwidth, for generalized MSK modulation, a smoother pulse $h(t)$ may be used instead [22] (e.g., decreasing the value of BT in (2.12) for Gaussian MSK signal). This however is done at the expense of increasing the induced inter-symbol interference within the modulated signal, which degrades the bit-error rate performance and increases the complexity of the receiver.

Though generalized MSK is attractive for its high power and bandwidth efficiency, it has very complex optimum demodulators with complexity increasing exponentially with the modulation memory L. This complexity is due to the size of the matched filter bank

and to the large number of trellis states (see Fig. 2.8).

In general, the Euclidean distance between signals generated from combining a channel encoder with generalized MSK modulator cannot be linearly related to the Hamming distance of corresponding symbol sequences produced by the channel encoder. This is due to the *non-linearity* and *memory* inherent in the modulator. Therefore the search for good channel codes, for generalized MSK, is considered a difficult task. Most of the work that has been done in constructing good codes for CPM signals was conducted using computer-aided search and simulation [32]-[33], [35] without regard to the increase in the complexity of the receiver [19].

For generalized MSK with modulation memory $L = 2$ and $L = 3$, we will show that by imposing a particular structure on the codes, we can achieve good coding gains while optimally demodulating the coded signal using a simple linear receiver. We will demonstrate that with these structured codes, no inter-symbol interference is introduced at the output of the linear receiver and, in AWGN environment, the noise samples are independent. In these cases, the Euclidean distance between waveforms is linearly related to the Hamming distance between symbol sequences which simplifies the task of searching for good codes for such generalized MSK systems.

4.1.1 Euclidean vs. Hamming Distance

Coded linear modulation, such as coded BPSK, QPSK or OQPSK, has the property that the Euclidean distance between different transmitted signals is proportional to the Hamming distance between corresponding coded sequences. In designing codes for such modulation schemes we need only consider the Hamming distance properties of the code, particularly seeking to maximize the *minimum* Hamming distance of the code. Since generalized MSK is a non-linear modulation scheme, Euclidean distance and Hamming distance are not directly related, so codes designed based on Hamming distance consideration may not produce matching Euclidean distance properties. This difficulty in

relating Hamming distance to Euclidean distance can be removed in the case of modulation memory of two symbol duration ($L = 2$) by imposing a simple nondebilitating constraint on the code as expressed by the following result:

Theorem 1. *Let C_W be any rate R_c binary code for which the coded bits satisfy the relationship that for all k,*

$$c_{2k} = c_{2k+1}. \tag{4.1}$$

Then the $\mathbf{NSED}(i,j)$ *for generalized MSK signals with modulation memory $L = 2$, and the Hamming distance between sequences generated by C_W (i.e., $H_W(\mathbf{c}^i, \mathbf{c}^j)$) are related by*

$$\mathbf{NSED}(i,j) = 2R_c H_W(\mathbf{c}^i, \mathbf{c}^j). \tag{4.2}$$

Proof. From (4.1) we have that $c_{2k-1} = c_{2k-2}$, and the even and odd symbols of v_n (defined in (3.25)) are given by

$$v_{2k} = (-1)^{2k+1} c_{2k} \underbrace{c_{2k-1}c_{2k-2}}_{=1} = -c_{2k}, \tag{4.3}$$

$$v_{2k+1} = (-1)^{2k+2} \underbrace{c_{2k+1}c_{2k}}_{=1} c_{2k-1} = c_{2k-1}. \tag{4.4}$$

Substituting (4.1), (4.3) and (4.4) into the expression for $\chi(i,j)$ given in (3.57), we obtain

$$\begin{aligned}
\chi(i,j) &= \sum_{k=0}^{\infty} \left[c_{2k}^i - c_{2k}^j\right] \underbrace{\left[c_{2k-2}^i - c_{2k-2}^j\right]}_{\left[c_{2k-1}^i - c_{2k-1}^j\right]} + \sum_{k=0}^{\infty} \underbrace{\left[v_{4k}^i - v_{4k}^j\right]}_{-\left[c_{4k}^i - c_{4k}^j\right]} \left[c_{2k-1}^i - c_{2k-1}^j\right] \\
&+ \sum_{k=0}^{\infty} \underbrace{\left[c_{2k+1}^i - c_{2k+1}^j\right]}_{\left[c_{2k}^i - c_{2k}^j\right]} \left[c_{2k-1}^i - c_{2k-1}^j\right] - \sum_{k=0}^{\infty} \underbrace{\left[v_{2k+1}^i - v_{2k+1}^j\right]}_{\left[c_{2k-1}^i - c_{2k-1}^j\right]} \left[c_{2k}^i - c_{2k}^j\right] \\
&= \sum_{k=0}^{\infty} \left[c_{2k}^i - c_{2k}^j\right] \left[c_{2k-1}^i - c_{2k-1}^j\right] - \sum_{k=0}^{\infty} \left[c_{2k}^i - c_{2k}^j\right] \left[c_{2k-1}^i - c_{2k-1}^j\right] \\
&+ \sum_{k=0}^{\infty} \left[c_{2k}^i - c_{2k}^j\right] \left[c_{2k-1}^i - c_{2k-1}^j\right] - \sum_{k=0}^{\infty} \left[c_{2k-1}^i - c_{2k-1}^j\right] \left[c_{2k}^i - c_{2k}^j\right] \\
&= 0.
\end{aligned} \tag{4.5}$$

The Hamming distance between the v_n sequences is given by

$$H(\mathbf{v}^i, \mathbf{v}^j) = \frac{1}{4} \sum_{n=0}^{\infty} |v_n^i - v_n^j|^2$$

$$= \frac{1}{4}\left[\sum_{k=0}^{\infty}|v_{2k}^i - v_{2k}^j|^2 + \sum_{k=0}^{\infty}|v_{2k+1}^i - v_{2k+1}^j|^2\right]$$
$$= \frac{1}{4}\left[\sum_{k=0}^{\infty}|c_{2k}^i - c_{2k}^j|^2 + \sum_{k=0}^{\infty}|c_{2k-1}^i - c_{2k-1}^j|^2\right],$$

and since $c_{-1}^i = c_{-1}^j = 1$ for all i, j, then

$$\begin{aligned} H(\mathbf{v}^i, \mathbf{v}^j) &= \frac{1}{4}\left[\sum_{k=0}^{\infty}|c_{2k}^i - c_{2k}^j|^2 + \sum_{k=1}^{\infty}|c_{2k-1}^i - c_{2k-1}^j|^2\right] \\ &= \frac{1}{4}\left[\sum_{k=0}^{\infty}|c_{2k}^i - c_{2k}^j|^2 + \sum_{k=0}^{\infty}|c_{2k+1}^i - c_{2k+1}^j|^2\right] \\ &= \frac{1}{4}\sum_{n=0}^{\infty}|c_n^i - c_n^j|^2 \\ &= H(\mathbf{c}^i, \mathbf{c}^j). \end{aligned} \tag{4.6}$$

Substituting (4.5) and (4.6) into (3.62) we obtain

$$\mathbf{NSED}(i, j) = 2R_c H_W(\mathbf{c}^i, \mathbf{c}^j)$$

as required. □

4.2 On The Usefulness of Repetition Codes for Generalized MSK Signals

The condition (4.1) on the coded symbol stream may be viewed as requiring the encoder incorporate a double repetition code in the encoding process following some other encoding process. An encoder then that meets this condition (that makes Euclidean distances between generated signals proportional to Hamming distances between corresponding coded sequences) can thus be broken down into a cascade of two encoders—a rate-R_o outer encoder $\mathbf{W}_{\text{out}}$ followed by the double repetition inner encoder $\mathbf{W}_{\text{in}}$. This situation is depicted in Fig. 4.1. As the double repetition code is a rate-1/2 code, the overall code rate is half the code rate of the outer encoder:

$$R_c = \frac{R_o}{2}. \tag{4.7}$$

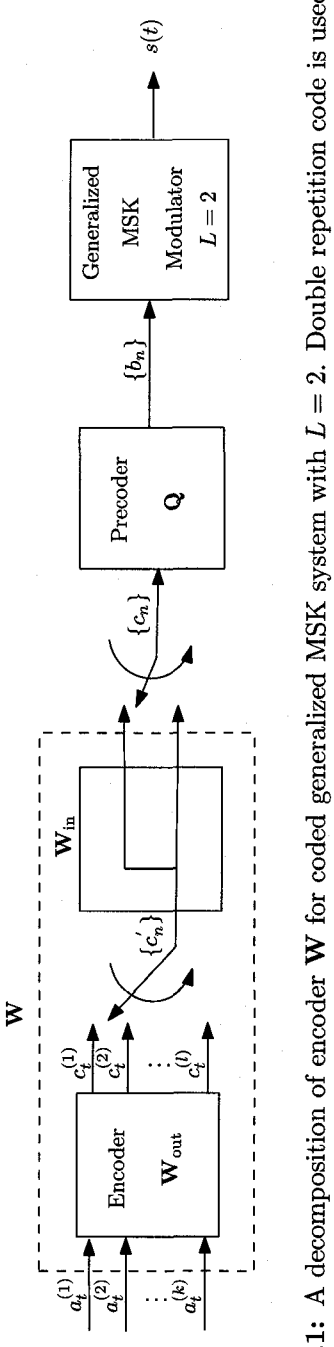

Fig. 4.1: A decomposition of encoder $\mathbf{W}$ for coded generalized MSK system with $L = 2$. Double repetition code is used as an inner encoder.

Any linear block encoder and almost all convolutional encoders (except possibly for catastrophic encoders) could be used as an outer encoder. We shall consider in this thesis outer encoders that are linear convolutional encoders since these codes are widely used in wireless applications to improve the performance, such as digital radio, mobile phones and satellite links, and Bluetooth implementations.

Let $\mathbf{a} = \mathbf{a}_0, \mathbf{a}_1, \mathbf{a}_2...$ and $\mathbf{c} = \mathbf{c}_0, \mathbf{c}_1, \mathbf{c}_2...$ be the input and output sequences of a rate $R = M/N$, $M \leq N$, convolutional encoder respectively, where $\mathbf{a}_i = (a_i^{(1)}...a_i^{(M)})$ and $\mathbf{c}_i = (c_i^{(1)}...c_i^{(N)})$. The relationship between the input $\mathbf{a}$ and output $\mathbf{c}$ can expressed as

$$\mathbf{c} = \mathbf{a}\mathbf{G}, \tag{4.8}$$

where $\mathbf{c}_i = \sum_{k=0}^{\infty} \mathbf{a}_{i-k}\mathbf{G}_k$. The semi-infinite matrix

$$\mathbf{G} = \begin{pmatrix} \mathbf{G}_0 & \mathbf{G}_1 & \mathbf{G}_2 & \dots & \mathbf{G}_m & & \\ \mathbf{0} & \mathbf{G}_0 & \mathbf{G}_1 & \mathbf{G}_2 & \dots & \mathbf{G}_m & \\ \mathbf{0} & \mathbf{0} & \mathbf{G}_0 & \mathbf{G}_1 & \mathbf{G}_2 & \dots & \mathbf{G}_m \\ & & & \ddots & \ddots & \ddots & \ddots \end{pmatrix}, \tag{4.9}$$

is called the *generator matrix*, where the sub-matrices $\mathbf{G}_k$, $0 \leq k \leq m$, are binary $M \times N$ matrices which can be expressed as

$$\mathbf{G}_k = \begin{pmatrix} g_{1k}^{(1)} & g_{1k}^{(2)} & \dots & g_{1k}^{(N)} \\ g_{2k}^{(1)} & g_{2k}^{(2)} & \dots & g_{2k}^{(N)} \\ \vdots & \vdots & \ddots & \vdots \\ g_{M,k}^{(1)} & g_{M,k}^{(2)} & \dots & g_{M,k}^{(N)} \end{pmatrix}. \tag{4.10}$$

Note that all operations in (4.8) are modulo-2 operation. For convolutional codes, it is convenient to express (4.8) in the $\mathcal{D}$-transform domain as $c(D) = a(D)\mathbf{G}(D)$, where

$$\mathbf{G}(D) = \begin{pmatrix} \mathbf{G}_1^{(1)}(D) & \mathbf{G}_1^{(2)}(D) & \dots & \mathbf{G}_1^{(N)}(D) \\ \mathbf{G}_2^{(1)}(D) & \mathbf{G}_2^{(2)}(D) & \dots & \mathbf{G}_2^{(N)}(D) \\ \vdots & \vdots & \ddots & \vdots \\ \mathbf{G}_M^{(1)}(D) & \mathbf{G}_M^{(2)}(D) & \dots & \mathbf{G}_M^{(N)}(D) \end{pmatrix}, \tag{4.11}$$

Each of the entries in (4.11) is a polynomial given by $\mathbf{G}_i^{(j)}(D) = g_{i0}^{(j)} + g_{i1}^{(j)} D + ... + g_{i,\nu_i}^{(j)} D^{\nu_i}$, for $i = 1, 2..., M$, and $j = 1, 2, ..., N$. Let

$$\nu_i = \max_{1 \le j \le N} \left[\deg \mathbf{G}_i^{(j)}(D) \right]. \tag{4.12}$$

The overall constraint length of the convolutional encoder is [36]

$$\nu = \sum_{i=1}^{M} \nu_i, \tag{4.13}$$

where the memory order of the encoder is $m = \max_{1 \le i \le M} [\nu_i]$.

Consider now the case where two convolutional codes are cascaded as depicted in Fig. 4.2. The equivalent convolutional code is a cascade of an outer code $\mathbf{G}_{\text{out}}$ of rate $R_o = k/l$ followed by an inner code $\mathbf{G}_{\text{in}}$ of rate $R_i = m/r$.

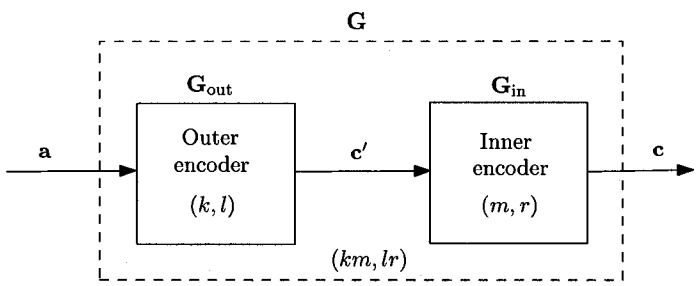

Fig. 4.2: A cascading of two convolutional encoder.

The cascaded generator matrix $\mathbf{G}$ is given by

$$\mathbf{G} = \mathbf{G}_{\text{out}} \mathbf{G}_{\text{in}}. \tag{4.14}$$

where $\mathbf{G}_{\text{out}}$ and $\mathbf{G}_{\text{in}}$ are the semi-infinite matrices of the outer and inner encoders respectively. It can easily be seen that the rate of the cascaded code R_c will be

$$R_c = R_o R_i = \frac{km}{lr}. \tag{4.15}$$

If $l = m$, then the outer and inner encoders are said to have matched rates [40]. In that case (4.14) can, equivalently, be expressed as

$$\mathbf{G}(D) = \mathbf{G}_{\text{out}}(D) \mathbf{G}_{\text{in}}(D), \tag{4.16}$$

while if $l \neq m$, the two cascaded encoders are said to have unmatched rates and the matrix multiplication in (4.16) is not defined, but (4.14) is still valid [40, Ch. 4].

Theorem 2. *Let $C_{W_{\text{out}}}$ be any rate-R_o ($R_o = k/l$, $k \leq l$) outer convolutional code cascaded with a double repetition code as an inner code, and let $\mathbf{W}_{\text{out}}(D)$ and $\mathbf{W}(D)$ be the generator matrices of the outer and cascaded encoders respectively. Let the entries of the generator matrix $\mathbf{W}^o(D)$ be $w^o_{i,j}(D)$ for $i \in \{1, 2, ..., k\}$ and $j \in \{1, 2, ..., l\}$. If $\mathbf{W}_{\text{out}}(D)$ is a polynomial matrix then*

$$\mathbf{W}(D) = \begin{pmatrix} w^o_{11}(D) & w^o_{11}(D) & \dots & w^o_{1l}(D) & w^o_{1l}(D) \\ w^o_{21}(D) & w^o_{21}(D) & \dots & w^o_{2l}(D) & w^o_{2l}(D) \\ \vdots & \vdots & \ddots & \vdots & \vdots \\ w^o_{k1}(D) & w^o_{k1}(D) & \dots & w^o_{kl}(D) & w^o_{kl}(D) \end{pmatrix}, \tag{4.17}$$

where the cascaded encoder $\mathbf{W}$ is a rate-$k/2l$ convolutional encoder.

Proof. Except for the case of $R_o = 1$ (i.e., $k = l = 1$), the two generator matrices of the inner and outer encoders cannot be multiplied in the $\mathcal{D}$-transform representation to find the generator matrix of the cascaded encoder (since $l \neq 1$), i.e., $\mathbf{W}(D) \neq \mathbf{W}_{\text{out}}(D)\mathbf{W}_{\text{in}}(D)$. Instead one has to multiply the semi-infinite matrices $\mathbf{W}_{\text{out}}$ and $\mathbf{W}_{\text{in}}$ to determine the generator matrix of the cascaded encoder $\mathbf{W} = \mathbf{W}_{\text{out}}\mathbf{W}_{\text{in}}$. However, the matrix $\mathbf{W}(D)$, for unmatched rates, can be found by considering $l \times 2l$ sub-matrices instead of 1×2 sub-matrices in $\mathbf{W}_{\text{in}}$. The resulting matrices $\mathbf{W}_{\text{out}}(D)$ and $\mathbf{W}^l_{\text{in}}(D)$ then have matched rates and can be multiplied. The inner generator matrix can be written as

$$\mathbf{W}_{\text{in}} = \begin{pmatrix} 11 & 00 & 00 & \dots & 00 & & \\ 00 & 11 & 00 & 00 & \dots & 00 & \\ 00 & 00 & 11 & 00 & 00 & \dots & 00 \\ & & & \ddots & \ddots & \ddots & & \ddots \end{pmatrix}.$$

If we consider $l \times 2l$ sub-matrices of $\mathbf{W}_{\text{in}}$, then the $\mathcal{D}$-transform representation of $\mathbf{W}_{\text{in}}$, (i.e., $\mathbf{W}^l_{\text{in}}(D)$) would be given by

$$\mathbf{W}_{\text{in}}^{l}(D) = \begin{pmatrix} 1 & 1 & 0 & 0 & \dots & 0 & 0 & 0 & 0 \\ 0 & 0 & 1 & 1 & \dots & 0 & 0 & 0 & 0 \\ \vdots & \vdots & & & \ddots & & & \vdots & \vdots \\ 0 & 0 & 0 & 0 & \dots & 0 & 0 & 1 & 1 \end{pmatrix}. \tag{4.18}$$

The outer generator matrix is

$$\mathbf{W}_{\text{out}}(D) = \begin{pmatrix} w_{11}^{o}(D) & w_{12}^{o}(D) & \dots & w_{1l}^{o}(D) \\ w_{21}^{o}(D) & w_{21}^{o}(D) & \dots & w_{2l}^{o}(D) \\ \vdots & \vdots & \ddots & \vdots \\ w_{k1}^{o}(D) & w_{k2}^{o}(D) & \dots & w_{kl}^{o}(D) \end{pmatrix}. \tag{4.19}$$

Using (4.18) and (4.19), the semi-infinite matrix multiplication $\mathbf{W} = \mathbf{W}_{\text{out}}\mathbf{W}_{\text{in}}$ can be equivalently represented by

$$\begin{aligned} \mathbf{W}(D) &= \mathbf{W}_{\text{out}}(D)\mathbf{W}_{\text{in}}^{l}(D) \\ &= \begin{pmatrix} w_{11}^{o}(D) & w_{11}^{o}(D) & \dots & w_{1l}^{o}(D) & w_{1l}^{o}(D) \\ w_{21}^{o}(D) & w_{21}^{o}(D) & \dots & w_{2l}^{o}(D) & w_{2l}^{o}(D) \\ \vdots & \vdots & \ddots & \vdots & \vdots \\ w_{k1}^{o}(D) & w_{k1}^{o}(D) & \dots & w_{kl}^{o}(D) & w_{kl}^{o}(D) \end{pmatrix}. \end{aligned}$$

□

Corollary 1. *Let encoder $\mathbf{W}(D)$ be any $k \times 2l$ polynomial matrix. If $\mathbf{W}(D)$ is partitioned into (k, l) convolutional encoder $\mathbf{W}_{\text{out}}(D)$ and double repetition encoder as illustrated in Fig. 4.1, then*

$$\mathbf{NSED}(i, j) = 2\frac{k}{l} H_{W_{\text{out}}}(\mathbf{c}'^{i}, \mathbf{c}'^{j}). \tag{4.20}$$

where $H_{W_{\text{out}}}(\mathbf{c}'^{i}, \mathbf{c}'^{j})$ is the Hamming distance between sequences generated by outer encoder $\mathbf{W}_{\text{out}}$.

Proof. Using a double repetition code doubles the Hamming distance between sequences generated by the outer code $\mathbf{W}_{\text{out}}$, i.e., $H_W(\mathbf{c}^i, \mathbf{c}^j) = 2H_{W_{\text{out}}}(\mathbf{c}'^{i}, \mathbf{c}'^{j})$. Therefore, from (4.2) and (4.7)

$$\mathbf{NSED}(i, j) = 2R_c H_W(\mathbf{c}^i, \mathbf{c}^j)$$

$$\begin{aligned} &= 2\frac{R_o}{2}\left[2H_{W_{\text{out}}}(\mathbf{c}'^i, \mathbf{c}'^j)\right] \\ &= 2R_o H_{W_{\text{out}}}(\mathbf{c}'^i, \mathbf{c}'^j), \end{aligned}$$

where $R_o = k/l$ is the rate of outer encoder $\mathbf{W}_{\text{out}}$. □

From (4.20), we have that the normalized squared free Euclidean distance is given by

$$\mathbf{NSFED} = 2(k/l)H_{\text{min}}^{W_{\text{out}}}, \tag{4.21}$$

where $H_{\text{min}}^{W_{\text{out}}}$ is the minimum Hamming distance of C_{W^o}. Therefore, to maximize the free Euclidean distance of coded generalized MSK with modulation memory $L = 2$ employing a double a repetition code, for a given rate k/l and constraint length ν^o of the code C_{W^o}, the minimum Hamming distance of the outer encoder must be maximized.

The immediate consequence of Theorem 4.1, is that the dependency of the Euclidean distance on the pulse shape $h(t)$ is totally eliminated (i.e., the performance of the overall system is independent of $h(t)$). The main impact, then, of a choice of pulse shape relates to the spectral properties of the signals [22] where this subject is beyond the scope of this thesis.

4.3 Optimum Linear Receiver Design for Length $2T$ Coded Generalized MSK

It has been shown previously, that a precoded MSK signal can be expressed exactly as an OQPSK signal, which allows us to form this signal using an I-Q modulator. For "uncoded" generalized MSK signals with pulse shapes $h(t)$ of duration more than a symbol period, it was demonstrated by Galko [8, p. 18] that it is impossible to express the signals in I-Q form. However, Galko showed that it is not necessary for generalized MSK to be expressed as an I-Q signal in order for it to be demodulated using a simple I-Q receiver. The optimum choice of the filter in such a simple I-Q receiver depends on

the signal-to-noise ratio, leading to the concept of "Average Matched Filter" (AMF) and "Asymptotic Optimal Filter" (AOF). It was shown that, for duobinary MSK and tamed MSK (TFM), the simple I-Q receiver with AOF has a degradation performance of 0.91 dB and 2.63 dB respectively, compared to simple MSK and only 0.28 dB and 1.24 dB poorer than the optimal (Viterbi) receiver at high SNR.

Surprisingly, using the double repetition code that was introduced previously, for any $h(t)$ of duration $2T$ satisfying (3.58), a coded generalized MSK signal may be expressed in I-Q form. This easily seen from the following result:

Theorem 3. *Precoded generalized MSK signals with a pulse shape $h(t)$ of duration up to two symbol periods can be expressed as an inphase-quadrature signal (with Euclidean distances between generated signals proportional to Hamming distances between corresponding coded sequences) if and only if the c_n symbol sequence satisfies the condition*

$$c_{2k+1}c_{2k-1} = c_{2k}c_{2k-2}, \quad \textit{for all } k \in \mathbb{Z}. \tag{4.22}$$

The generalized MSK signal can then be written as

$$s(t) = I(t)\cos(2\pi f_c t + \theta_0) - Q(t)\sin(2\pi f_c t + \theta_0),$$

where the inphase signal $I(t)$ and quadrature signal $Q(t)$ are given by

$$I(t) = \sqrt{\frac{2E}{T}}\cos\phi(t) = \sqrt{\frac{2E}{T}}\sum_{n \text{ odd}} c_n p(t - nT), \tag{4.23}$$

$$Q(t) = \sqrt{\frac{2E}{T}}\sin\phi(t) = \sqrt{\frac{2E}{T}}\sum_{n \text{ even}} c_n \tilde{p}(t - nT), \tag{4.24}$$

with the inphase pulse $p(t)$ and quadrature pulse $\tilde{p}(t)$ given by

$$p(t) = C_0(t) - C_1(t + T), \tag{4.25}$$

$$\tilde{p}(t) = C_1(t - 3T) - C_0(t). \tag{4.26}$$

The functions $C_0(t)$ and $C_1(t)$ are the Laurent pulses given by (3.16) and (3.17) respectively.

Proof. First we prove that if the constraint (4.22) holds then the inphase and quadrature signals can be expressed as in (4.23) and (4.24) respectively. Substituting (4.22) into (3.25), we have that the even and odd symbols of v_n are given by

$$v_{2k} = (-1)^{2k+1} c_{2k} c_{2k-1} c_{2k-2} = -c_{2k} c_{2k} c_{2k+1} = -c_{2k+1}, \tag{4.27}$$

and

$$v_{2k+1} = (-1)^{2k+2} c_{2k+1} c_{2k} c_{2k-1} = c_{2k+1} c_{2k+1} c_{2k-2} = c_{2k-2}. \tag{4.28}$$

Substituting (4.27) into (3.23) we get

$$\begin{aligned} I(t) &= \sqrt{\frac{2E}{T}} \left[\sum_k c_{2k+1} C_0(t - [2k+1]\,T) - \sum_k c_{2k+1} C_1(t - 2kT) \right] \\ &= \sqrt{\frac{2E}{T}} \sum_k c_{2k+1} \left[C_0(t - [2k+1]\,T) - C_1(t - 2kT) \right] \\ &= \sqrt{\frac{2E}{T}} \sum_{n \text{ odd}} c_n p(t - nT), \end{aligned}$$

where $p(t) = C_0(t) - C_1(t+T)$, as required. Now, substituting (4.28) into (3.24) we get

$$\begin{aligned} Q(t) &= \sqrt{\frac{2E}{T}} \left[-\sum_k c_{2k-2} C_0(t - [2k-2]\,T) + \sum_k c_{2k-2} C_1(t - [2k+1]\,T) \right] \\ &= \sqrt{\frac{2E}{T}} \sum_k c_{2k-2} \left[C_1(t - [2k+1]\,T) - C_0(t - [2k-2]\,T) \right] \\ &= \sqrt{\frac{2E}{T}} \sum_{n \text{ even}} c_n \tilde{p}(t - nT), \end{aligned}$$

where $\tilde{p}(t) = C_1(t - 3T) - C_0(t)$, as required.

For the converse statement, we want to show that if $I(t)$ and $Q(t)$ can be expressed as in (4.23) and (4.24) respectively, where $p(t)$ and $\tilde{p}(t)$ are given by (4.25) and (4.26) respectively, then (4.22) must be satisfied for all k.

Consider the inphase and quadrature signals, $I(t)$ and $Q(t)$, on the interval $t \in [0, T]$. The signals $I(t)$ and $Q(t)$ can be expressed as

$$I(t) = A\left[-c_1 C_0(t) + c_{-1} C_0(t+T)\right],$$

$$Q(t) = A\left[-c_0 C_0(t) - c_{-2} C_0(t+2T)\right],$$

where $A = \sqrt{2E/T}$. The square of the envelope of $s(t)$ for all $t \in [0, T]$

$$\begin{aligned} I^2(t) + Q^2(t) &= A^2\Big\{C_1^2(t) + C_0^2(t+T) - 2c_1c_{-1}C_0(t+T)C_1(t) \\ &\quad + C_0^2(t) + C_0^2(t+2T) + 2c_0c_{-2}C_0(t)C_0(t+2T)\Big\}, \end{aligned} \tag{4.29}$$

where $C_1(t) = S(t)S(t+3T)$ and $C_0(t) = S(t)S(t+T)$. Substituting these values into (4.29) gives us

$$\begin{aligned} I^2(t) + Q^2(t) &= A^2\Big\{S^2(t)S^2(t+3T) + S^2(t+T)S^2(t+2T) - 2c_1c_{-1}\beta(t) \\ &\quad + S^2(t)S^2(t+T) + S^2(t+2T)S^2(t+3T) + 2c_0c_{-2}\beta(t)\Big\} \\ &= A^2\Big\{\left[S^2(t) + S^2(t+2T)\right]\left[S^2(t+T) + S^2(t+3T)\right] \\ &\quad + 2\left[c_0c_{-2} - c_1c_{-1}\right]\beta(t)\Big\}, \end{aligned} \tag{4.30}$$

where $\beta(t) = S(t)S(t+T)S(t+2T)S(t+3T)$. Now for the square of the envelope for $t \in [T, 2T]$, we have that

$$I(t) = A\left[c_1C_0(t-T) + c_{-1}C_0(t+T)\right],$$

$$Q(t) = A\left[c_{-2}C_1(t-T) - c_0C_0(t)\right],$$

therefore,

$$\begin{aligned} I^2(t) + Q^2(t) &= A^2\Big\{C_0^2(t-T) + C_0^2(t+T) + 2c_1c_{-1}C_0(t-T)C_0(t+T) \\ &\quad + C_1^2(t-T) + C_0^2(t) - 2c_0c_{-2}C_1(t-T)C_0(t)\Big\}, \end{aligned} \tag{4.31}$$

where $C_1(t) = S(t)S(t+3T)$ and $C_0(t) = S(t)S(t+T)$. Substituting these values into (4.31) gives us

$$\begin{aligned} I^2(t) + Q^2(t) &= A^2\Big\{S^2(t)S^2(t-T) + S^2(t+T)S^2(t+2T) + 2c_1c_{-1}\gamma(t) \\ &\quad + S^2(t-T)S^2(t+2T) + S^2(t)S^2(t+T) - 2c_0c_{-2}\gamma(t)\Big\} \\ &= A^2\Big\{\left[S^2(t-T) + S^2(t+T)\right]\left[S^2(t) + S^2(t+2T)\right] + \end{aligned}$$

$$2\left[c_1c_{-1} - c_0c_{-2}\right]\gamma(t)\Big\}, \tag{4.32}$$

where $\gamma(t) = S(t)S(t+T)S(t+2T)S(t-T)$. Now, for $t \in [0,T]$,

$$S^2(t) + S^2(t+2T) = \sin^2\left(\frac{\pi t}{2T}\int_0^t h(t)\right) + \cos^2\left(\frac{\pi t}{2T}\int_0^t h(t)\right) = 1,$$

and

$$S^2(t+T) + S^2(t+3T) = \sin^2\left(\frac{\pi t}{2T}\int_0^{t+T} h(t)\right) + \cos^2\left(\frac{\pi t}{2T}\int_0^{t+T} h(t)\right) = 1,$$

while for $t \in [T,2T]$,

$$S^2(t-T) + S^2(t+T) = \sin^2\left(\frac{\pi t}{2T}\int_0^{t-T} h(t)\right) + \cos^2\left(\frac{\pi t}{2T}\int_0^{t-T} h(t)\right) = 1,$$

and

$$S^2(t) + S^2(t+2T) = \sin^2\left(\frac{\pi t}{2T}\int_0^t h(t)\right) + \cos^2\left(\frac{\pi t}{2T}\int_0^t h(t)\right) = 1.$$

Therefore, for $t \in [0,T]$ (4.30) reduces to

$$I^2(t) + Q^2(t) = A^2\left\{1 + 2\left[c_0c_{-2} - c_1c_{-1}\right]\beta(t)\right\}, \tag{4.33}$$

and for $t \in [T,2T]$ (4.32) reduces to

$$I^2(t) + Q^2(t) = A^2\left\{1 + 2\left[c_1c_{-1} - c_0c_{-2}\right]\gamma(t)\right\}. \tag{4.34}$$

For the signal $s(t)$ to be constant envelope, $I^2(t)+Q^2(t)$ (i.e., the square of the envelope) must be constant for all $t \in [0,2T]$. Since $\beta(t)$ and $\gamma(t)$ cannot be identically zero for all t, for $s(t)$ to have a constant envelope on $[0,2T]$, $c_0c_{-2} - c_1c_{-1} = 0$, i.e.,

$$c_1c_{-1} = c_0c_{-2}. \tag{4.35}$$

A similar analysis shows that for $t \in [2kT,(2k+2)T]$, the envelope of $s(t)$ is constant only if

$$c_{2k+1}c_{2k-1} = c_{2k}c_{2k-2}.$$

□

We see that since in a repetition code, $c_{2k} = c_{2k+1}$, (4.22) holds and thus all coded generalized MSK signals with pulse shapes $h(t)$ of length $2T$, involves a double repetition code can be expressed in I-Q form.

As an example, Fig. 4.3 shows the inphase and quadrature pulses given in (4.25) and (4.26) respectively, for the case of DMSK signal. As expected, since the pulse shape $h(t)$ is nonzero outside the interval $[0, T]$, the pulse $p(t)$ and $\tilde{p}(t)$ each has a duration greater than $2T$.

In general, for any coded generalized MSK with pulse shape $h(t)$ of length $2T$, the signal can be expressed in I-Q form with inphase and quadrature pulses of duration $4T$ given by (4.25) and (4.26). Each channel (inphase and quadrature) waveform is a PAM signal that carries the (odd and even) coded sequence at a rate of $1/2T$. Therefore, inter-symbol interference exists in this coded signal, where it affects a finite number of symbols. Inter-symbol interference (ISI) introduces *memory* in the signal, which is the case for generalized MSK. The optimum detection of signals with ISI is based on *maximum-likelihood sequence estimation* (MLSE) which is typically implemented using the Viterbi algorithm (see Chapter 2). The complexity of such detector increases exponentially with the length of the pulse shape LT.

Employing a double repetition code will allow us to generate coded generalized MSK signals with pulse shapes of length $2T$, using a simple I-Q modulator. Fig. 4.4 shows a block diagram for a modulator based on these results. We shall show in the next section that expressing this coded signal in an I-Q form may result in a significant reduction in the complexity of the optimum receiver.

4.3.1 Demodulation and Detection of Length $2T$ Coded generalized MSK in AWGN Channel

Based on (4.23) and (4.24), i.e., expressing generalized MSK with modulation memory $L = 2$ as two PAM signals in quadrature, we can design a simple I-Q receiver (assuming

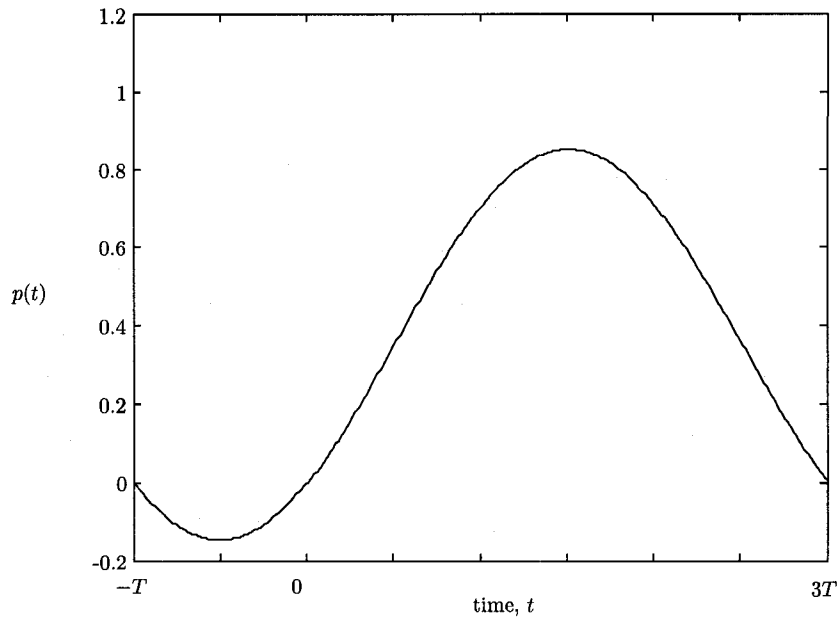

a. Inphase channel pulse shape $p(t)$

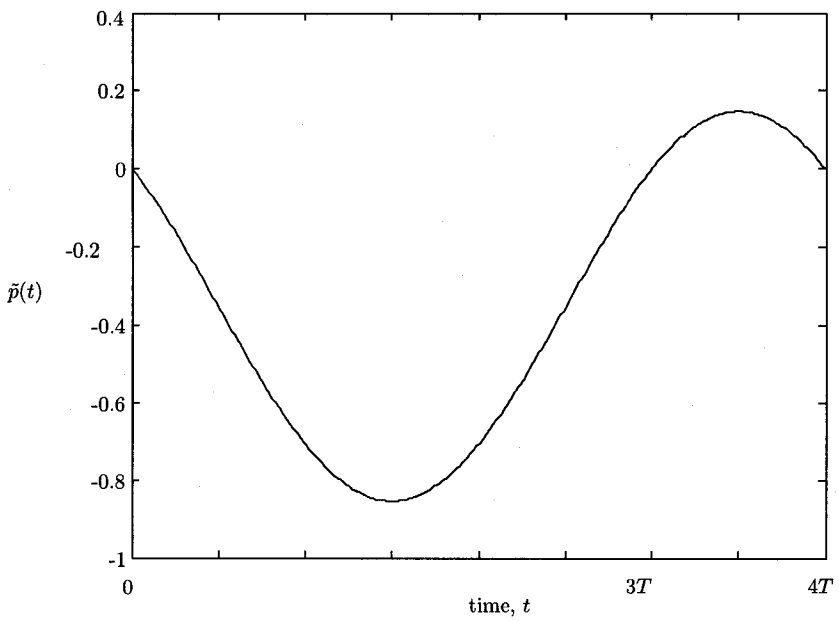

b.Quadrature channel pulse shape $\tilde{p}(t)$

Fig. 4.3: Impulse response of Inphase (a) and Quadrature (b) pulses for Coded, $L = 2$, generalized MSK signals.

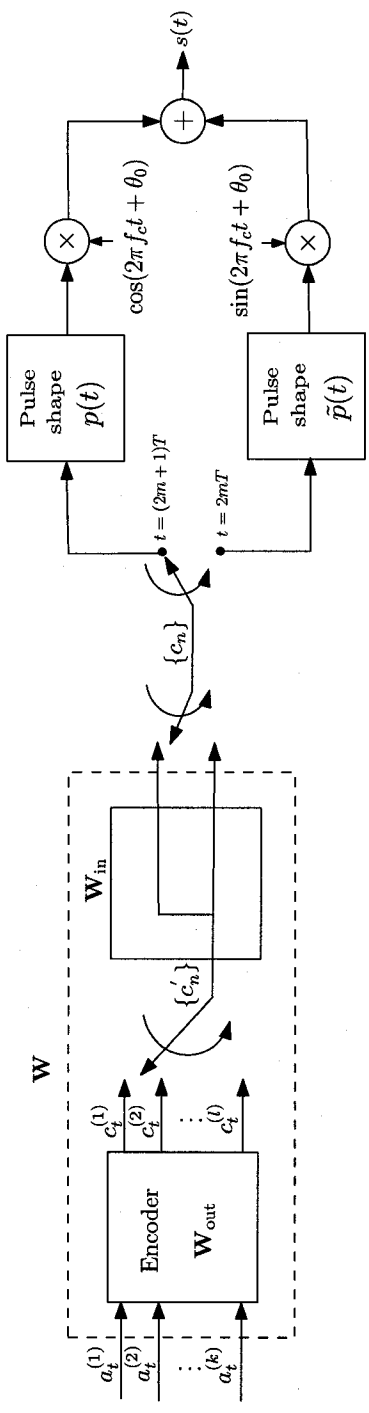

Fig. 4.4: Equivalent I-Q modulator for coded generalized MSK signals with modulation memory $L = 2$. Pulses $p(t)$ and $\tilde{p}(t)$ are as given in (4.25) and (4.26).

$f_cT \gg 1$) for recovering the coded symbols c_n. Fig. 4.5 shows a linear coherent I-Q receiver used to (soft) detect coded generalized MSK with modulation memory $L = 2$. This receiver is similar to that of MSK (Fig. 2.7.c), except that a different predetection filter on each channel is used instead of the cosine pulse shape.

Let us assume the received signal $r(t)$ is simply the transmitted signal $s(t)$ corrupted by an additive white Gaussian noise process $n(t)$ with power spectrum $\mathcal{N}_0/2$. Thus the received signal can be expressed as

$$r(t) = s(t) + n(t). \tag{4.36}$$

We can express $n(t)$ in I-Q form as $n(t) = n_I(t)\cos(2\pi f_c t) - n_Q(t)\sin(2\pi f_c t)$, where $n_I(t)$ and $n_Q(t)$ are independent white Gaussian noise processes with power spectrum $\mathcal{N}_o$.
It has been shown in Section 4.3 that the transmitted signal $s(t)$ for generalized MSK with modulation memory $L = 2$, can be expressed as an I-Q signal, where each channel waveform is a PAM signal with a pulse of finite duration. Therefore, the inphase and quadrature components of the received signal are then both PAM signals with overlapping pulse shapes corrupted by additive white Gaussian noise. For each of these I-Q components separately, it is well-known [34, p. 600] that filtering the signal with filter matched to the pulse shape and sampling the filtered signal at the end of the symbol periods produces a set of *sufficient statistics* for the symbol stream, from which the symbols can then be recovered. Fig. 4.5 shows a receiver that implements this approach to arrive at an optimal receiver. For the I and Q channels we employ filters matched to $p(t)$ and $\tilde{p}(t)$ whose outputs are sampled at $t = (2m+1)T$ and $t = 2mT$ to generate quantities z_{2m+1} and z_{2m}, respectively. We are going to consider only the detection of the inphase channel signal, since similar analysis for quadrature channel signal leads to the same results.

The sampled output of the matched filter in the inphase channel (assuming $f_cT \gg 1$)

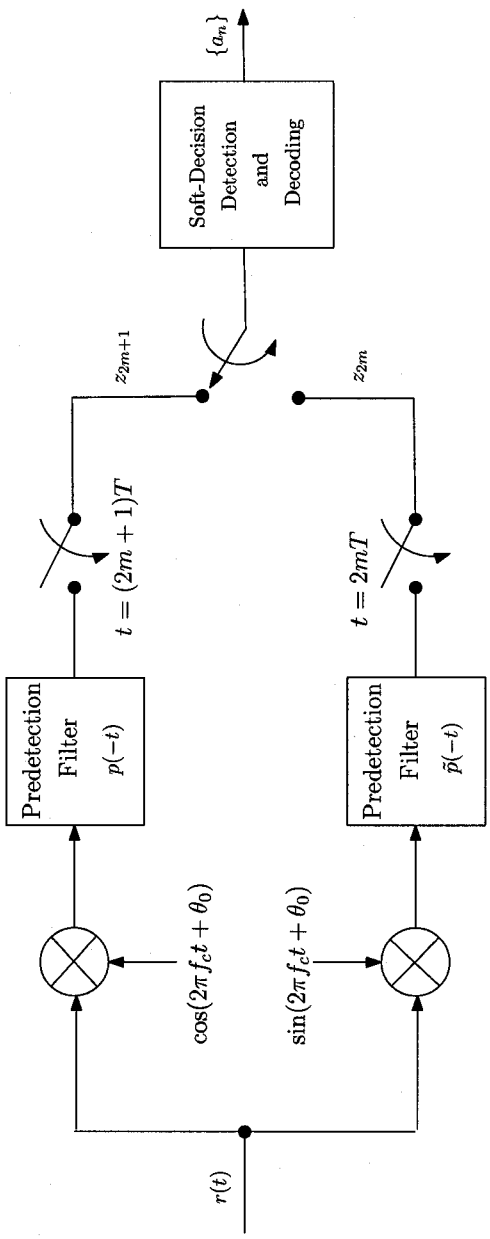

Fig. 4.5: Simple I-Q receiver for precoded generalized MSK signals with pulse shape of length $2T$ coded by double repetition code as inner encoder. The decoder used here is the inverse of the cascaded encoder $\mathbf{W}$.

at $t = (2m+1)T$, is given by

$$z_{2m+1} = \sqrt{\frac{E}{2T}} \sum_k \left\{ c_{2k+1} \int_{-\infty}^{\infty} p(t - [2m+1]\,T) p(t - [2k+1]\,T)\, dt \right\} + n_{2m+1}, \quad (4.37)$$

where n_{2m+1} is a zero-mean Gaussian random variable given by

$$n_{2m+1} = \frac{1}{2} \int_{-\infty}^{\infty} n_I(t) p(t - [2m+1])\, dt. \quad (4.38)$$

We can simplify (4.37) by noting that

$$\int_{-\infty}^{\infty} p(t - [2m+1]\,T) p(t - [2k+1]\,T)\, dt = \begin{cases} T, & m = k; \\ \gamma, & |m-k| = 1; \\ 0, & \text{otherwise}, \end{cases} \quad (4.39)$$

where γ is given by

$$\begin{aligned} \gamma &= \int_{-\infty}^{\infty} p(t - [2m+1]\,T) p(t - [2m-1]\,T)\, dt, \\ &= \int_{-\infty}^{\infty} p(t - [2m+1]\,T) p(t - [2m+3]\,T)\, dt. \end{aligned} \quad (4.40)$$

In that case,

$$z_{2m+1} = \sqrt{\frac{ET}{2}} c_{2m+1} + \sqrt{\frac{ET}{2}} \underbrace{\gamma\,(c_{2m-1} + c_{2m+3})}_{\text{ISI}} + n_{2m+1}. \quad (4.41)$$

As expected, since the duration of the pulse $p(t)$ extends more than two symbol periods, the matched filter's sampled output z_{2m+1} depends on more than one symbol.

The sampled random variables $\{n_{2k+1}\}$ are in general zero-mean possibly *correlated* Gaussian random variables with

$$\begin{aligned} \mathcal{E}\{n_{2i-1} n_{2j-1}\} &= \frac{\mathcal{N}_o}{4} \int_{-\infty}^{\infty} p(t - [2i-1]\,T) p(t - [2j-1]\,T)\, dt \\ &= \begin{cases} \frac{\mathcal{N}_o}{4} T, & i = j; \\ \frac{\mathcal{N}_o}{4} \gamma, & |i-j| = 1; \\ 0, & \text{otherwise}. \end{cases} \end{aligned} \quad (4.42)$$

From (4.40) we have that,

$$\gamma = \int_{-\infty}^{\infty} p(t-[2m-1]\,T)p(t-[2m+1]\,T)\,dt,$$

where $p(t)$ is given by (4.25). Therefore,

$$\begin{aligned}
\gamma &= \int_{-\infty}^{\infty} \Big\{C_0(t-[2m-1]\,T) - C_1(t-[2m-2]\,T)\Big\} \\
&\qquad \times \Big\{C_0(t-[2m+1]\,T) - C_1(t-2mT)\Big\}\,dt \\
&= \int_{-\infty}^{\infty} C_0(t-[2m-1]\,T)C_0(t-[2m+1]\,T)\,dt \\
&\quad + \int_{-\infty}^{\infty} \underbrace{C_1(t-[2m-2]\,T)C_1(t-2mT)}_{=0}\,dt \\
&\quad - \int_{-\infty}^{\infty} \underbrace{C_1(t-[2m-2]\,T)C_0(t-[2m+1]\,T)}_{=0}\,dt \\
&\quad - \int_{-\infty}^{(2m+2)T} C_0(t-[2m-1]\,T)C_1(t-2mT)\,dt \\
&= \int_{(2m+1)T}^{(2m+2)T} C_0(t-[2m-1]\,T)C_0(t-[2m+1]\,T)\,dt \\
&\quad - \int_{2mT}^{(2m+1)T} C_0(t-[2m-1]\,T)C_1(t-2mT)\,dt.
\end{aligned}$$

By a change of variables ($t' = t-(2m+1)T$) in the first integral and ($t' = t-2mT$) in the second integral we get

$$\begin{aligned}
\gamma &= \int_0^T C_0(t)C_0(t+2T)\,dt - \int_0^T C_1(t)C_0(t+T)\,dt \\
&= \int_0^T S(t)S(t+T)S(t+2T)S(t+3T)\,dt - \int_0^T S(t)S(t+T)S(t+2T)S(t+3T)\,dt \\
&= 0.
\end{aligned}$$

From this, the sampled output of the matched filter for the inphase channel at $t =$

$(2m+1)T$ (i.e., z_{2m+1}) reduces simply to

$$z_{2m+1} = \sqrt{\frac{ET}{2}} c_{2m+1} + n_{2m+1} \tag{4.43}$$

where $\{n_{2k+1}\}$ are *uncorrelated* zero-mean Gaussian random variables (hence independent) with variance equal to $\mathcal{N}_o T/4$.

A similar analysis shows that for quadrature channel, the sampled output of the matched filter at $t = 2mT$, is given by

$$z_{2m} = \sqrt{\frac{ET}{2}} c_{2m} + n_{2m}, \tag{4.44}$$

where $\{n_{2k}\}$ is a sequence of independent identically distributed zero-mean Gaussian random variables with variance $\mathcal{N}_o T/4$. Therefore, the detection problem for the recovery of the symbols sequence $\{c_n\}$ from the decision variable sequence $\{z_k\}$ is one corresponding to *memoryless* linear modulation.

If the sequence $\{z_k\}$ is the input to the soft-decision detector and decoder for the $\{a_k\}$ symbol stream, then the bit error probability (for high SNR) $\mathcal{P}_{b,\text{asymp}}$ can be expressed as [34, p.487]

$$\begin{aligned} \mathcal{P}_{b,\text{asymp}} &= Q\left(\frac{\sqrt{ET/2H_{\min}^W}}{\sqrt{\mathcal{N}_o T/4}}\right) \\ &= Q\left(\sqrt{2R_c H_{\min}^W \frac{E_b}{\mathcal{N}_o}}\right), \end{aligned} \tag{4.45}$$

Using the result in Theorem 1, we have that $\mathbf{NSFED} = 2R_c H_{\min}^W$. Therefore $\mathcal{P}_{b,\text{asymp}}$ can be expressed as

$$\mathcal{P}_{b,\text{asymp}} = Q\left(\sqrt{\mathbf{NSFED}\frac{E_b}{\mathcal{N}_o}}\right). \tag{4.46}$$

It is interesting to note that the simple I-Q receiver, depicted in Fig. 4.5, has performance that is equivalent to the Viterbi receiver, where the bit error rate of the latter (for high SNR) is also given by (4.46). Therefore the receiver shown in Fig. 4.5 is asymptotically *optimal* in the sense of minimizing the asymptotic probability of error.

If both encoders **W** applied to precoded MSK and generalized MSK with pulse shape $h(t)$ of length $2T$ are identical, the expression in (4.45) is equivalent to the asymptotic bit error probability performance evaluated for OQPSK-MSK receiver for recovering $\{a_n\}$ symbols. The overall asymptotic performance for coded MSK (using soft-decision decoding) is also given by (4.46) (i.e., no degradation in performance when compared to coded MSK). This result has been achieved by the use of a simple double repetition code.

It can be shown that other possible inphase and quadrature pulses can be used to express coded generalized MSK with pulse shapes $h(t)$ of length $2T$, as an I-Q signal. These pulses, however, may cause a degradation in the performance and ISI in the demodulated signal at the receiver. Table 4.1 shows these pulses with the corresponding conditions for the coded symbols to preserve the constant envelope property of the signal. The relation between Euclidean distance and Hamming distance, and the existence of ISI in the sampled outputs of the matched filter are also shown.

4.3.2 Design of A Simplified Receiver

The optimum receiver's objective is to recover the stream of information symbols (the $\{a_n\}$ sequence) minimizing the probability of an information symbol error. The optimal receiver for generalized MSK signals cannot make decisions on any isolated symbol without taking the entire sequence of transmitted symbols into account. This requires a Maximum Likelihood Sequence Estimator (MLSE), that is efficiently implemented using the Viterbi algorithm as depicted in Fig. 4.6.*a*. The Viterbi algorithm chooses the information sequence ($\{a_n\}$) that maximizes the following correlation metric

$$Z_n(\mathbf{a}_n, \phi_n) = \int_{nT}^{(n+1)T} r(t)\cos(2\pi f_c t + \phi(t) + \phi_n)\, dt,$$

which can be obtained from a coherent quadrature receiver using a bank of matched filters and samplers [42]. It can be shown [42] that for binary generalized MSK of modulation memory L, there are 2^{L+1} different values of $Z_n(\mathbf{a}_n, \phi_n)$ computed in each signal interval.

Inphase Pulse Shape $p(t)$	Quadrature Pulse Shape $\tilde{p}(t)$	Condition on c_n for $t \in [2kT, (2k+2)T]$	**NSED** (Performance)	Inter-Symbol Interference (ISI)
$\pm(C_0(t) - C_1(t+T))$	$\pm(C_1(t-3T) - C_0(t))$	$c_{2k+1}c_{2k-1} = c_{2k}c_{2k-2}$	$= 2R_cH_W$	No
$\pm(C_0(t) + C_1(t+T))$	$\pm(C_1(t-3T) + C_0(t))$	$c_{2k+1}c_{2k-1} = -c_{2k}c_{2k-2}$	$\neq 2R_cH_W$	Yes

Table 4.1: Comparisons of different possible inphase and quadrature channel pulses ($p(t)$ and $\tilde{p}(t)$) in terms of coded symbol constraint, **NSED**, and existence of ISI.

Using the Laurent decomposition of generalized MSK as a superposition of PAM signals suggests another strategy for optimal detection of the information sequence which is depicted in Fig. 4.6.*b*. This receiver was derived by Kaleh [16] where it was shown that the complexity of the receiver (the state transitions and trellis diagram) is nearly the same as the one shown in Fig.4.6.*a*.

It is well known [43] that the performance of the optimum receiver based on the Viterbi algorithm (i.e., the bit error probability $\mathcal{P}_b$) is upper bounded by

$$\mathcal{P}_b \leq \sum_{d=d_{\min}}^{\infty} C_d \, Q\left(\sqrt{d^2 \frac{E_b}{\mathcal{N}_o}}\right),$$

where $d^2 = \mathbf{NSED}(i,j)$, $d^2_{\min} = \mathbf{NSFED}$ is the smallest Euclidean distance among all distances in the set of all error events, and C_d is a constant.

It is usually difficult to obtain an exact expression of $\mathcal{P}_b$ for all SNR. Therefore, an approximation is preferably made for high SNR to obtain the asymptotic performance of the overall system, which is given by

$$\mathcal{P}_{b,\text{asymp}} = Q\left(\sqrt{\mathbf{NSFED}\frac{E_b}{\mathcal{N}_o}}\right).$$

Let us consider the case of precoded generalized MSK with pulse shape $h(t)$ of length $2T$, where only a double repetition code is applied as a channel encoder (i.e., the outer encoder $\mathbf{W}_{\text{out}}$ is the identity mapper). Using (4.21) the normalized minimum Euclidean distance **NSFED** is equal to 2. Therefore, the asymptotic performance of the overall coded system can be approximated by

$$\mathcal{P}_{b,\text{asymp}} = Q\left(\sqrt{\frac{2E_b}{\mathcal{N}_o}}\right). \tag{4.47}$$

The optimum receiver based on MLSE is considered complex in terms of the computational load and hardware implementation. Therefore, we would like to propose in this section a simplified receiver in which it is able to detect the information symbols with minimum probability of error. Let us consider again the case where no outer encoder is applied. Fig. 4.6.*c* shows a block diagram of the proposed simple receiver. It will be

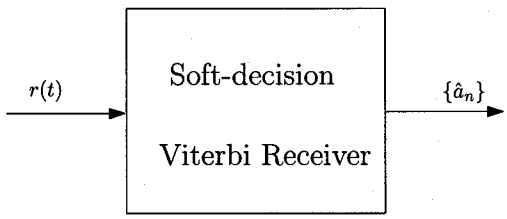

a. Optimum MLSE receiver implemented using Viterbi algorithm.

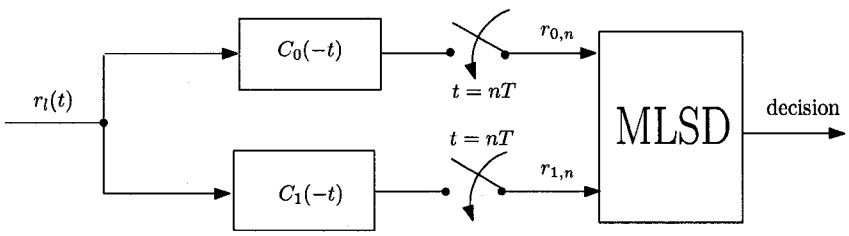

b. Optimum receiver based on Laurent decomposition of generalized MSK as superposition of PAM signals. $r_l(t)$ is the lowpass equivalent of the receiver signal.

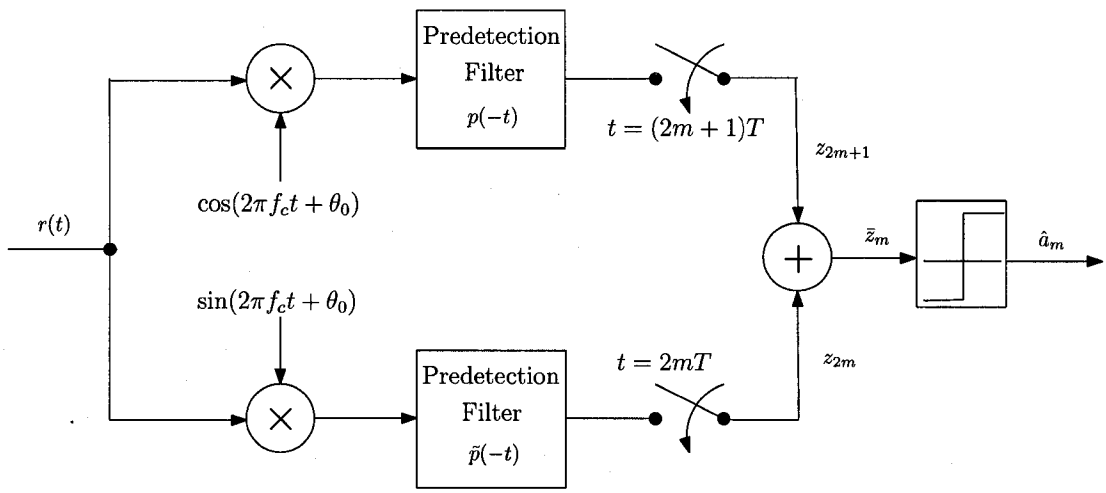

c. Simple *I-Q* receiver that uses hard decision detection.

Fig. 4.6: Three different *optimum* receivers used to detect generalized MSK with pulse shapes of duration $2T$ employing a double repetition code only.

demonstrated that *symbol-by-symbol* detection is optimal in the sense of minimizing the probability of error of detecting the information symbol a_n.

The sampled output of the matched filter on each channel, z_{2m+1} and z_{2m}, is given by (4.43) and (4.44) respectively. Since no outer encoding is presented here, the symbol $c_{2m+1} = c_{2m} = a_m$. Adding z_{2m+1} and z_{2m} we produce the decision variable $\bar{z}_m$ given by

$$\bar{z}_m = \sqrt{2ET}a_m + \bar{n}_m, \tag{4.48}$$

where a_m (the information symbols) are assumed to be independent identically distributed that takes values ± 1, with equal probabilities, and the sequence $\{\bar{n}_m = n_{2m+1} + n_{2m}\}$ are independent zero-mean Gaussian random variables with variance $\mathcal{N}_o T/2$. If $\bar{z}_m$ is passed into a slicer (hard-decision), then the probability of error of detection a_m is given by

$$\begin{aligned} \mathcal{P}_b &= Q\left(\frac{\sqrt{2ET}}{\sqrt{\mathcal{N}_o T/2}}\right) \\ &= Q\left(\sqrt{\frac{4E}{\mathcal{N}_o}}\right), \end{aligned}$$

and since $E = E_b/2$ then the probability of error $\mathcal{P}_e$ can be written in terms of $E_b/\mathcal{N}_o$ as

$$\mathcal{P}_b = Q\left(\sqrt{\frac{2E_b}{\mathcal{N}_o}}\right). \tag{4.49}$$

Consider the case of duobinary MSK. The simple I-Q receiver depicted in Fig. 4.6.*c* has an asymptotic performance that is equivalent to the one evaluated for MLSE receiver. Therefore, this simple receiver is asymptotically optimal.

It must be noted that the expression given in (4.49) is also valid for low SNR, in contrast to the MLSE receiver where it is difficult to derive a closed expression for $\mathcal{P}_e$ at low SNR. A coding gain of at least 0.63 dB could be achieved compared to the uncoded duobinary MSK (where **NSFED** ≈ 1.73). Therefore, a great reduction in the receiver complexity and an increase in the power efficiency have been achieved by the use of a

simple double repetition code. The price of these improvements is achieved at the cost of increasing the bandwidth compared to the uncoded case. Nevertheless, error control coding is usually applied in all practical communication systems, therefore the comparison in bandwidth-efficiency between different modulation schemes must be made for the same code rate of the channel encoder. Therefore, we believe that considering spectrum, performance and receiver complexity, precoded generalized MSK with modulation memory $L = 2$ employing double repetition code is an improvement over simple MSK.

4.4 Simple Modulator/Demodulator Design of Length $3T$ Coded Generalized MSK

Since the number of Laurent pulses, i.e., $C_k(t)$, increases exponentially as the memory L increases, the structure of the Viterbi (optimum) receiver becomes more complex and the amount of needed computations increases. We will consider in this section a new method of representing certain coded generalized MSK with modulation memory $L = 3$, involving "quadruple" repetition code, as an I-Q signal. Such coded signals can then be demodulated using a simple I-Q receiver.

Theorem 4. *Let C_W be any rate R_c binary code for which the coded bits satisfy the relationship that for all k,*

$$c_{4k} = c_{4k+1} = c_{4k+2} = c_{4k+3}. \tag{4.50}$$

The **NSED**(i, j)*, for generalized MSK signals with pulse shape duration $3T$, and the Hamming distance between corresponding sequences generated by C_W are related by*

$$\mathbf{NSED}(i, j) = 2R_c H_W(\mathbf{c}^i, \mathbf{c}^j). \tag{4.51}$$

Proof. See Appendix C. □

Equation (4.50) suggests that a quadruple repetition code can be applied as an inner encoder to satisfy (4.51). Fig. 4.7 shows coded generalized MSK system with modulation memory $L = 3$ where the channel encoder is decomposed into outer encoder and a quadruple repetition encoder (inner encoder). The outer rate-R_o encoder $\mathbf{W}_{\text{out}}$ with memory ν_o and inner quadruple repetition encoder are combined into an encoder $\mathbf{W}$ with code rate

$$R_c = \frac{R_o}{4}. \tag{4.52}$$

Again, any linear block encoder and almost all convolutional encoders (except possibly catastrophic encoders) could be used as an outer encoder. We shall consider here, outer encoders that are linear convolutional encoders.

Theorem 5. *Let $C_{W_{\text{out}}}$ be any rate-R_o ($R_0 = k/l$, $k \leq l$) outer convolutional code cascaded with a quadruple repetition code as an inner code, and let $\mathbf{W}_{\text{out}}(D)$ and $\mathbf{W}(D)$ be the generator matrices of the outer and cascaded encoders respectively. Let the entries of the generator matrix $\mathbf{W}^o(D)$ be $w^o_{i,j}(D)$ for $i \in \{1, 2, ..., k\}$ and $j \in \{1, 2, ..., l\}$. If $\mathbf{W}_{\text{out}}(D)$ is a polynomial matrix then*

$$\mathbf{W}(D) = \begin{pmatrix} w^o_{11}(D) & w^o_{11}(D) & w^o_{11}(D) & w^o_{11}(D) & \dots & w^o_{1l}(D) & w^o_{1l}(D) & w^o_{1l}(D) & w^o_{1l}(D) \\ w^o_{21}(D) & w^o_{21}(D) & w^o_{21}(D) & w^o_{21}(D) & \dots & w^o_{2l}(D) & w^o_{2l}(D) & w^o_{2l}(D) & w^o_{2l}(D) \\ \vdots & \vdots & \vdots & \vdots & \ddots & \vdots & \vdots & \vdots & \vdots \\ w^o_{k1}(D) & w^o_{k1}(D) & w^o_{k1}(D) & w^o_{k1}(D) & \dots & w^o_{kl}(D) & w^o_{kl}(D) & w^o_{kl}(D) & w^o_{kl}(D) \end{pmatrix}, \tag{4.53}$$

where the combined encoder $\mathbf{W}(D)$ is a rate-$k/4l$ convolutional encoder.

Proof. Except for the case of $R_0 = 1$ (i.e., $k = l = 1$), the two generator matrices of the inner and outer encoders cannot be multiplied in the $\mathcal{D}$-transform representation to find the generator matrix of the cascaded encoder (since $l \neq 1$) (i.e., $\mathbf{W}(D) \neq \mathbf{W}_{\text{in}}(D)\mathbf{W}_{\text{out}}(D)$). Instead one has to multiply the semi-infinite matrices $\mathbf{W}_{\text{out}}$ and $\mathbf{W}_{\text{in}}$ to determine the generator matrix of the cascaded encoder $\mathbf{W} = \mathbf{W}_{\text{out}}\mathbf{W}_{\text{in}}$. However, the matrix $\mathbf{W}(D)$ can be found by considering $l \times 4l$ sub-matrices instead of 1×4 sub-matrices in $\mathbf{W}_{\text{in}}$. The

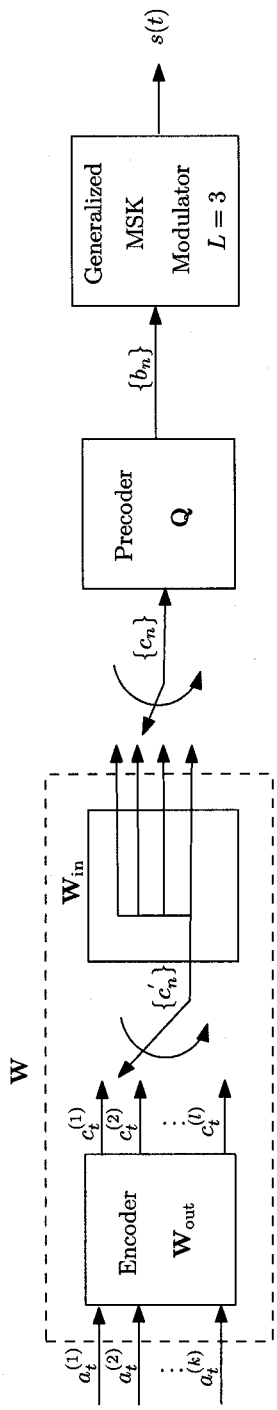

Fig. 4.7: A decomposition of encoder **W** for coded generalized MSK system with modulation memory $L = 3$. Quadruple (rate-1/4) repetition code is used as an inner encoder.

resulting matrices $\mathbf{W}^o(D)$ and $\mathbf{W}^l_{\text{in}}(D)$ then have matched rates and can be multiplied. The inner generator matrix can be written as

$$\mathbf{W}^l_{\text{in}} = \begin{pmatrix} 1111 & 0000 & \dots & 0000 & & \\ 0000 & 1111 & 0000 & \dots & 0000 & \\ 0000 & 0000 & 1111 & 0000 & \dots & 0000 \\ & & & \ddots & \ddots & \ddots \end{pmatrix}.$$

Instead of 1×4 sub-matrices we consider l times larger ones, $l \times 4l$, and express the matrix in the $\mathcal{D}$-transform representation which is given by

$$\mathbf{W}_{\text{in}}(D) = \begin{pmatrix} 1 & 1 & 1 & 1 & 0 & 0 & 0 & 0 & \dots & 0 & 0 & 0 & 0 & 0 & 0 & 0 & 0 \\ 0 & 0 & 0 & 0 & 1 & 1 & 1 & 1 & \dots & 0 & 0 & 0 & 0 & 0 & 0 & 0 & 0 \\ \vdots & \vdots & & & & & & & \ddots & & & & & & & \vdots & \vdots \\ 0 & 0 & 0 & 0 & 0 & 0 & 0 & 0 & \dots & 0 & 0 & 0 & 0 & 1 & 1 & 1 & 1 \end{pmatrix}. \tag{4.54}$$

The outer generator matrix is

$$\mathbf{W}_{\text{out}}(D) = \begin{pmatrix} w^o_{11}(D) & w^o_{12}(D) & \dots & w^o_{1l}(D) \\ w^o_{21}(D) & w^o_{21}(D) & \dots & w^o_{2l}(D) \\ \vdots & \vdots & \ddots & \vdots \\ w^o_{k1}(D) & w^o_{k2}(D) & \dots & w^o_{kl}(D) \end{pmatrix}. \tag{4.55}$$

Using (4.54) and (4.55), the semi-infinite matrix multiplication $\mathbf{W} = \mathbf{W}_{\text{out}}\mathbf{W}_{\text{in}}$ can be equivalently represented by

$$\mathbf{W}(D) = \begin{pmatrix} w^o_{11}(D) & w^o_{11}(D) & w^o_{11}(D) & w^o_{11}(D) & \dots & w^o_{1l}(D) & w^o_{1l}(D) & w^o_{1l}(D) & w^o_{1l}(D) \\ w^o_{21}(D) & w^o_{21}(D) & w^o_{21}(D) & w^o_{21}(D) & \dots & w^o_{2l}(D) & w^o_{2l}(D) & w^o_{2l}(D) & w^o_{2l}(D) \\ \vdots & \vdots & \vdots & \vdots & \ddots & \vdots & \vdots & \vdots & \vdots \\ w^o_{k1}(D) & w^o_{k1}(D) & w^o_{k1}(D) & w^o_{k1}(D) & \dots & w^o_{kl}(D) & w^o_{kl}(D) & w^o_{kl}(D) & w^o_{kl}(D) \end{pmatrix}.$$

□

Corollary 2. *Let encoder $\mathbf{W}(D)$ be any $k \times 4l$ polynomial matrix. If $\mathbf{W}$ is partitioned into (k, l) convolutional encoder $\mathbf{W}_{\text{out}}(D)$ and a quadruple repetition encoder as illustrated in Fig. 4.7, then*

$$\mathbf{NSED}(i, j) = 2\frac{k}{l} H_{W_{\text{out}}}(\mathbf{c}'^i, \mathbf{c}'^j). \tag{4.56}$$

Proof. Using a quadruple repetition code times the Hamming distance of the outer code $\mathbf{W}_{\text{out}}(D)$ by a factor of 4, i.e., $H_W(\mathbf{c}^i, \mathbf{c}^j) = 4H_{W_{\text{out}}}(\mathbf{c}'^i, \mathbf{c}'^j)$. Therefore, from (4.51)

$$\begin{aligned} \mathbf{NSED}(i,j) &= 2R_c H_W(\mathbf{c}^i, \mathbf{c}^j) \\ &= 2\frac{R_o}{4}\left[4H_{W_{\text{out}}}(\mathbf{c}'^i, \mathbf{c}'^j)\right] \\ &= 2R_o H_{W_{\text{out}}}(\mathbf{c}'^i, \mathbf{c}'^j), \end{aligned} \tag{4.57}$$

where $R_o = k/l$ is the rate of outer encoder $\mathbf{W}_{\text{out}}(D)$. □

The immediate consequence of (4.56) is that convolutional codes $C_{W_{\text{out}}}$ with large minimum Hamming distance ($H_{\text{min}}^{W_{\text{out}}}$) are good candidates to generate signal waveforms (generalized MSK signals with pulse shapes $h(t)$ of length $3T$) with large **NSFED**. Theorem 4 shows that employing a quadruple repetition code to the encoding process, the dependency of the Euclidean distance on the premodulation filter $h(t)$ can also be eliminated. Again, the main impact, then, of a choice of pulse shape relates to the spectral properties of the signals.

Let us now consider the effect of applying a quadruple repetition code to the inphase and quadrature channel signals. The inphase channel signal is equal to

$$\begin{aligned} I(t) = \sqrt{\frac{2E}{T}}\cos\phi(t) &= \sqrt{\frac{2E}{T}}\Bigg\{\sum_{k=0}^{\infty} c_{4k-3}C_0(t-[4k-3]\,T) \\ &+ \sum_{k=0}^{\infty} c_{4k-1}C_0(t-[4k-1]\,T) + \sum_{k=0}^{\infty} v_{4k}C_1(t-4kT) \\ &+ \sum_{k=0}^{\infty} v_{4k+2}C_1(t-[4k-2]\,T) + \sum_{k=0}^{\infty} x_{4k}C_2(t-4kT) \\ &+ \sum_{k=0}^{\infty} x_{4k+2}C_2(t-[4k+2]\,T) + \sum_{k=0}^{\infty} y_{4k+1}C_3(t-[4k+1]\,T) \\ &+ \sum_{k=0}^{\infty} y_{4k+3}C_3(t-[4k+3]\,T)\Bigg\} \end{aligned} \tag{4.58}$$

and the quadrature channel signal is equal to

$$Q(t) = \sqrt{\frac{2E}{T}}\sin\phi(t) = \sqrt{\frac{2E}{T}}\Bigg\{-\sum_{k=0}^{\infty} c_{4k}C_0(t-4kT)$$

$$
\begin{aligned}
&-\sum_{k=0}^{\infty} c_{4k+2}C_0(t-[4k+2]\,T)+\sum_{k=0}^{\infty} v_{4k+1}C_1(t-[4k+1]\,T)\\
&+\sum_{k=0}^{\infty} v_{4k+3}C_1(t-[4k+3]\,T)+\sum_{k=0}^{\infty} x_{4k+1}C_2(t-[4k+1]\,T)\\
&+\sum_{k=0}^{\infty} x_{4k+3}C_2(t-[4k+3]\,T)-\sum_{k=0}^{\infty} y_{4k}C_3(t-4kT)\\
&-\sum_{k=0}^{\infty} y_{4k+2}C_3(t-[4k+2]\,T)\Big\}. \qquad (4.59)
\end{aligned}
$$

Applying (C.1)–(C.3) to (4.58) and (4.59), the inphase and quadrature channel signals each reduces to a PAM signal with finite pulse duration that is given by

$$I(t)=\sqrt{\frac{2E}{T}}\sum_{k} c_{4k+1}p(t-[4k+1]T), \qquad (4.60)$$

and

$$Q(t)=\sqrt{\frac{2E}{T}}\sum_{k} c_{4k+2}\tilde{p}(t-[4k+2]T), \qquad (4.61)$$

where the pulses $p(t)$ and $\tilde{p}(t)$ are expressed as

$$
\begin{aligned}
p(t) \;=\;& C_0(t)+C_0(t-2T)-C_1(t+T)-C_1(t-T)\\
&+C_2(t+T)+C_2(t-5T)+C_3(t-4T)+C_3(t-2T), \qquad (4.62)
\end{aligned}
$$

and

$$
\begin{aligned}
\tilde{p}(t) \;=\;& -C_0(t+2T)-C_0(t)+C_1(t-T)+C_1(t-3T)\\
&-C_2(t+T)-C_2(t-T)-C_3(t+2T)-C_3(t-4T). \qquad (4.63)
\end{aligned}
$$

The functions $C_0(t)$, $C_1(t)$, $C_2(t)$, and $C_3(t)$ are the Laurent pulses given by (3.29), (3.30), (3.31) and (3.32) respectively. In this case, it is possible to express the generalized MSK signal as

$$s(t)=I(t)\cos(2\pi f_c t+\theta_0)-Q(t)\sin(2\pi f_c t+\theta_0),$$

where the inphase signal $I(t)$ and quadrature signal $Q(t)$ are given by (4.60) and (4.61) respectively.

As an example, Fig. 4.8 shows a plot of $p(t)$ and $\tilde{p}(t)$ for coded TFM signal. Again, this pulse has a duration that is greater than $2T$. Therefore, any precoded generalized MSK with modulation memory $L = 3$ that are encoded by a quadruple repetition code can be expressed as an I-Q signal where each channel waveform is a PAM signal with finite ISI. Fig. 4.9 shows a block diagram of a simple I-Q modulator that generates such coded signals.

4.4.1 Simplified Detection for Length $3T$ Coded generalized MSK

The exact I-Q representation of coded generalized MSK with modulation memory $L = 3$ using a quadruple repetition code, suggests another strategy of demodulating the coded signal (in AWGN channel) using a simplified I-Q receiver similar to the one designed for coded generalized MSK with pulse shapes of duration $2T$. It is to be expected that inter-symbol interference would likely exist at the output of the matched filter and thus post equalization would be required to achieve the best performance. It will be shown however that, if $h(t)$ satisfies a certain condition, inter-symbol interference can totally be eliminated, therefore avoiding the use of an equalizer, which simplifies the detection problem.

It will be shown that a simple I-Q receiver can be used to demodulate the coded signal where the predetection filter on each channel is matched to the pulses $p(t)$ and $\tilde{p}(t)$ given in (4.62) and (4.63), respectively. The output of the matched filter is then sampled every $4T$ seconds (i.e., at $t = (4m+1)T$ on the I channel and $t = (4m+2)T$ on the Q channel. Again, let us consider the detection of the inphase channel signal, since similar analysis applied to quadrature channel signal leads to the same results.

Let us assume the received signal is given by (4.36), then the sampled output of the

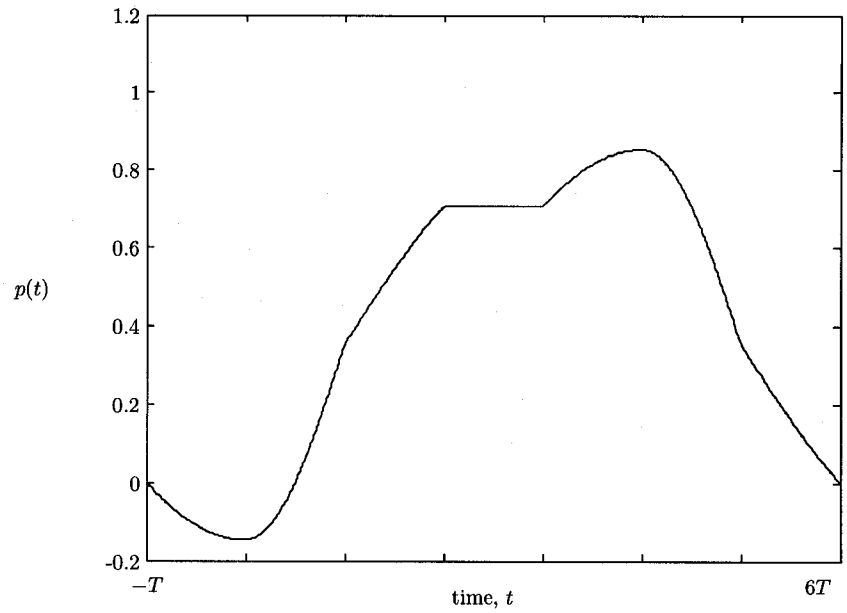

a. Inphase channel pulse shape $p(t)$

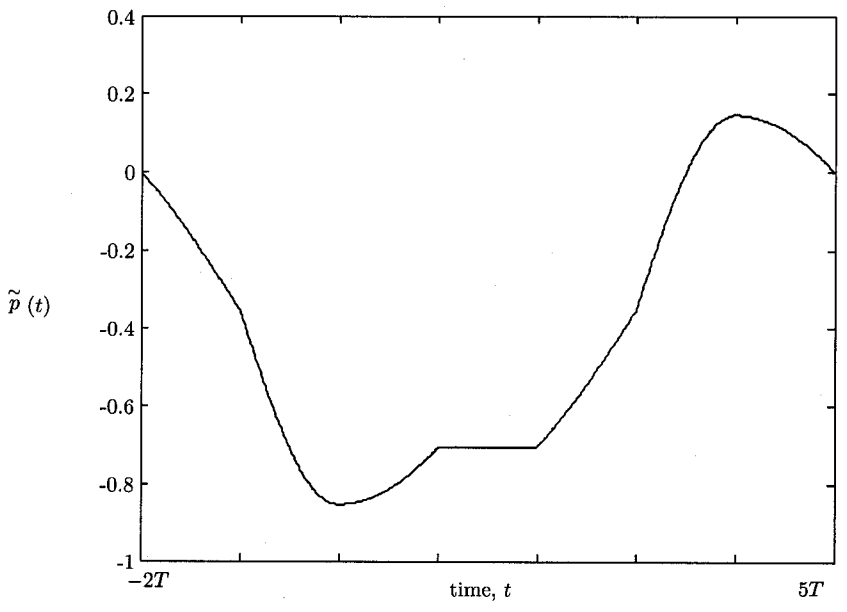

*b.*Quadrature pulse shape $\tilde{p}$ (t)

Fig. 4.8: The pulse shape of *a.* inphase channel $p(t)$, *b.* quadrature channel $\tilde{p}(t)$, for coded TFM signal. Pulses $p(t)$ and $\tilde{p}(t)$ are as given in (4.62) and (4.26).

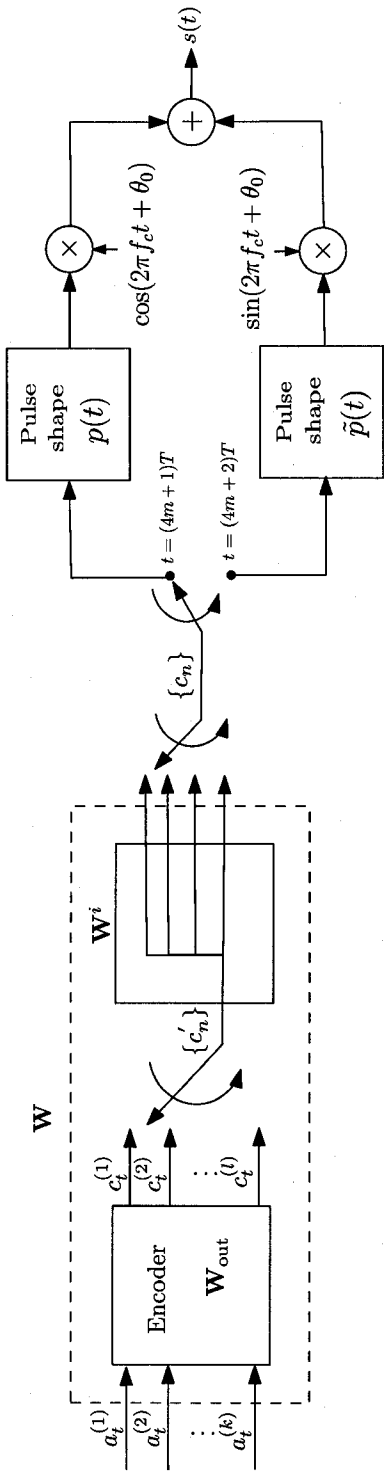

Fig. 4.9: Equivalent I-Q modulator for generating coded generalized MSK with modulation memory $L = 3$

predetection (matched) filter in the inphase channel at $t = (4m+1)T$ is

$$z_{4m+1} = \sqrt{\frac{E}{2T}} \sum_k \left\{ c_{4k+1} \int_{-\infty}^{\infty} p(t-[4m+1]\,T) p(t-[4k+1]\,T)\; dt \right\} + n_{4m+1}, \tag{4.64}$$

where n_{4m+1} is a zero-mean Gaussian random variable given by

$$n_{4m+1} = \frac{1}{2} \int_{-\infty}^{\infty} n_I(t) p(t-[4m+1])\; dt. \tag{4.65}$$

We can simplify (4.64) by noting that

$$\int_{-\infty}^{\infty} p(t-[4m+1]\,T) p(t-[4k+1]\,T)\; dt = \begin{cases} 2T, & m=k; \\ \beta, & |m-k|=1; \\ 0, & \text{otherwise}, \end{cases} \tag{4.66}$$

where β is given by

$$\begin{aligned} \beta &= \int_{-\infty}^{\infty} p(t-[4k+1]\,T) p(t-[4k+5]\,T)\; dt \\ &= \int_{-\infty}^{\infty} p(t-[4k-3]\,T) p(t-[4k+1]\,T)\; dt. \end{aligned} \tag{4.67}$$

In that case,

$$z_{4m+1} = \sqrt{2ET} c_{4m+1} + \sqrt{2ET} \underbrace{\beta\,(c_{4m-3} + c_{4m+5})}_{\text{ISI}} + n_{4m+1}. \tag{4.68}$$

As expected, the output of the demodulator (matched filter) at the sampling instants is corrupted by ISI as indicated by (4.68) which affects a finite number of symbols.

The sampled random variables $\{n_{4k+1}\}$ are zero-mean possibly correlated Gaussian random variables with

$$\begin{aligned} \mathcal{E}\left\{n_{4i+1} n_{4j+1}\right\} &= \frac{\mathcal{N}_o}{4} \int_{-\infty}^{\infty} p(t-[4i+1]\,T) p(t-[4j+1]\,T)\; dt \\ &= \begin{cases} \frac{\mathcal{N}_o}{2} T, & i=j; \\ \frac{\mathcal{N}_o}{4} \beta, & |i-j|=1; \\ 0, & \text{otherwise}. \end{cases} \end{aligned} \tag{4.69}$$

Fortunately, for a symmetric pulse shape[3] $h(t)$, the value of β is zero which is shown as follows:

Using the expression given in (4.62) for the inphase pulse $p(t)$, we have the following:

$$\begin{aligned}\beta = \int_{-\infty}^{\infty} \Big\{ & C_0(t-[4k-3]\,T) + C_0(t-[4k-1]) - C_1(t-[4k-4]\,T) - \\ & C_1(t-[4k-2]\,T) + C_2(t-[4k-4]\,T) + C_2(t-[4k+2]\,T) \\ & + C_3(t-[4k+1]\,T) + C_3(t-[4k-1]\,T)\Big\} \cdot \Big\{ C_0(t-[4k+1]\,T) \\ & + C_0(t-[4k+3]) - C_1(t-4kT) - C_1(t-[4k+2]\,T) + C_2(t-4kT) \\ & + C_2(t-[4k+6]\,T) + C_3(t-[4k+5]\,T) + C_3(t-[4k+3]\,T)\Big\}\, dt. \end{aligned} \quad (4.70)$$

For simplicity let

$$C_{ij}(n,m) = \int_{-\infty}^{\infty} C_i(t-nT)C_j(t-mT)\, dt, \qquad \text{for } 1 \le i,j \le 3.$$

It can be shown that all $C_{i,j}(n,m)$ are identically zero (since the two pulses $C_i(t-nT)$ and $C_j(t-mT)$ do not overlap in time) except for

$$\begin{aligned} C_{00}(4k-1,4k+1) &= \int_{(4k+1)T}^{(4k+3)T} C_0(t-[4k-1])C_0(t-[4k+1]\,T)\, dt \\ &= \int_0^{2T} C_0(t)C_0(t+2T)\, dt \\ &= \int_0^{2T} S(t)S(t+T)S^2(t+2T)S(t+3T)S(t+4T)\, dt, \end{aligned} \quad (4.71)$$

$$\begin{aligned} C_{01}(4k-1,4k) &= \int_{4kT}^{(4k+2)T} C_0(t-[4k-1])C_1(t-4kT)\, dt \\ &= \int_0^{2T} C_1(t)C_0(t+T)\, dt \end{aligned}$$

[3]Most of the signals of interest (e.g. $(1+D)^2/4$ MSK, 3-Raised Cosine MSK, and Gaussian MSK) involve pulse-shapes that are symmetric about $\tau = 3T/2$, i.e., $h(\tau+t) = h(\tau-t)$.

$$= \int_0^{2T} S(t)S(t+T)S^2(t+2T)S(t+3T)S(t+4T)\,dt, \quad (4.72)$$

$$\begin{aligned} C_{30}(4k+1,4k+1) &= \int_{(4k+1)T}^{(4k+2)T} C_3(t-[4k+1])C_0(t+[4k+1]\,T)\,dt \\ &= \int_0^T C_0(t)C_3(t)\,dt \\ &= \int_0^T S^2(t)S(t+T)S(t+2T)S(t+4T)S(t+5T)\,dt, \end{aligned} \quad (4.73)$$

$$\begin{aligned} C_{21}(4k+2,4k+2) &= \int_{(4k+2)T}^{(4k+3)T} C_2(t-[4k+2])C_1(t-[4k+2]\,T)\,dt \\ &= \int_0^T C_1(t)C_2(t)\,dt \\ &= \int_0^T S^2(t)S(t+T)S(t+2T)S(t+4T)S(t+5T)\,dt, \end{aligned} \quad (4.74)$$

$$\begin{aligned} C_{02}(4k-3,4k) &= \int_{4kT}^{(4k+1)T} C_0(t-[4k-3])C_2(t-4kT)\,dt \\ &= \int_0^T C_2(t)C_0(t+3T)\,dt \\ &= \int_0^T S(t)S(t+T)S(t+3T)S(t+4T)S^2(t+5T)\,dt, \end{aligned} \quad (4.75)$$

$$\begin{aligned} C_{31}(4k+1,4k+1) &= \int_{(4k+1)T}^{(4k+2)T} C_3(t-[4k+1])C_1(t-4kT)\,dt \\ &= \int_0^T C_3(t)C_1(t+T)\,dt \end{aligned}$$

$$= \int_0^T S(t)S(t+T)S(t+3T)S(t+4T)S^2(t+5T)\,dt, \quad (4.76)$$

$$C_{20}(4k+2,4k+1) = \int_{(4k+2)T}^{(4k+3)T} C_2(t-[4k+2])C_0(t-[4k+1]\,T)\,dt$$
$$= \int_0^T C_2(t)C_0(t+T)\,dt$$
$$= \int_0^T S(t)S^2(t+T)S(t+2T)S(t+3T)S(t+5T)\,dt, \quad (4.77)$$

and

$$C_{01}(4k-1,4k+2) = \int_{(4k+2)T}^{(4k+3)T} C_0(t-[4k-1])C_1(t-[4k+2]\,T)\,dt$$
$$= \int_0^T C_1(t)C_0(t+3T)\,dt$$
$$= \int_0^T S(t)S(t+2T)S(t+3T)S^2(t+4T)S(t+5T)\,dt. \quad (4.78)$$

Substituting (4.71)–(4.78) into (4.70), β reduces to

$$\begin{aligned}\beta = {} & C_{00}(4k-1,4k+1) - C_{01}(4k-1,4k) + \\ & C_{30}(4k+1,4k+1) - C_{01}(4k+2,4k+2) \\ & + C_{02}(4k-3,4k) - C_{31}(4k+1,4k) \\ & + C_{20}(4k+2,4k+1) - C_{01}(4k-1,4k+2). \end{aligned} \quad (4.79)$$

Each term in (4.79) would cancel with the next term (since they are equal) except for the last two terms. In that case β is equal to

$$\beta = \int_0^T S(t)S(t+2T)S(t+3T)S(t+5T)\left[S^2(t+T) - S^2(t+4T)\right]\,dt. \quad (4.80)$$

To see how the integral in (4.80) would equal zero for symmetric $h(t)$, let

$$f(t) = \frac{\pi}{2T}\int_0^t h(\tau)\,d\tau.$$

Since $h(t) = h(3T - t)$, $f(t)$ is also equal to

$$f(t) = \frac{\pi}{2T} \int_{3T-t}^{3T} h(\tau)\, d\tau. \tag{4.81}$$

Equation (4.80) can be written in terms of the function $f(t)$ as

$$\begin{aligned} \beta &= \int_0^T \sin(f(t)) \sin(f(t+2T)) \cos(f(t)) \times \\ &\qquad \cos(f(t+2T)) \left[\sin^2(f(t+T) - \cos^2(f(t+T))\right]\, dt \\ &= (-1/4) \int_0^T \sin(2f(t)) \sin(2f(t+2T)) \cos(2f(t+T))\, dt. \end{aligned}$$

By a change of variable ($t' = t - T/2$) we get

$$\beta = (-1/4) \int_{-T/2}^{T/2} \sin(2f(t+T/2)) \sin(2f(t+5T/2)) \cos(2f(t+3T/2))\, dt.$$

Now let $\rho(t)$ be

$$\rho(t) = \sin(2f(t+T/2)) \sin(2f(t+5T/2)) \cos(2f(t+3T/2)).$$

We will show that $\rho(t)$ is an odd function for $t \in [-T/2, T/2]$. This is shown as follows:

$$\rho(-t) = \sin(2f(T/2-t)) \sin(2f(5T/2-t)) \cos(2f(3T/2-t)). \tag{4.82}$$

Using (4.81) we have that

$$f(T/2-t) = \frac{\pi}{2T} \int_{t+5T/2}^{3T} h(\tau)\, d\tau = \frac{\pi}{2} - \frac{\pi}{2T} \int_0^{t+5T/2} h(\tau)\, d\tau = \frac{\pi}{2} - f(t+5T/2), \tag{4.83}$$

and

$$f(3T/2-t) = \frac{\pi}{2T} \int_{t+3T/2}^{3T} h(\tau)\, d\tau = \frac{\pi}{2} - \frac{\pi}{2T} \int_0^{t+3T/2} h(\tau)\, d\tau = \frac{\pi}{2} - f(t+3T/2). \tag{4.84}$$

From (4.83) we have that

$$f(5T/2-t) = \frac{\pi}{2} - f(t+T/2). \tag{4.85}$$

Now substituting (4.83)-(4.85) into (4.82) we have that

$$\begin{aligned}\rho(-t) &= \sin\left(2\left[\frac{\pi}{2} - f(t+5T/2)\right]\right)\sin\left(2\left[\frac{\pi}{2} - f(t+T/2)\right]\right)\cos\left(2\left[\frac{\pi}{2} - f(t+3T/2)\right]\right) \\ &= \sin(\pi - 2f(t+5T/2))\sin(\pi - f(t+T/2))\cos(\pi - 2f(t+3T/2)) \\ &= -\sin(2f(t+5T/2))\sin(f(t+T/2))\cos(2f(t+3T/2)) \\ &= -\rho(t). \end{aligned} \tag{4.86}$$

Clearly, from (4.86) $\rho(t)$ is an odd function in $[-T/2, T/2]$. Hence, we have that

$$\beta = (-1/4)\int_{-T/2}^{T/2} \rho(t)\, dt = 0.$$

For example, consider the premodulation pulse shape given in (3.43), $h(t)$ can be made symmetric if $k_0 = k_2 = (1 - k_1)/2$. Fig. 4.10.*a* shows such symmetric pulse shape. For $k_1 = 1/2$, we have that $k_0 = k_2 = 1/4$ which is the case for TFM. Another important example for symmetric $h(t)$ is the Gaussian pulse given in (2.10). Figure 4.10.*b* shows a plot of Gaussian premodulation pulse truncated at $|t - 3T/2| \geq 3T/2$ for the case of $BT = 0.3, 0.4$ and 0.5, where $h(t)$ with $BT = 0.3$ is used in GSM mobile systems.

In that case the sampled output of the matched filter at $t = (4m+1)T$ (i.e., z_{4m+1}) reduces simply to

$$z_{4m+1} = \sqrt{2ET}c_{4m+1} + n_{4m+1}, \tag{4.87}$$

where $\{n_{4m+1}\}$ is a sequence of independent identically distributed zero-mean Gaussian random variables with variance $\mathcal{N}_o T/2$. A similar analysis shows that, the sampled output of the matched filter on the quadrature channel at $t = (4m+2)T$ is given by

$$z_{4m+2} = \sqrt{2ET}c_{4m+2} + n_{4m+2}, \tag{4.88}$$

where $\{n_{4m+2}\}$ is a sequence of independent identically distributed zero-mean Gaussian random variables with variance $\mathcal{N}_o T/2$.

Since the sampled output of the matched filter on the I and Q channel (i.e., z_{4m+1} and z_{4m+2}) contains only half of the coded symbols sequence $\{c_n\}$ plus noise, the sequence

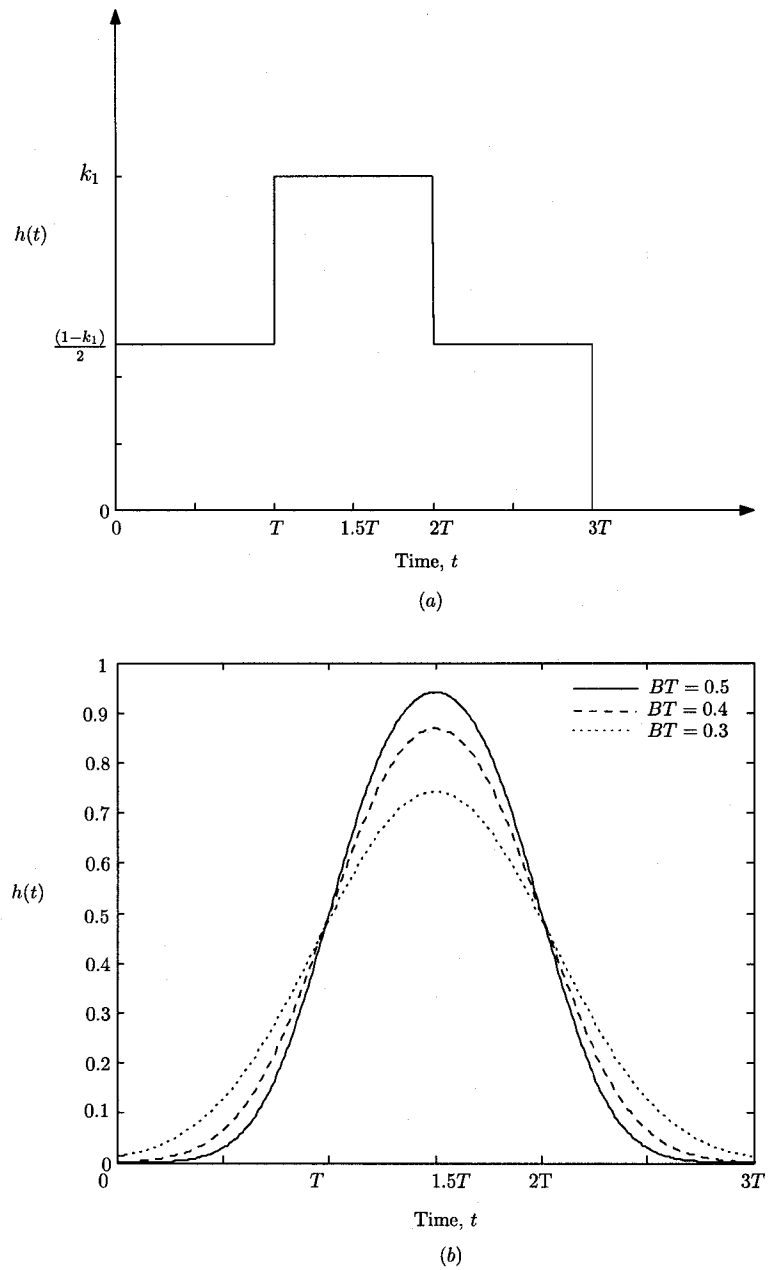

Fig. 4.10: Symmetric premodulation filters $h(t)$ of length $3T$ that produces no ISI at the output of the matched filter. (a) $h(t)$ given in (3.43), generated using correlative coding where $k_0 = k_2$. (b) Gaussian pulse shape filter truncated at $|t - 3T/2| \geq 3T/2$ for $BT = 0.3, 0.4$ and 0.5.

$\{z_n\}$ cannot be used directly for the detection and decoding of the $\{a_n\}$ symbol stream. However, since a quadruple repetition code is applied, using (4.50) we know that, $c_{4m+1} = c_{4m+2} = c'_m$, where $\{c'_n\}$ is the outer encoder's ($\mathbf{W}_{\text{out}}$) output sequence. This suggests another strategy of processing the sampled output of the matched filter on both channels, which is adding z_{4m+1} and z_{4m+2} and then using the sum to make a decision. This receiver is depicted in Fig. 4.11.

The decision variable $\bar{z}_m$ is given by

$$\bar{z}_m = z_{4m+1} + z_{4m+2} = \sqrt{8ET}c'_m + \bar{n}_m, \tag{4.89}$$

where $\{\bar{n}_m = n_{4m+1} + n_{4m+2}\}$ is a sequence of independent identically distributed Gaussian random variables with variance $\mathcal{N}_o T$. Again, the detection problem for the recovery of the symbols sequence $\{c'_n\}$ from the decision variable sequence $\{\bar{z}_n\}$ is one corresponding to memoryless linear modulation. If the sequence $\{\bar{z}_n\}$ is used at the input of the (soft-decision) detector and decoder for the $\{a_n\}$ symbol stream, then, the bit error probability (for high SNR) of can be expressed as

$$\begin{aligned} \mathcal{P}_{b,\text{asymp}} &= Q\left(\frac{\sqrt{8ETH_{\min}^{W_{\text{out}}}}}{\sqrt{\mathcal{N}_o T}}\right) \\ &= Q\left(\sqrt{8R_c H_{\min}^{W_{\text{out}}}\frac{E_b}{\mathcal{N}_o}}\right), \end{aligned}$$

and since $H_{\min}^{W_{\text{out}}} = H_{\min}^{W}/4$, then we have that

$$\mathcal{P}_{b,\text{asymp}} = Q\left(\sqrt{2R_c H_{\min}^{W}\frac{E_b}{\mathcal{N}_o}}\right).$$

Using the result shown in Theorem 4, we have that $\mathbf{NSFED} = 2R_c H_{\min}^{W}$. Therefore, the asymptotic bit error probability can be expressed as

$$\mathcal{P}_{b,\text{asymp}} = Q\left(\sqrt{\mathbf{NSFED}\frac{E_b}{\mathcal{N}_o}}\right). \tag{4.90}$$

This is exactly equivalent to the asymptotic performance of the Viterbi (optimum) receiver (Fig. 4.12.*a*) . Therefore, the simple I-Q receiver depicted in Fig. 4.11, is *optimum*

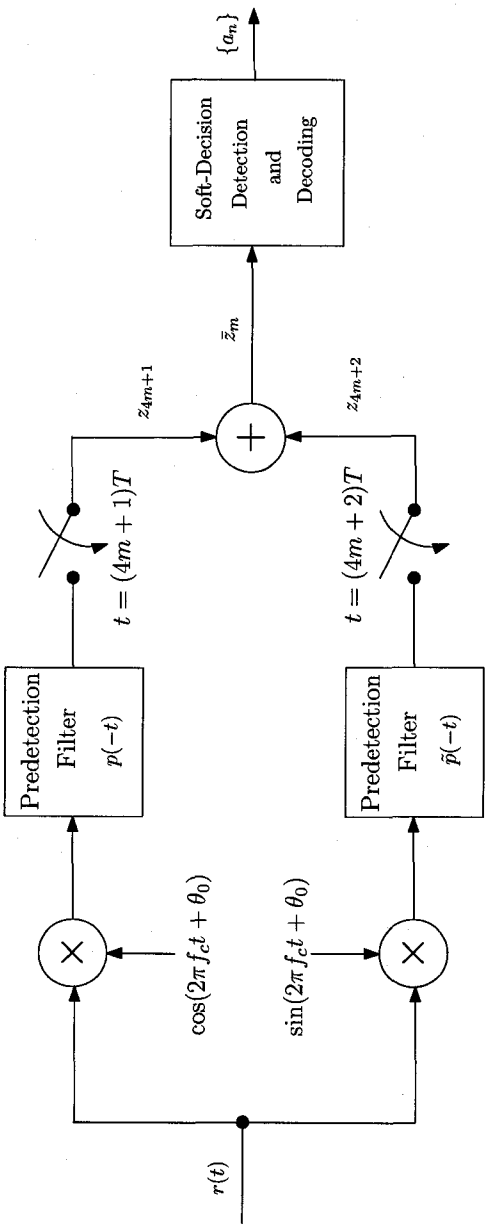

Fig. 4.11: Modified I-Q receiver for coded generalized MSK with modulation memory $L = 3$, using a quadruple repetition code (inner encoder). The decoder used here is the inverse of the outer encoder $\mathbf{W}_{\text{out}}$.

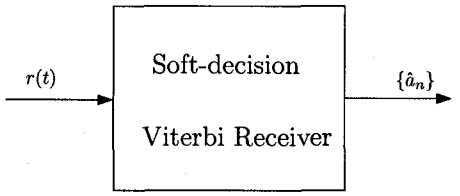

a. Optimum MLSE receiver implemented using Viterbi algorithm.

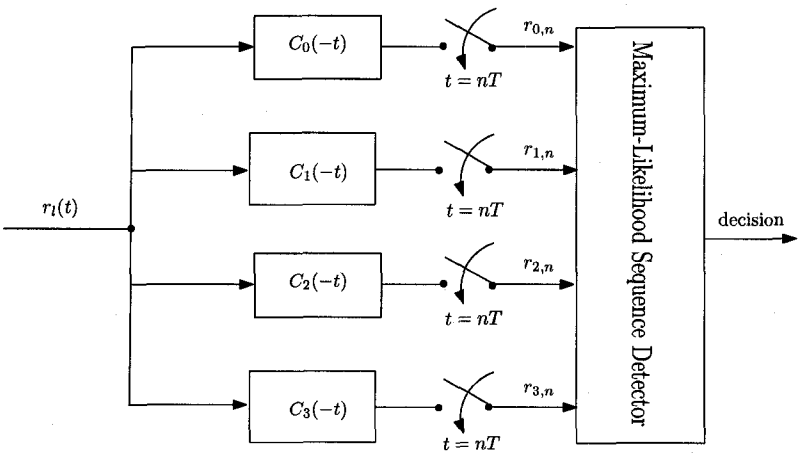

b. Optimum receiver based on Laurent decomposition of generalized MSK as superposition of PAM signals. $r_l(t)$ is the lowpass equivalent of the receiver signal.

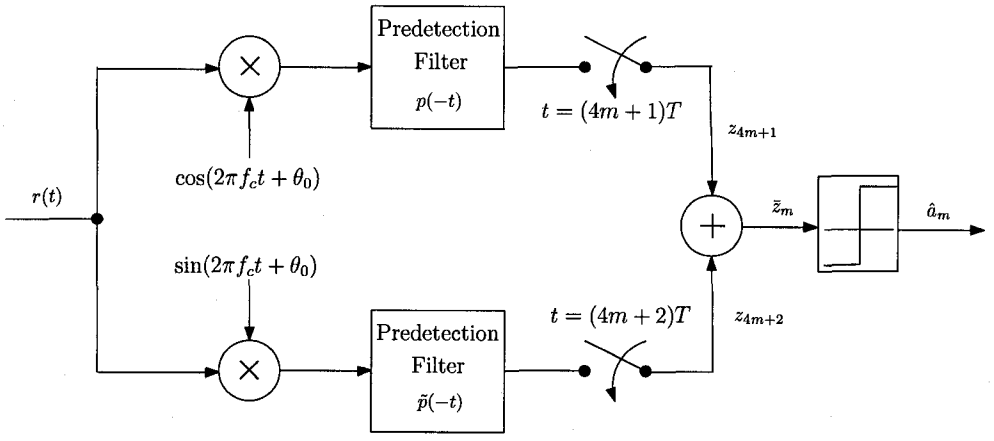

c. Simple *I-Q* receiver that uses hard decision detection.

Fig. 4.12: Three different *optimum* receivers used to detect generalized MSK with pulse shapes of duration $3T$ employing a quadruple repetition code only.

in the sense of minimizing the asymptotic probability of error.

It is interesting to note that with quadruple repetition coding only, the simplified receiver shown in Fig. 4.12.*c* can also be used to optimally detect coded generalized MSK signals with pulse shapes of duration $3T$. The receiver performs symbol-by-symbol detection on the decision variable $\bar{z}_m$ where the performance of that receiver (with no outer encoding) in detecting the a_m symbol is also given by (4.49) for all SNR.

Consider, for example, TFM modulation scheme. This signal, combining it with quadruple repetition code, can be optimally demodulated using the receiver depicted in Fig. 4.12.*c* while achieving a coding gain of at least 1.40 dB compared to uncoded TFM ($\mathbf{NSFED}_{\text{uncoded}} \approx 1.45$). If we compare the two receivers depicted in Fig. 4.12.*b* and Fig. 4.12.*c*, the reduction in the complexity of the former receiver compared to the latter can be found in two places: the first one is that the number of the matched filters used in the demodulator is reduced by a factor of 2 and the second is in using a *slicer* instead of the MLSE detection (e.g. Viterbi algorithm).

It must be noted at this point that, although a quadruple repetition code has simplified the detection problem of coded generalized MSK with pulse shapes of duration $3T$, it is not considered an efficient code when it comes to issues related to spectrum and bandwidth-efficiency. Nevertheless, for MSK system that uses the same code rate, considering performance, bandwidth and receiver complexity, generalized MSK signals with $h(t)$ of length $3T$ employing a quadruple repetition code is again an improvement over simple MSK or generalized MSK with pulse shape of length $2T$.

4.5 Searching for good convolutional codes for Generalized MSK

We have seen in the preceding sections, the difficulty of relating the Euclidean distance between transmitted generalized MSK signals to the Hamming distance between corre-

sponding coded sequences can be eliminated by the use of repetition codes. Since the asymptotic performance of any coded modulation system depends on the minimum Euclidean distance between possible transmitted signals, to increase the performance of the overall generalized MSK system shown in Fig. 4.1 and 4.7 for modulation memory $L = 2$ and $L = 3$ respectively, one has to search for those rate-k/l outer convolutional codes C_{W^o}, of a given constraint length ν^o, that have maximum $H_{\min}^{W^o}$ (for that rate and constraint length).

Finding the code which maximizes $H_{\min}^{W^o}$ is done for each code using those optimum convolutional codes that have been reported in literature (see for example [36],[37]). This optimum outer encoder $\mathbf{W}_{\text{out}}(D)$ is then combined with the repetition code to generate the corresponding encoder $\mathbf{W}(D)$. The search for good convolutional codes bas been done for precoded generalized MSK signals with memory $L = 1, 2$ and 3. These special (convolutional) codes, when combined with the CPFSK modulator, can be detected *optimally* using a simple I-Q receiver.

In general, encoder $\mathbf{W}$ constructed for generalized MSK with modulation memory $L = 2$ and $L = 3$ (Fig. 4.1 and 4.7), is not optimum in the sense of maximizing the minimum Hamming distance for a given rate R_c and constrained length ν. MSK signal does not require the information symbols to be encoded by a double repetition code in order to demodulate it using an I-Q receiver. Therefore, no constraint on the rate of encoder C_W is necessary, and optimum encoders (for a given rate and constraint length) that maximize the minimum Hamming distance can be applied.

4.5.1 Best Codes for "Precoded" MSK

For the special case where the modulation scheme is MSK, a repetition code is not necessary for the signal to be demodulated using a simple I-Q receiver. Therefore the channel encoder $\mathbf{W}$ is equivalent to the outer encoder $\mathbf{W}_{\text{out}}$. The results are reported in tables 4.2-4.5.

Best rate-1/2 convolutional encoder			
ν	**W**	**NSFED**	Coding gain (dB)
1	[3 1]	3	1.761
2	[5 7]	5	3.98
3	[13 17]	6	4.77
4	[27 31]	7	5.44
5	[53 75]	8	6.02
6	[117 155]	10	6.99

Table 4.2: Best rate-1/2 convolutional encoder **W** for use of "precoded" MSK in Fig. 2.4.

Best rate-1/3 convolutional encoder			
$\nu = \nu^o$	**W**	**NSFED**	Coding gain (dB)
1	[1 3 3]	5	3.98
2	[5 7 7]	8	6.02
3	[13 15 17]	10	6.99
4	[25 33 37]	12	7.78
5	[47 53 75]	13	8.13
6	[117 127 155]	15	8.75

Table 4.3: Best rate-1/3 convolutional encoder **W** for use of "precoded" MSK in Fig. 2.4.

Best rate-1/4 convolutional encoder			
ν	**W**	**NSFED**	Coding gain (dB)
1	[1 1 3 3]	3	1.76
2	[5 5 7 7]	5	3.98
3	[13 13 15 17]	7.5	5.74
4	[25 27 33 37]	8	6.02
5	[45 53 67 77]	9	6.532
6	[117 127 155 171]	10	6.99

Table 4.4: Best rate-1/4 convolutional encoder **W** for use of "precoded" MSK in Fig. 2.4.

Best rate-2/3 convolutional encoder			
ν	**W**	**NSFED**	Coding gain (dB)
2	$\begin{pmatrix} 3 & 1 & 0 \\ 2 & 3 & 3 \end{pmatrix}$	3	1.76
3	$\begin{pmatrix} 3 & 2 & 1 \\ 4 & 1 & 7 \end{pmatrix}$	4	3.01
4	$\begin{pmatrix} 6 & 5 & 1 \\ 7 & 2 & 5 \end{pmatrix}$	5	3.98
5	$\begin{pmatrix} 07 & 06 & 03 \\ 12 & 01 & 13 \end{pmatrix}$	6	4.77
6	$\begin{pmatrix} 06 & 13 & 13 \\ 13 & 06 & 17 \end{pmatrix}$	7	5.44

Table 4.5: Best rate-2/3 convolutional encoder **W** for use of "precoded" MSK in Fig. 2.4.

The codes' generators are given in octal notation. Note that these codes have been previously reported in literature (for memoryless modulation) [37] where only encoders **W** of rate 1/2, 1/3, 1/4 and 2/3 are reported of constraint length up to 6. For every best code found, the (normalized) minimum square Euclidean distance is given as well as the asymptotic coding gain, CG=10 log ($\mathbf{NSFED}_{,\text{coded}}/\mathbf{NSFED}_{,\text{uncoded}}$), is calculated with respect to the uncoded MSK (where **NSFED** = 2). All codes that are reported here for MSK achieve the same free Euclidean distance for the same codes applied to linear modulation schemes such as BPSK and OQPSK. Moreover, in most cases these codes achieve better performance when applied to precoded MSK than the codes reported in [38].

4.5.2 Good Codes for "Precoded" Generalized MSK with $L = 2$

As have been shown previously that for generalized MSK signals with memory $L = 2$ to be demodulated using a linear receiver a repetition code of rate 1/2 must be applied as an inner code. This causes a limitation in the encoder **W**'s rate, where we are only restricted for code rates of $k/2l$. These codes are not optimum in the sense of maximizing the free Hamming distance of the code C_W, for a given rate R_c and constraint length ν.

Numerical results are presented in tables 4.6,4.7 of our search for the best rate 1/2 and rate 1/4 convolutional codes for use with DMSK of constraint length up to 5. Again, for every good code found, the **NSFED** is given and coding gain is calculated with respect to uncoded DMSK ($\mathbf{NSFED}_{,\text{uncoded}} \approx 1.73$). These codes are also applicable for any generalized MSK with premodulation filter, $h(t)$, of length $2T$, where the only difference is in the calculation of the coding gain. This is because the value of $\mathbf{NSFED}_{,\text{uncoded}}$ depends on the pulse shape of $h(t)$.

Best rate-1/2 convolutional encoder						
ν^o	$\mathbf{W}_{\text{out}} = w^{o(0)}$	ν	$\mathbf{W}$		NSFED	Coding gain (dB)
0	1	0	1	1	2	0.63
1	2	1	2	2	2	0.63
2	7	2	7	7	4	3.64
3	13	3	13	13	4	3.64
4	31	4	31	31	6	5.40
5	75	5	75	75	6	5.40

Table 4.6: Best rate-1/2 convolutional encoder $\mathbf{W}$ generated by cascading best rate-1/1 convolutional encoder $\mathbf{W}_{\text{out}}$ with rate-1/2 repetition code for use of "precoded" generalized MSK with $L = 2$ in Fig. 4.1.

Best rate-1/4 convolutional encoder									
ν^o	$\mathbf{W}_{\text{out}}$		ν	$\mathbf{W}$				NSFED	Coding gain (dB)
0	1	1	0	1	1	1	1	2	0.63
1	1	3	1	1	1	3	3	3	2.39
2	5	7	2	5	5	7	7	5	4.61
3	13	17	3	13	13	17	17	6	5.40
4	27	31	4	27	27	31	31	7	6.07
5	53	75	5	53	53	75	75	8	6.65

Table 4.7: Best rate-1/4 convolutional encoder $\mathbf{W}$ generated by cascading best rate-1/2 convolutional encoder $\mathbf{W}_{\text{out}}$ with rate-1/2 repetition code for use of "precoded" generalized MSK with $L = 2$ in Fig. 4.1.

4.5.3 Good Codes for "Precoded" Generalized MSK with $L = 3$

As have been shown previously that for generalized MSK signals with memory $L = 3$ to be demodulated using a linear receiver a repetition code of rate 1/4 must be applied as an inner code. This causes a limitation in the encoder $\mathbf{W}$'s rate, where we are only restricted for code rates of $k/4l$.

Numerical results are presented in table 4.8 of our search for the best rate 1/4 convolutional codes for use with TFM of constraint length up to 5. Again, for every best code found, the NSFED is given and coding gain is calculated with respect to uncoded DMSK ($\mathbf{NSFED}_{,\text{uncoded}} \approx 1.45$). These codes are also optimum for any generalized MSK with symmetric premodulation filter, $h(t)$, of length $3T$, where the only difference is in the calculation of the coding gain. This is because the value of $\mathbf{NSFED}_{,\text{uncoded}}$ depends on the pulse shape of $h(t)$.

Best rate-1/4 convolutional encoder									
ν^o	$\mathbf{W}_{\text{out}}$	ν	$\mathbf{W}$					NSFED	Coding gain (dB)
0	1	0	1	1		1	1	2	1.40
1	2	1	2	2		2	2	2	1.40
2	7	2	7	7		7	7	4	4.41
3	13	3	13	13		13	13	4	4.41
4	31	4	31	31		31	31	6	6.17
5	75	5	75	75		75	75	6	6.17

Table 4.8: Best rate-1/4 convolutional encoder $\mathbf{W}$ generated by cascading best rate-1/1 convolutional encoder $\mathbf{W}_{\text{out}}$ with rate-1/4 repetition code for use of "precoded" generalized MSK with $L = 3$ in Fig. 4.7.

Chapter 5

Discussion and Conclusion

5.1 Summary

In this thesis we proposed a simple linear receiver for coded generalized MSK especially for signals with modulation memory $L = 2$ and 3. In Chapter 2, we have given an overview on the special case of such modulation scheme called MSK and its generalization to a larger class referred to *generalized* MSK. In Chapter 3, the application of the Laurent representation of CPM to generalized MSK signals has been investigated. Finally, the design of a linear receiver for coded generalized MSK signal with modulation memory $L = 2$ and 3 in additive white Gaussian noise channel has been developed in Chapter 4.

In Chapter 2, it has been shown that the coding design problem for MSK signals generated by CPFSK-MSK modulator can be simplified by the use of precoding. The precoder is applied between the channel encoder and CPFSK-MSK modulator where its objective is to relate the Euclidean distance between generated MSK signals linearly to the Hamming distance between corresponding sequences generated by channel encoder, i.e., the criterion of optimization of the combinations (encoder and modulator) was translated to a criterion of maximization of Hamming distance. Another advantage of using such precoder is that the signal can be optimally demodulated using simple

inphase-quadrature (I-Q) receiver.

In Chapter 3, the representation of generalized MSK signal with modulation memory of $L = 2$ and $L = 3$ as PAM using the Laurent representation was studied. The squared Euclidean distance between different signals were considered and closed form expressions computed for the Euclidean distance of such signals. It has been shown that in general the Euclidean distance depends on the premodulation filter used to shape the symbols prior modulation. The PAM representation of generalized MSK signals generated by correlative coding with coding polynomial (k_0+k_1D) and $(k_0+k_1D+k_2D^2)$ were considered and an exact expression of the free Euclidean distance was computed for the "uncoded" case of such signals.

In Chapter 4, the proposed linear receiver for detecting coded generalized MSK signal in additive white Gaussian noise channel was examined. It has been shown that imposing a particular structure on the code applied to generalized MSK signals with modulation memory $L = 2$ and $L = 3$, the square Euclidean distance becomes linearly related to the Hamming distance between sequences generated by channel encoder. The dependency of Euclidean distance on the premodulation filter is totally removed, therefore the difficulty of the code design for such signals has been eliminated. The optimization criterion for such signals is maximizing the free Hamming distance of the channel encoder. For generalized MSK with $L = 2$ and $L = 3$, the code structure is just a double (rate-1/2) and quadruple (rate-1/4) *repetition* code, respectively. Using such coding technique, it was shown that the precoder (derived for MSK) combined with CPFSK modulator used to generate generalized MSK with $L = 2$ and 3 can be replaced by a simple I-Q modulator where the I and Q channel pulses are linear combination of the Laurent pulses. This will allow us to demodulate the signal using a simple I-Q receiver. An interesting result, is that for generalized MSK with any pulse shape $h(t)$ of length $2T$ no inter-symbol interference is introduced at the output of the matched filter, where for $h(t)$ of length $3T$, only symmetrical pulse shapes do not produce ISI. Moreover, the noise

samples are independent and therefore, soft-decision detection and decoding, applied to memoryless linear modulation schemes, is considered *optimum*. Finally, searching for good convolutional codes, which can optimally be detected using the proposed linear receiver, for generalized MSK is reported for some rates and constraint length.

5.2 Suggestions for further research

It was shown that the power efficiency of some generalized MSK signals may be improved through the application of repetition codes. For generalized MSK with pulse shapes duration of length $3T$, it has been shown that a quadruple repetition code can be used to simplify the detection problem. This is done at the expense of increasing the bandwidth which is not desirable for communication systems with adjacent channel interference such as mobile and wireless communication systems. It is shown (this work has not been demonstrated in this thesis and will be reported elsewhere) that by increasing the modulation memory of generalized MSK to $L = 4$, using a quadruple repetition code the I-Q receiver can still be used to optimally detect such signals. This might have a great influence on the improvement of the spectrum-efficiency of the coded signal.

It is believed that for generalized MSK signals with modulation memory of $L \geq 5$ to be optimally detected using a simple I-Q receiver (employing soft-decision detection and decoding), a repetition code of rate $R_i \leq 1/6$ may be applied as an inner code (further research is being performed for such problem). Since repetition coding is considered inefficient coding process in data transmission, the search for other efficient coding schemes can be investigated.

As proposed in [39], repetition codes exhibits unique properties when it is used over faded mobile channel. Hence, one of the primary focuses for further research at this point might well be the performance of these coding techniques on fading channel.

Appendix A

Squared Euclidean Distance of Precoded CPFSK-MSK

The squared Euclidean distance $d^2(i,j)$ between any two transmitted coded signals $s_i(t)$ and $s_j(t)$ which corresponds to two different symbol sequences $\mathbf{c}^i$ and $\mathbf{c}^j$, for $t \geq 0$, is defined by

$$d^2(i,j) \triangleq \|s_i(t) - s_j(t)\|^2 = \int_0^\infty |s_i(t) - s_j(t)|^2 \, dt, \tag{A.1}$$

where $s(t)$ is defined by (2.1).

Assuming that $f_cT \gg 1$, the squared Euclidean distance can be written as

$$d^2(i,j) = \frac{E}{T}\int_0^\infty [\cos\phi_i(t) - \cos\phi_j(t)]^2 \, dt + \frac{E}{T}\int_0^\infty [\sin\phi_i(t) - \sin\phi_j(t)]^2 \, dt, \tag{A.2}$$

Using the OQPSK description of MSK given in (2.4), (A.2) can be expressed as

$$\begin{aligned} d^2(i,j) &= \frac{E}{T}\int_0^\infty \left(\sum_{n \text{ odd}} [c_n^i - c_n^j]\, p(t-nT)\right)^2 dt + \frac{E}{T}\int_0^\infty \left(\sum_{n \text{ even}} [c_n^i - c_n^j]\, p(t-nT)\right)^2 dt \\ &= \frac{E}{T}\sum_{n \text{ odd}}\sum_{m \text{ odd}} [c_n^i - c_n^j]\,[c_m^i - c_m^j] \int_0^\infty p(t-nT)p(t-mT)\, dt \\ &\quad + \frac{E}{T}\sum_{n \text{ even}}\sum_{m \text{ even}} [c_n^i - c_n^j]\,[c_m^i - c_m^j] \int_0^\infty p(t-nT)p(t-mT)\, dt \end{aligned} \tag{A.3}$$

where $p(t)$ is given by (2.5) and the integral in (A.3) is given by

$$\int_0^\infty p(t-nT)p(t-mT)\,dt = \begin{cases} \|p(t)\|^2 = T, & n = m, \\ 0, & \text{otherwise.} \end{cases} \tag{A.4}$$

where $\|p(t)\|^2$ is defined by the energy of the pulse $p(t)$. Therefore, equation (A.3) reduces to

$$\begin{aligned} d^2(i,j) &= E\sum_n \left[c_n^i - c_n^j\right]^2 \\ &= 4EH(\mathbf{c}^i, \mathbf{c}^j), \end{aligned} \tag{A.5}$$

where $H(\mathbf{c}^i, \mathbf{c}^j)$ is defined by the Hamming distance between the two sequences $\mathbf{c}^i$ and $\mathbf{c}^j$.

Appendix B

Squared Euclidean Distance of Length $3T$ Generalized MSK

Using the expression given in (3.45), the normalized squared Euclidean distance for coded generalized MSK signals, for $t \geq 0$ can be expressed as (assuming $f_c T \gg 1$)

$$\mathbf{NSED}(i,j) = \frac{R_c}{2}\left\{\frac{1}{T}\int_0^{\infty}\left[\cos(\phi_i(t)) - \cos(\phi_j(t))\right]^2\, dt + \frac{1}{T}\int_0^{\infty}\left[\sin(\phi_i(t)) - \sin(\phi_j(t))\right]^2\, dt\right\}, \tag{B.1}$$

where R_c is the code rate of encoder $\mathbf{W}$. Let $I_{i,j}$ and $Q_{i,j}$ be equal to the following

$$I_{i,j} = \frac{1}{T}\int_0^{\infty}\left[\cos(\phi_i(t)) - \cos(\phi_j(t))\right]^2\, dt, \tag{B.2}$$

$$Q_{i,j} = \frac{1}{T}\int_0^{\infty}\left[\sin(\phi_i(t)) - \sin(\phi_j(t))\right]^2\, dt. \tag{B.3}$$

Then $I_{i,j}$ and $Q_{i,j}$ can be expressed as

$$\begin{aligned} I_{i,j} \;=\; & \sum_{n\ \text{odd}}\sum_{m\ \text{odd}}\left[c_n^i - c_n^j\right]\left[c_m^i - c_m^j\right]\frac{1}{T}\int_0^{\infty} C_0(t-nT)C_0(t-mT)\, dt \\ & + \sum_{n\ \text{even}}\sum_{m\ \text{even}}\left[v_n^i - v_n^j\right]\left[v_m^i - v_m^j\right]\frac{1}{T}\int_0^{\infty} C_1(t-nT)C_1(t-mT)\, dt \\ & + \sum_{n\ \text{even}}\sum_{m\ \text{even}}\left[x_n^i - x_n^j\right]\left[x_m^i - x_m^j\right]\frac{1}{T}\int_0^{\infty} C_2(t-nT)C_2(t-mT)\, dt + \end{aligned}$$

$$\sum_{n\text{ odd}}\sum_{m\text{ odd}}[y_n^i-y_n^j]\,[y_m^i-y_m^j]\,\frac{1}{T}\int_0^\infty C_3(t-nT)C_3(t-mT)\,dt$$
$$+2\sum_{n\text{ odd}}\sum_{m\text{ even}}[c_n^i-c_n^j]\,[v_m^i-v_m^j]\,\frac{1}{T}\int_0^\infty C_0(t-nT)C_1(t-mT)\,dt$$
$$+2\sum_{n\text{ odd}}\sum_{m\text{ even}}[c_n^i-c_n^j]\,[x_m^i-x_m^j]\,\frac{1}{T}\int_0^\infty C_0(t-nT)C_2(t-mT)\,dt$$
$$+2\sum_{n\text{ odd}}\sum_{m\text{ odd}}[c_n^i-c_n^j]\,[y_m^i-y_m^j]\,\frac{1}{T}\int_0^\infty C_0(t-nT)C_3(t-mT)\,dt$$
$$+2\sum_{n\text{ even}}\sum_{m\text{ even}}[v_n^i-v_n^j]\,[x_m^i-x_m^j]\,\frac{1}{T}\int_0^\infty C_1(t-nT)C_2(t-mT)\,dt$$
$$+2\sum_{n\text{ even}}\sum_{m\text{ odd}}[v_n^i-v_n^j]\,[y_m^i-y_m^j]\,\frac{1}{T}\int_0^\infty C_1(t-nT)C_3(t-mT)\,dt$$
$$+2\sum_{n\text{ even}}\sum_{m\text{ odd}}[x_n^i-x_n^j]\,[y_m^i-y_m^j]\,\frac{1}{T}\int_0^\infty C_2(t-nT)C_3(t-mT)\,dt, \qquad \text{(B.4)}$$

and

$$\begin{aligned}
Q_{i,j} \;=\; & \sum_{n\text{ even}}\sum_{m\text{ even}}[c_n^i-c_n^j]\,[c_m^i-c_m^j]\,\frac{1}{T}\int_0^\infty C_0(t-nT)C_0(t-mT)\,dt \\
& +\sum_{n\text{ odd}}\sum_{m\text{ odd}}[v_n^i-v_n^j]\,[v_m^i-v_m^j]\,\frac{1}{T}\int_0^\infty C_1(t-nT)C_1(t-mT)\,dt \\
& +\sum_{n\text{ odd}}\sum_{m\text{ odd}}[x_n^i-x_n^j]\,[x_m^i-x_m^j]\,\frac{1}{T}\int_0^\infty C_2(t-nT)C_2(t-mT)\,dt \\
& +\sum_{n\text{ even}}\sum_{m\text{ even}}[y_n^i-y_n^j]\,[y_m^i-y_m^j]\,\frac{1}{T}\int_0^\infty C_3(t-nT)C_3(t-mT)\,dt \\
& -2\sum_{n\text{ even}}\sum_{m\text{ odd}}[c_n^i-c_n^j]\,[v_m^i-v_m^j]\,\frac{1}{T}\int_0^\infty C_0(t-nT)C_1(t-mT)\,dt \\
& -2\sum_{n\text{ even}}\sum_{m\text{ odd}}[c_n^i-c_n^j]\,[x_m^i-x_m^j]\,\frac{1}{T}\int_0^\infty C_0(t-nT)C_2(t-mT)\,dt \\
& +2\sum_{n\text{ even}}\sum_{m\text{ even}}[c_n^i-c_n^j]\,[y_m^i-y_m^j]\,\frac{1}{T}\int_0^\infty C_0(t-nT)C_3(t-mT)\,dt \\
& +2\sum_{n\text{ odd}}\sum_{m\text{ odd}}[v_n^i-v_n^j]\,[x_m^i-x_m^j]\,\frac{1}{T}\int_0^\infty C_1(t-nT)C_2(t-mT)\,dt -
\end{aligned}$$

$$2\sum_{n\text{ odd}}\sum_{m\text{ even}}\left[v_n^i - v_n^j\right]\left[y_m^i - y_m^j\right]\frac{1}{T}\int_0^\infty C_1(t-nT)C_3(t-mT)\,dt$$
$$-2\sum_{n\text{ odd}}\sum_{m\text{ even}}\left[x_n^i - x_n^j\right]\left[y_m^i - y_m^j\right]\frac{1}{T}\int_0^\infty C_2(t-nT)C_3(t-mT)\,dt. \tag{B.5}$$

The integrals shown in (B.4) and (B.5) can be evaluated as follows:

$$\int_0^\infty C_0(t-nT)C_0(t-mT)\,dt = \begin{cases} \|C_0(t)\|^2, & n=m; \\ \langle C_0(t), C_0(t-2T)\rangle, & |n-m|=2; \\ 0, & \text{otherwise.} \end{cases} \tag{B.6}$$

$$\int_0^\infty C_1(t-nT)C_1(t-mT)\,dt = \begin{cases} \|C_1(t)\|^2, & n=m; \\ 0, & \text{otherwise.} \end{cases} \tag{B.7}$$

$$\int_0^\infty C_2(t-nT)C_2(t-mT)\,dt = \begin{cases} \|C_2(t)\|^2, & n=m; \\ 0, & \text{otherwise.} \end{cases} \tag{B.8}$$

$$\int_0^\infty C_3(t-nT)C_3(t-mT)\,dt = \begin{cases} \|C_3(t)\|^2, & n=m; \\ 0, & \text{otherwise.} \end{cases} \tag{B.9}$$

$$\int_0^\infty C_0(t-nT)C_1(t-mT)\,dt = \begin{cases} \langle C_0(t-T), C_1(t)\rangle, & m-n=-1; \\ \langle C_0(t-T), C_1(t-2T)\rangle, & m-n=1; \\ \langle C_0(t-T), C_1(t-4T)\rangle, & m-n=3; \\ 0, & \text{otherwise.} \end{cases} \tag{B.10}$$

$$\int_0^\infty C_0(t-nT)C_2(t-mT)\,dt = \begin{cases} \langle C_0(t-T), C_2(t-2T)\rangle, & m-n=1; \\ \langle C_0(t-T), C_2(t-4T)\rangle, & m-n=3; \\ 0, & \text{otherwise.} \end{cases} \tag{B.11}$$

$$\int_0^\infty C_0(t-nT)C_3(t-mT)\,dt = \begin{cases} \langle C_0(t-T), C_3(t-T)\rangle, & m=n; \\ \langle C_0(t-T), C_3(t-3T)\rangle, & m-n=2; \\ 0, & \text{otherwise.} \end{cases} \tag{B.12}$$

$$\int_0^\infty C_1(t-nT)C_2(t-mT)\,dt = \begin{cases} \langle C_1(t), C_2(t)\rangle, & m=n; \\ 0, & \text{otherwise.} \end{cases} \tag{B.13}$$

$$\int_0^\infty C_1(t-nT)C_3(t-mT)\,dt = \begin{cases} \langle C_1(t), C_3(t)\rangle, & m-n=1; \\ 0, & \text{otherwise.} \end{cases} \tag{B.14}$$

$$\int_0^\infty C_2(t-nT)C_3(t-mT)\,dt = 0. \tag{B.15}$$

It can be shown that,

$$\begin{aligned}
\langle C_0(t), C_0(t-2T)\rangle &= \langle C_0(t-T), C_1(t-2T)\rangle\,,\\
\langle C_0(t-T), C_1(t)\rangle &= \langle C_0(t-T), C_2(t-2T)\rangle\,,\\
\langle C_0(t-T), C_1(t-4T)\rangle &= \langle C_0(t-T), C_3(t-3T)\rangle\,,\\
\langle C_0(t-T), C_2(t-4T)\rangle &= \langle C_1(t), C_3(t-T)\rangle\,,\\
\langle C_0(t-T), C_3(t-T)\rangle &= \langle C_1(t), C_2(t)\rangle\,.
\end{aligned} \tag{B.16}$$

Substituting (B.6)-(B.16) into (B.4) and (B.5), and by rearranging terms, $\mathbf{NSED}(i,j)$ reduces to

$$\begin{aligned}
\mathbf{NSED}(i,j) = \frac{R_c}{2T}\Big\{ & 4\|C_0(t)\|^2 H(\mathbf{c}^i,\mathbf{c}^j) + 4\|C_1(t)\|^2 H(\mathbf{v}^i,\mathbf{v}^j)\\
& +4\|C_2(t)\|^2 H(\mathbf{x}^i,\mathbf{x}^j) + 4\|C_3(t)\|^2 H(\mathbf{y}^i,\mathbf{y}^j)\\
& +2\langle C_0(t), C_0(t-2T)\rangle\,\chi(i,j) + 2\langle C_0(t-T), C_1(t)\rangle\,\eta(i,j)\\
& +2\langle C_0(t-T), C_1(t-4T)\rangle\,\lambda(i,j) + 2\langle C_0(t-T), C_2(t-4T)\rangle\,\zeta(i,j)\\
& +2\langle C_0(t-T), C_3(t-T)\rangle\,\delta(i,j)\Big\},
\end{aligned} \tag{B.17}$$

where $\chi(i,j)$ is still expressed by (3.57) and

$$\begin{aligned}
\eta(i,j) = & \sum_{n\text{ odd}} \left[c_n^i - c_n^j\right]\left[v_{n-1}^i - v_{n-1}^j\right] - \sum_{n\text{ even}} \left[c_n^i - c_n^j\right]\left[v_{n-1}^i - v_{n-1}^j\right]\\
& + \sum_{n\text{ even}} \left[c_{n-1}^i - c_{n-1}^j\right]\left[x_n^i - x_n^j\right] - \sum_{n\text{ odd}} \left[c_{n-1}^i - c_{n-1}^j\right]\left[x_n^i - x_n^j\right],
\end{aligned} \tag{B.18}$$

$$\begin{aligned}
\lambda(i,j) = & \sum_{n\text{ even}} \left[c_{n-3}^i - c_{n-3}^j\right]\left[v_n^i - v_n^j\right] - \sum_{n\text{ odd}} \left[c_{n-3}^i - c_{n-3}^j\right]\left[v_n^i - v_n^j\right]\\
& + \sum_{n\text{ odd}} \left[c_{n-2}^i - c_{n-2}^j\right]\left[y_n^i - y_n^j\right] + \sum_{n\text{ even}} \left[c_{n-2}^i - c_{n-2}^j\right]\left[y_n^i - y_n^j\right],
\end{aligned} \tag{B.19}$$

$$\begin{aligned}
\zeta(i,j) = & \sum_{n\text{ even}} \left[c_{n-3}^i - c_{n-3}^j\right]\left[x_n^i - x_n^j\right] - \sum_{n\text{ odd}} \left[c_{n-3}^i - c_{n-3}^j\right]\left[x_n^i - x_n^j\right]\\
& + \sum_{n\text{ odd}} \left[v_{n-1}^i - v_{n-1}^j\right]\left[y_n^i - y_n^j\right] - \sum_{n\text{ even}} \left[v_{n-1}^i - v_{n-1}^j\right]\left[y_n^i - y_n^j\right],
\end{aligned} \tag{B.20}$$

$$\begin{aligned}\delta(i,j) &= \sum_{n \text{ odd}} \left[c^i_{n-2} - c^j_{n-2}\right] \left[y^i_n - y^j_n\right] + \sum_{n \text{ even}} \left[c^i_{n-2} - c^j_{n-2}\right] \left[y^i_n - y^j_n\right] \\ &\quad + \sum_{n \text{ even}} \left[v^i_n - v^j_n\right] \left[x^i_n - x^j_n\right] + \sum_{n \text{ odd}} \left[v^i_n - v^j_n\right] \left[x^i_n - x^j_n\right]. \end{aligned} \tag{B.21}$$

Appendix C

Theorem 4 Proof

Applying (4.50) used in Theorem 4 to each even and odd symbols of v_n, x_n, and y_n, we get the following:

For v_n symbols,

$$\begin{aligned} v_{4k} &= (-1)^{4k+1} c_{4k} c_{4k-1} c_{4k-2} = -c_{4k}, \\ v_{4k+1} &= (-1)^{4k+2} c_{4k+1} c_{4k} c_{4k-1} = c_{4k-1}, \\ v_{4k+2} &= (-1)^{4k+3} c_{4k+2} c_{4k+1} c_{4k} = -c_{4k}, \\ v_{4k+3} &= (-1)^{4k+4} c_{4k+3} c_{4k+2} c_{4k+1} = c_{4k+1}. \end{aligned} \tag{C.1}$$

For x_n symbols,

$$\begin{aligned} x_{4k} &= (-1)^{4k} c_{4k} c_{4k-2} c_{4k-3} = c_{4k}, \\ x_{4k+1} &= (-1)^{4k+1} c_{4k+1} c_{4k-1} c_{4k-2} = -c_{4k+1}, \\ x_{4k+2} &= (-1)^{4k+2} c_{4k+2} c_{4k} c_{4k-1} = c_{4k-1}, \\ x_{4k+3} &= (-1)^{4k+3} c_{4k+3} c_{4k+3} c_{4k+1} = -c_{4k+1}. \end{aligned} \tag{C.2}$$

For y_n symbols,

$$\begin{aligned} y_{4k} &= c_{4k} c_{4k-1} c_{4k-3} = c_{4k}, \\ y_{4k+1} &= c_{4k+1} c_{4k} c_{4k-2} = c_{4k-2}, \\ y_{4k+2} &= c_{4k+2} c_{4k+1} c_{4k-1} = c_{4k-1}, \\ y_{4k+3} &= c_{4k+3} c_{4k+2} c_{4k} = c_{4k}. \end{aligned} \tag{C.3}$$

From (4.50) we have that $c_{4k-1} = c_{4k-2} = c_{4k-3} = c_{4k-4}$, and substituting (4.50) and (C.1)–(C.3) into $\chi(i,j)$ that is defined in (3.57), we obtain that

$$\begin{aligned}
\chi(i,j) &= \sum_{k=0}^{\infty}\left[c_{4k}^i - c_{4k}^j\right]\underbrace{\left[c_{4k-2}^i - c_{4k-2}^j\right]}_{\left[c_{4k-1}^i - c_{4k-1}^j\right]} + \sum_{k=0}^{\infty}\underbrace{\left[v_{4k}^i - v_{4k}^j\right]}_{-\left[c_{4k}^i - c_{4k}^j\right]}\left[c_{4k-1}^i - c_{4k-1}^j\right] \\
&\quad + \sum_{k=0}^{\infty}\underbrace{\left[c_{4k+2}^i - c_{4k+2}^j\right]}_{\left[c_{4k+1}^i - c_{4k+1}^j\right]}\left[c_{4k}^i - c_{4k}^j\right] + \sum_{k=0}^{\infty}\underbrace{\left[v_{4k+2}^i - v_{4k+2}^j\right]}_{-\left[c_{4k}^i - c_{4k}^j\right]}\left[c_{4k+1}^i - c_{4k+1}^j\right] \\
&\quad + \sum_{k=0}^{\infty}\underbrace{\left[c_{4k+1}^i - c_{4k+1}^j\right]}_{\left[c_{4k}^i - c_{4k}^j\right]}\left[c_{4k-1}^i - c_{4k-1}^j\right] - \sum_{k=0}^{\infty}\underbrace{\left[v_{4k+1}^i - v_{4k+1}^j\right]}_{\left[c_{4k-1}^i - c_{4k-1}^j\right]}\left[c_{4k}^i - c_{4k}^j\right] \\
&\quad + \sum_{k=0}^{\infty}\underbrace{\left[c_{4k+3}^i - c_{4k+3}^j\right]}_{\left[c_{4k+2}^i - c_{4k+2}^j\right]}\left[c_{4k+1}^i - c_{4k+1}^j\right] - \sum_{k=0}^{\infty}\underbrace{\left[v_{4k+3}^i - v_{4k+3}^j\right]}_{\left[c_{4k+1}^i - c_{4k+1}^j\right]}\left[c_{4k+2}^i - c_{4k+2}^j\right] \\
&= 0. \qquad \text{(C.4)}
\end{aligned}$$

Substituting (4.50) and (C.1)–(C.3) into $\eta(i,j)$ that is defined in (B.18), we obtain that

$$\begin{aligned}
\eta(i,j) &= \sum_{k=0}^{\infty}\left[c_{4k+1}^i - c_{4k+1}^j\right]\underbrace{\left[v_{4k}^i - v_{4k}^j\right]}_{-\left[c_{4k}^i - c_{4k}^j\right]} + \sum_{k=0}^{\infty}\left[c_{4k+3}^i - c_{4k+3}^j\right]\underbrace{\left[v_{4k+2}^i - v_{4k+2}^j\right]}_{-\left[c_{4k}^i - c_{4k}^j\right]} \\
&\quad - \sum_{k=0}^{\infty}\left[c_{4k}^i - c_{4k}^j\right]\underbrace{\left[v_{4k-1}^i - v_{4k-1}^j\right]}_{\left[c_{4k-1}^i - c_{4k-1}^j\right]} - \sum_{k=0}^{\infty}\left[c_{4k+2}^i - c_{4k+2}^j\right]\underbrace{\left[v_{4k+1}^i - v_{4k+1}^j\right]}_{-\left[c_{4k-1}^i - c_{4k-1}^j\right]} \\
&\quad + \sum_{k=0}^{\infty}\left[c_{4k-1}^i - c_{4k-1}^j\right]\underbrace{\left[x_{4k}^i - x_{4k}^j\right]}_{\left[c_{4k}^i - c_{4k}^j\right]} + \sum_{k=0}^{\infty}\left[c_{4k+1}^i - c_{4k+1}^j\right]\underbrace{\left[x_{4k+2}^i - x_{4k}^j\right]}_{\left[c_{4k-1}^i - c_{4k-1}^j\right]} \\
&\quad - \sum_{k=0}^{\infty}\left[c_{4k}^i - c_{4k}^j\right]\underbrace{\left[x_{4k+1}^i - x_{4k+1}^j\right]}_{-\left[c_{4k+1}^i - c_{4k+1}^j\right]} - \sum_{k=0}^{\infty}\left[c_{4k+2}^i - c_{4k+2}^j\right]\underbrace{\left[x_{4k+3}^i - x_{4k+3}^j\right]}_{-\left[c_{4k+1}^i - c_{4k+1}^j\right]} \\
&= 0. \qquad \text{(C.5)}
\end{aligned}$$

Substituting (4.50) and (C.1)–(C.3) into $\lambda(i,j)$ that is defined in (B.19), we obtain that

$$\begin{aligned}
\lambda(i,j) &= \sum_{k=0}^{\infty}\left[c_{4k-3}^i - c_{4k-3}^j\right]\underbrace{\left[v_{4k}^i - v_{4k}^j\right]}_{-\left[c_{4k}^i - c_{4k}^j\right]} + \sum_{k=0}^{\infty}\left[c_{4k-1}^i - c_{4k-1}^j\right]\underbrace{\left[v_{4k+2}^i - v_{4k+2}^j\right]}_{-\left[c_{4k}^i - c_{4k}^j\right]} \\
&\quad - \sum_{k=0}^{\infty}\left[c_{4k-2}^i - c_{4k-2}^j\right]\underbrace{\left[v_{4k+1}^i - v_{4k+1}^j\right]}_{\left[c_{4k-1}^i - c_{4k-1}^j\right]} - \sum_{k=0}^{\infty}\left[c_{4k}^i - c_{4k}^j\right]\underbrace{\left[v_{4k+3}^i - v_{4k+3}^j\right]}_{\left[c_{4k+1}^i - c_{4k+1}^j\right]} +
\end{aligned}$$

$$\begin{aligned}
&\sum_{k=0}^{\infty}\left[c_{4k-1}^{i}-c_{4k-1}^{j}\right]\underbrace{\left[y_{4k+1}^{i}-y_{4k+1}^{j}\right]}_{\left[c_{4k-2}^{i}-c_{4k-2}^{j}\right]}+\sum_{k=0}^{\infty}\left[c_{4k+1}^{i}-c_{4k+1}^{j}\right]\underbrace{\left[y_{4k+3}^{i}-y_{4k+3}^{j}\right]}_{\left[c_{4k}^{i}-c_{4k}^{j}\right]}\\
&+\sum_{k=0}^{\infty}\left[c_{4k-2}^{i}-c_{4k-2}^{j}\right]\underbrace{\left[y_{4k}^{i}-y_{4k}^{j}\right]}_{\left[c_{4k}^{i}-c_{4k}^{j}\right]}+\sum_{k=0}^{\infty}\left[c_{4k}^{i}-c_{4k}^{j}\right]\underbrace{\left[y_{4k+2}^{i}-y_{4k+2}^{j}\right]}_{\left[c_{4k-1}^{i}-c_{4k-1}^{j}\right]}\\
=\;&0. \qquad \text{(C.6)}
\end{aligned}$$

Substituting (4.50) and (C.1)–(C.3) into $\zeta(i,j)$ that is defined in (B.20), we obtain that

$$\begin{aligned}
\zeta(i,j) =\;&\sum_{k=0}^{\infty}\left[c_{4k-3}^{i}-c_{4k-3}^{j}\right]\underbrace{\left[x_{4k}^{i}-x_{4k}^{j}\right]}_{\left[c_{4k}^{i}-c_{4k}^{j}\right]}+\sum_{k=0}^{\infty}\left[c_{4k-1}^{i}-c_{4k-1}^{j}\right]\underbrace{\left[x_{4k+2}^{i}-x_{4k+2}^{j}\right]}_{\left[c_{4k-1}^{i}-c_{4k-1}^{j}\right]}\\
&-\sum_{k=0}^{\infty}\left[c_{4k-2}^{i}-c_{4k-2}^{j}\right]\underbrace{\left[x_{4k+1}^{i}-x_{4k+1}^{j}\right]}_{-\left[c_{4k+1}^{i}-c_{4k+1}^{j}\right]}-\sum_{k=0}^{\infty}\left[c_{4k}^{i}-c_{4k}^{j}\right]\underbrace{\left[x_{4k+3}^{i}-x_{4k+3}^{j}\right]}_{-\left[c_{4k+1}^{i}-c_{4k+1}^{j}\right]}\\
&+\sum_{k=0}^{\infty}\underbrace{\left[v_{4k}^{i}-v_{4k}^{j}\right]}_{-\left[c_{4k}^{i}-c_{4k}^{j}\right]}\underbrace{\left[y_{4k+1}^{i}-y_{4k+1}^{j}\right]}_{\left[c_{4k-2}^{i}-c_{4k-2}^{j}\right]}+\sum_{k=0}^{\infty}\underbrace{\left[v_{4k+2}^{i}-v_{4k+2}^{j}\right]}_{-\left[c_{4k}^{i}-c_{4k}^{j}\right]}\underbrace{\left[y_{4k+3}^{i}-y_{4k+3}^{j}\right]}_{\left[c_{4k}^{i}-c_{4k}^{j}\right]}\\
&-\sum_{k=0}^{\infty}\underbrace{\left[v_{4k-1}^{i}-v_{4k-1}^{j}\right]}_{\left[c_{4k-3}^{i}-c_{4k-3}^{j}\right]}\underbrace{\left[y_{4k}^{i}-y_{4k}^{j}\right]}_{\left[c_{4k}^{i}-c_{4k}^{j}\right]}-\sum_{k=0}^{\infty}\underbrace{\left[v_{4k+1}^{i}-v_{4k+1}^{j}\right]}_{\left[c_{4k-1}^{i}-c_{4k-1}^{j}\right]}\underbrace{\left[y_{4k+2}^{i}-y_{4k+2}^{j}\right]}_{\left[c_{4k-1}^{i}-c_{4k-1}^{j}\right]}\\
=\;&0. \qquad \text{(C.7)}
\end{aligned}$$

Substituting (4.50) and (C.1)– (C.3) into $\delta(i,j)$ that is defined in (B.21), we obtain that

$$\begin{aligned}
\delta(i,j) =\;&\sum_{k=0}^{\infty}\left[c_{4k-1}^{i}-c_{4k-1}^{j}\right]\underbrace{\left[y_{4k+1}^{i}-x_{4k+1}^{j}\right]}_{\left[c_{4k-2}^{i}-c_{4k-2}^{j}\right]}+\sum_{k=0}^{\infty}\left[c_{4k+1}^{i}-c_{4k+1}^{j}\right]\underbrace{\left[y_{4k+3}^{i}-y_{4k+3}^{j}\right]}_{\left[c_{4k}^{i}-c_{4k}^{j}\right]}\\
&+\sum_{k=0}^{\infty}\left[c_{4k-2}^{i}-c_{4k-2}^{j}\right]\underbrace{\left[y_{4k}^{i}-y_{4k}^{j}\right]}_{\left[c_{4k}^{i}-c_{4k}^{j}\right]}+\sum_{k=0}^{\infty}\left[c_{4k}^{i}-c_{4k}^{j}\right]\underbrace{\left[y_{4k+2}^{i}-y_{4k+2}^{j}\right]}_{\left[c_{4k-1}^{i}-c_{4k-1}^{j}\right]}\\
&+\sum_{k=0}^{\infty}\underbrace{\left[v_{4k}^{i}-v_{4k}^{j}\right]}_{-\left[c_{4k}^{i}-c_{4k}^{j}\right]}\underbrace{\left[x_{4k}^{i}-x_{4k}^{j}\right]}_{\left[c_{4k}^{i}-c_{4k}^{j}\right]}+\sum_{k=0}^{\infty}\underbrace{\left[v_{4k+2}^{i}-v_{4k+2}^{j}\right]}_{-\left[c_{4k}^{i}-c_{4k}^{j}\right]}\underbrace{\left[x_{4k+2}^{i}-x_{4k+2}^{j}\right]}_{\left[c_{4k-1}^{i}-c_{4k-1}^{j}\right]}\\
&+\sum_{k=0}^{\infty}\underbrace{\left[v_{4k+1}^{i}-v_{4k+1}^{j}\right]}_{\left[c_{4k-1}^{i}-c_{4k-1}^{j}\right]}\underbrace{\left[x_{4k+1}^{i}-x_{4k+1}^{j}\right]}_{-\left[c_{4k+1}^{i}-c_{4k+1}^{j}\right]}+\sum_{k=0}^{\infty}\underbrace{\left[v_{4k+3}^{i}-v_{4k+3}^{j}\right]}_{\left[c_{4k+1}^{i}-c_{4k+1}^{j}\right]}\underbrace{\left[x_{4k+3}^{i}-x_{4k+3}^{j}\right]}_{-\left[c_{4k+1}^{i}-c_{4k+1}^{j}\right]}\\
=\;&0. \qquad \text{(C.8)}
\end{aligned}$$

The Hamming distance between the v_n sequences is given by

$$H(\mathbf{v}^i,\mathbf{v}^j) = \frac{1}{4}\sum_{n=0}^{\infty}|v_n^i-v_n^j|^2$$

$$= \frac{1}{4}\left[\sum_{n\text{ even}}^{\infty}\underbrace{|v_n^i - v_n^j|^2}_{|c_n^i - c_n^j|^2} + \sum_{k=0}^{\infty}\underbrace{|v_{4k+1}^i - v_{4k+1}^j|^2}_{|c_{4k-1}^i - c_{4k-1}^j|^2} + \sum_{k=0}^{\infty}\underbrace{|v_{4k+3}^i - v_{4k+3}^j|^2}_{|c_{4k+1}^i - c_{4k+1}^j|^2}\right]$$

Using the fact that $c_{-1}^i = c_{-1}^j = 1$ for all i, j and $c_{4k+1} = c_{4k+3}$, then

$$\begin{aligned}
H(\mathbf{v}^i, \mathbf{v}^j) &= \frac{1}{4}\left[\sum_{n\text{ even}}^{\infty}|c_n^i - c_n^j|^2 + \sum_{k=1}^{\infty}|c_{2k-1}^i - c_{2k-1}^j|^2 + \sum_{k=0}^{\infty}|c_{4k+3}^i - c_{4k+3}^j|^2\right] \\
&= \frac{1}{4}\left[\sum_{n\text{ even}}^{\infty}|c_n^i - c_n^j|^2 + \sum_{k=0}^{\infty}|c_{2k+1}^i - c_{2k+1}^j|^2 + \sum_{k=0}^{\infty}|c_{4k+3}^i - c_{4k+3}^j|^2\right] \\
&= \frac{1}{4}\left[\sum_{n\text{ even}}^{\infty}|c_n^i - c_n^j|^2 + \sum_{n\text{ odd}}^{\infty}|c_n^i - c_n^j|^2\right] \\
&= \frac{1}{4}\sum_{n=0}^{\infty}|c_n^i - c_n^j|^2 \\
&= H(\mathbf{c}^i, \mathbf{c}^j). \qquad \text{(C.9)}
\end{aligned}$$

The Hamming distance between the x_n sequences is given by

$$\begin{aligned}
H(\mathbf{x}^i, \mathbf{x}^j) &= \frac{1}{4}\sum_{n=0}^{\infty}|x_n^i - x_n^j|^2 \\
&= \frac{1}{4}\left[\sum_{n\text{ odd}}^{\infty}\underbrace{|x_n^i - x_n^j|^2}_{|c_n^i - c_n^j|^2} + \sum_{k=0}^{\infty}\underbrace{|x_{4k+2}^i - x_{4k+2}^j|^2}_{|c_{4k-1}^i - c_{4k-1}^j|^2} + \sum_{k=0}^{\infty}\underbrace{|x_{4k+3}^i - x_{4k+3}^j|^2}_{|c_{4k+1}^i - c_{4k+1}^j|^2}\right]
\end{aligned}$$

Since $c_{-1}^i = c_{-1}^j = 1$ for all i, j and $c_{4k} = c_{4k+1} = c_{4k+2}$, then

$$\begin{aligned}
H(\mathbf{x}^i, \mathbf{x}^j) &= \frac{1}{4}\left[\sum_{n\text{ odd}}^{\infty}|c_n^i - c_n^j|^2 + \sum_{k=1}^{\infty}|c_{4k-1}^i - c_{4k-1}^j|^2 + \sum_{k=0}^{\infty}|c_{4k+2}^i - c_{4k+2}^j|^2\right] \\
&= \frac{1}{4}\left[\sum_{n\text{ odd}}^{\infty}|c_n^i - c_n^j|^2 + \sum_{k=0}^{\infty}|c_{2k+1}^i - c_{2k+1}^j|^2 + \sum_{k=0}^{\infty}|c_{4k+2}^i - c_{4k+2}^j|^2\right] \\
&= \frac{1}{4}\left[\sum_{n\text{ odd}}^{\infty}|c_n^i - c_n^j|^2 + \sum_{k=0}^{\infty}|c_{2k}^i - c_{2k}^j|^2 + \sum_{k=0}^{\infty}|c_{4k+2}^i - c_{4k+2}^j|^2\right] \\
&= \frac{1}{4}\left[\sum_{n\text{ odd}}^{\infty}|c_n^i - c_n^j|^2 + \sum_{n\text{ even}}^{\infty}|c_n^i - c_n^j|^2\right] \\
&= \frac{1}{4}\sum_{n=0}^{\infty}|c_n^i - c_n^j|^2 \\
&= H(\mathbf{c}^i, \mathbf{c}^j). \qquad \text{(C.10)}
\end{aligned}$$

The Hamming distance between the y_n sequences is given by

$$H(\mathbf{y}^i, \mathbf{y}^j) = \frac{1}{4}\sum_{n=0}^{\infty}|y_n^i - y_n^j|^2$$

$$= \frac{1}{4}\Bigg[\sum_{k=0}^{\infty}\underbrace{|y_{4k}^i - y_{4k}^j|^2}_{|c_{4k}^i - c_{4k}^j|^2} + \sum_{k=0}^{\infty}\underbrace{|y_{4k+2}^i - y_{4k+2}^j|^2}_{|c_{4k-1}^i - c_{4k-1}^j|^2}$$
$$+ \sum_{k=0}^{\infty}\underbrace{|y_{4k+1}^i - y_{4k+1}^j|^2}_{|c_{4k-2}^i - c_{4k-2}^j|^2} + \sum_{k=0}^{\infty}\underbrace{|y_{4k+3}^i - y_{4k+3}^j|^2}_{|c_{4k}^i - c_{4k}^j|^2}\Bigg]$$

Since $c_{-2}^i = c_{-2}^j = 1$, $c_{-1}^i = c_{-1}^j = 1$ for all i, j and $c_{4k+1} = c_{4k+3}$, then

$$\begin{aligned}
H(\mathbf{y}^i, \mathbf{y}^j) &= \frac{1}{4}\Bigg[\sum_{k=0}^{\infty}|c_{4k}^i - c_{4k}^j|^2 + \sum_{k=1}^{\infty}|c_{4k-1}^i - c_{4k-1}^j|^2 \\
&\quad + \sum_{k=2}^{\infty}|c_{4k-2}^i - c_{4k-2}^j|^2 + \sum_{k=0}^{\infty}|c_{4k}^i - c_{4k}^j|^2\Bigg] \\
&= \frac{1}{4}\Bigg[\sum_{k=0}^{\infty}|c_{4k}^i - c_{4k}^j|^2 + \sum_{k=0}^{\infty}|c_{4k+1}^i - c_{4k+1}^j|^2 \\
&\quad + \sum_{k=0}^{\infty}|c_{4k+2}^i - c_{4k+2}^j|^2 + \sum_{k=0}^{\infty}|c_{4k+3}^i - c_{4k+3}^j|^2\Bigg] \\
&= \frac{1}{4}\Bigg[\sum_{n\text{ odd}}^{\infty}|c_n^i - c_n^j|^2 + \sum_{n\text{ even}}^{\infty}|c_n^i - c_n^j|^2\Bigg] \\
&= \frac{1}{4}\sum_{n=0}^{\infty}|c_n^i - c_n^j|^2 \\
&= H(\mathbf{c}^i, \mathbf{c}^j). \qquad \text{(C.11)}
\end{aligned}$$

Substituting (C.4)-(C.11) into (B.17) we obtain

$$\begin{aligned}
\mathbf{NSED}(i,j) &= 2R_c H(\mathbf{c}^i, \mathbf{c}^j)\frac{1}{T}\Bigg[\|C_0(t)\|^2 + \|C_1(t)\|^2 + \|C_2(t)\|^2 + \|C_3(t)\|^2\Bigg] \\
&= 2R_c H(\mathbf{c}^i, \mathbf{c}^j)\frac{1}{T}\sum_{k=0}^{3}\|C_k(t)\|^2. \qquad \text{(C.12)}
\end{aligned}$$

It can be shown that for any pre-modulation pulse shape $h(t)$ of length $3T$,

$$\sum_{k=0}^{3}\|C_k(t)\|^2 = T. \qquad \text{(C.13)}$$

For simplicity, let

$$f(t) = \frac{\pi}{2T}\int_0^t h(\tau)\,d\tau,$$

then

$$\sum_{k=0}^{3}\|C_k(t)\|^2 = \int_0^T \sin^2[f(t)]\sin^2[f(t+T)]\sin^2[f(t+2T)]\;dt$$

$$
\begin{aligned}
&+ \int_0^T \sin^2[f(t)] \sin^2[f(t+2T)] \cos^2[f(t+T)]\ dt \\
&+ \int_0^T \sin^2[f(t)] \sin^2[f(t+T)] \cos^2[f(t+2T)]\ dt \\
&+ \int_0^T \sin^2[f(t)] \cos^2[f(t+T)] \cos^2[f(t+2T)]\ dt \\
&+ \int_T^{2T} \sin^2[f(t)] \sin^2[f(t+T)] \cos^2[f(t-T)]\ dt \\
&+ \int_T^{2T} \sin^2[f(t)] \cos^2[f(t-T)] \cos^2[f(t+T)]\ dt \\
&+ \int_{2T}^{3T} \sin^2[f(t)] \cos^2[f(t-2T)] \cos^2[f(t-T)]\ dt \\
&+ \int_{3T}^{4T} \cos^2[f(t-3T)] \cos^2[f(t-2T)] \cos^2[f(t-T)]\ dt.
\end{aligned}
$$

By changing of variable ($t' = t - T$) in the last integral, we have

$$
\begin{aligned}
\sum_{k=0}^{3} \|C_k(t)\|^2 &= \int_0^T \sin^2[f(t)] \sin^2[f(t+2T)] \left\{ \underbrace{\sin^2[f(t+T)] + \cos^2[f(t+T)]}_{=1} \right\} dt \\
&+ \int_0^T \sin^2[f(t)] \cos^2[f(t+2T)] \left\{ \underbrace{\sin^2[f(t+T)] + \cos^2[f(t+T)]}_{=1} \right\} dt \\
&+ \int_T^{2T} \sin^2[f(t)] \cos^2[f(t-T)] \left\{ \underbrace{\sin^2[f(t+T)] + \cos^2[f(t+T)]}_{=1} \right\} dt \\
&+ \int_{2T}^{3T} \cos^2[f(t-T)] \cos^2[f(t-2T)] \left\{ \underbrace{\sin^2[f(t)] + \cos^2[f(t)]}_{=1} \right\} dt \\
&= \int_0^T \sin^2[f(t)] \sin^2[f(t+2T)]\ dt + \int_0^T \sin^2[f(t)] \cos^2[f(t+2T)]\ dt \\
&+ \int_{2T}^{3T} \cos^2[f(t-T)] \cos^2[f(t-2T)]\ dt + \int_T^{2T} \sin^2[f(t)] \cos^2[f(t-T)]\ dt.
\end{aligned}
$$

By changing of variable ($t' = t - T$) in the last integral, we have

$$
\sum_{k=0}^{3} \|C_k(t)\|^2 = \int_0^T \sin^2[f(t)] \left\{ \underbrace{\sin^2[f(t+2T)] + \cos^2[f(t+2T)]}_{=1} \right\} dt
$$

$$+ \int_{T}^{2T} \cos^2 [f(t-T)] \left\{ \underbrace{\sin^2 [f(t)] + \cos^2 [f(t)]}_{=1} \right\} dt.$$

By changing of variable ($t' = t - T$), we have that

$$\begin{aligned} \sum_{k=0}^{3} \|C_k(t)\|^2 &= \int_{T}^{2T} \cos^2 [f(t-T)] + \int_{0}^{T} \sin^2 [f(t)] \; dt \\ &= \int_{0}^{T} \left\{ \underbrace{\sin^2 [f(t)] + \cos^2 [f(t)]}_{=1} \right\} dt \\ &= T. \end{aligned}$$

Therefore, (C.12) reduces simply to

$$\mathbf{NSED}(i,j) = 2R_c H(\mathbf{c}^i, \mathbf{c}^j). \tag{C.14}$$

as required.

References

[1] R. Strauss, J. Bretting, R. Metivier, "Travelling-wave tubes for communication satellites", *Proc. IEEE*, vol. 65, pp. 387-400, March 1977.

[2] G. Lazzarin, S. Pupolin, A. Sarti, "Nonlinearity Compensation in Digital Radio Systems", *IEEE Trans. Commun.*, vol. 42, pp. 988-999, Feb./March/Apr. 1994.

[3] T. Aulin and C-E. Sundberg, "Continuous Phase Modulation-Part I & II: Full & Partial Response Signaling", *IEEE Trans. Commun.*, vol. Com-29, pp. 210-225, March 1981.

[4] P.J. McLane, "The Viterbi Receiver for Correlative Encoded MSK Signals", *IEEE Trans. Commun.*, vol. Com-31, no.2, Feb. 1983.

[5] T. Aulin, "Symbol Error Probability Bounds for Coherently Viterbi Detected Continuous Phase Modulated Signals", *IEEE Trans. Commun.*, vol. Com-29, no 11, Nov. 1981.

[6] P. Galko and S. Pasupathy, "Linear receiver for correlatively coded MSK", *IEEE Trans. Commun.*, vol. Com-33, pp.338-347, Apr. 1985.

[7] Pierre A. Laurent, "Exact and approximate construction of digital phase modulation by superposition of amplitude modulated pulses (AMP)", *IEEE Trans. of Commun.*, vol 34, No.2, Feb 1986.

[8] P. Galko, "Generalized MSK", *Ph.D. dissertation*, Dept. Elec. Eng., Univ. of Toronto, Toronto, 1982.

[9] M.S El-Tanany, S.A. Mahmoud,"Mean-square error optimization of quadrature receivers for CPM with modulation index 1/2", *IEEE J.Select. Areas Commun.*, vol. SAC-5, no.5, pp. 896-905 June 1978

[10] M. Luise, U. Mengali, "OQPSK-based approximation to generalized MSK", *Proc. ICC 89, Boston*, MA, pp. 1648-1652, June 1989.

[11] A. Svensson, C.E Sundberg, and T. Aulin, "A Class of Reduced- Complexity Viterbi Detectors for Partial Response Continuous Phase Modulation", *IEEE Trans. Commun.*, vol. Com-32, no.10, Oct 1984.

[12] T. Ertas and F.H. Ali, "Upper bounds on the free distance for trellis Codes Combined with CPFSK signals", *Electronics Letters*, vol. 33, no. 17, August 1997.

[13] T. Aulin, N. Rydbeck, and C.E. Sundberg, "Transmitter and receiver structures for M-ary Partial response FM", *in Proc. Int. Zurich Sem. Digital Commun.*, Zurich, Switzerland, pp. A.2.1-A.2.6, 1980.

[14] A. Svensson, "Reduced state sequence detection of partial response continuous phase modulation", *IEEE Proceedings*, part I, vol. 138, pp. 1079-1087, Oct. 1984.

[15] F. Morales-Moreno, "Matched Codes for Finite Memory", *Ph.D. dissertation*, Dept. Elec. Eng., Univ. of Toronto, Toronto, 1987.

[16] G.K. Kaleh, "Simple Coherent receivers for partial response continuous phase modulation", *IEEE J. Select. Areas Commun.*, vol. SAC-7, no. 7 pp. 1427-1436, Dec. 1989.

[17] S. Pasupathy, "Minimum Shift Keying: a spectral efficient modulation", *IEEE Commun. Soc. Mag.*, vol. 17, pp. 14-22, July 1979.

[18] S. A.Groneymeyer and A. L. McBride, "MSK and offset QPSK modulation", this issue, *IEEE Trans. Commun.*, vol. COM-24. no. 8, pp. 809- 19. Aug. 1976.

[19] G. Lindell, C. E. Sundberg, and T. Aulin, "Minimum Euclidean distance for the best combination of short rate 1/2 convolutional codes and CPFSK modulation", *IEEE Trans. Inform. Theory*, vol. 30, pp. 509-520, May 1984.

[20] P. Kabal and S. Pasupathy, "Partial-response Signaling", *IEEE Trans. Commun.*, pp. 921-034, Sept. 1975.

[21] S. Pasupathy, "Correlative Coding: A Bandwidth-Efficient Signaling Scheme", *IEEE Comm. Society Magazine*, pp. 4-11, July 1977.

[22] B. Sayar and S. Pasupathy, "Nyquist 3 Pulse Shaping in Continuous Phase Modulation", *IEEE Trans. Commun.*, vol. Com-35, pp. 57-67, Jan. 1987.

[23] K. Murota and K. Hirade, "GMSK modulation for digital mobile radio telephony", *IEEE Trans. Commun.*, vol. Com-29, pp. 1044-1050, Jul. 1981.

[24] T. Rappaport, *Wireless Communications: Principles and Practices*, NJ: Prentice-Hall PTR, 1996.

[25] H. Mathis, "Differential detection of GMSK signals with low *BT* using the SOVA", *IEEE Trans. Commun.*, vol. 46, pp. 428-430, Apr. 1998.

[26] J. Wu and G.J. Saulnier, "An adaptive soft output demodulator for small BT GMSK signals", *in Proc. IEEE Vehicular Technology Conf.* (VTC) Fall'02, Vancouver, BC, Canada, pp. 520-524, Sept. 2002.

[27] J.B. Anderson, T. Aulin and C.E. Sundberg, *Digital Phase Modulation*, New York; plenum, 1986.

[28] G. Colavolpe and R. Raheli, "Reduced- Complexity Detection and Phase Synchronization of CPM signals", *IEEE Trans. Commun.*, vol. 45, pp. 1070-1079, Sept. 1997.

[29] M. Figuera and J.V. Krogmeier, "Optimum and Suboptimum receivers for M-ary CPM signals based upon the Laurent representation", *VTC 2002*, Proc. Vol.4, pp. 2268-2272, Sept. 2002.

[30] O.Dural and J.G. Proakis, "The performance of simplified maximum-likelihood sequence detector for continuous phase modulation scheme", *ICC 2000*, vol.2, pp. 641-645, June 2000.

[31] J.P. Fonseka, "Block Encoding with Continuous Phase Modulation", *IEEE Trans. Commun.*, vol. 42, no.12, Dec. 1994.

[32] G. Benelli and R. Fantacci, "Euclidean Distance for Combinations of Some Hamming Codes and Binary CPFSK Modulation", *IEEE Trans. Inform. Theory*, vol. IT-33, No. 2, March 1987.

[33] S.V. Pizzi and S. G. Wilson, "Convolutional coding combined with continuous phase modulation", *IEEE Trans. Commun.*, vol. 33, pp. 20-29, Jan. 1985.

[34] J. G. Proakis, *Digital Communications*, Fourth Edition, New York, McGraw-Hill, 2001.

[35] W. Holubowicz and F. Morales-Moreno, "Convolutional Coding of Binary CPM Schemes with No Increase in Receiver Complexity", *IEEE Trans. Commun.*, vol. 43, pp. 1221-1224, Feb. 1995.

[36] E. Passke, "Short binary convolutional codes with maximal free distance for rates 2/3 and 3/4", *IEEE Trans. Inform. Theory*, vol. IT-20, pp. 683-688, Sept. 1974.

[37] J. Chang, D. Hwang, and M. Lin, "Some Extended Results on the Search for Good Convolutional Codes", *IEEE Trans. Inform. Theory*, vol. 43, no. 5, pp. 1683-1697, Sept. 1997.

[38] F. Morales-Moreno and S. Pasupathy, "Structure, optimization and realization of FFSK trellis codes", *IEEE Trans. Inform. Theory*, vol. IT-34, pp. 730-741, July 1988.

[39] Lee W.C. Lee, "The advantages of using repetition coding in mobile radio communication", *in Proc. 36th IEEE Vehicular Technology Conf.* Dallas, TX, pp. 157-161, May 1986.

[40] Stefan Host, *On Woven Convolutional Codes*, Lund University, 1999.

[41] G.D. Forney, Jr., "Maximum-Likelihood Sequence Estimation of Digital Sequences in the Presence of Intersymbol Interference", *IEEE Trans. Inform. Theory*, vol. IT-18, pp. 363-378, May 1972.

[42] J. B. Anderson, T. Aullin, C-E. Sundberg. *Digital Phase Modulation.* Plenum Press, New York, 1986.

[43] G. Lindell and C. E. Sundberg, "An Upper Bound on the Bit Error Probability of Combined Convolutional Coding and Continuous Phase Modulation", *IEEE Trans. Inform. Theory*, vol. 34, pp. 1263-1269, Sept. 1988.